USAAML TECHNICAL REPORT 65-5

A STUDY OF ROUGH-TERRAIN-INDUCED STRUCTURAL LANDING LOADS

PHASE III

May 1965

U.S. ARMY AVIATION MATERIEL LABORATORIES
FORT EUSTIS, VIRGINIA

CONTRACT DA 44-177-TC-735
DOUGLAS AIRCRAFT CO., INC.

DDC Availability Notices

Qualified requesters may obtain copies of this report from DDC.

This report has been furnished to the Department of Commerce for sale to the public.

Disclaimer

The findings in this report are not to be construed as an official Department of the Army position, unless so designated by other authorized documents.

When Government drawings, specifications, or othe. data are used for any purpose other than in connection with a definitely related Government procurement operation, the United States Government thereby incurs no responsibility nor any obligation whatsoever; and the fact that the Government may have formulated, furnished, or in any way supplied the said drawings, specifications, or other data is not to be regarded by implication or otherwise as in any manner licensing the holder or any other person or corporation, or conveying any rights or permission, to manufacture, use, or sell any patented invention that may in any way be related thereto.

Disposition Instructions

Destroy this report when it is no longer needed. Do not return it to the originator.

DISCLAIMER NOTICE

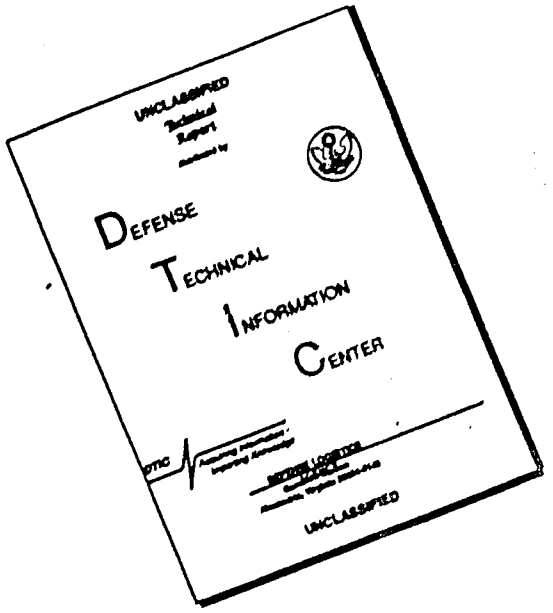

THIS DOCUMENT IS BEST QUALITY AVAILABLE. THE COPY FURNISHED TO DTIC CONTAINED A SIGNIFICANT NUMBER OF PAGES WHICH DO NOT REPRODUCE LEGIBLY.

HEADQUARTERS
U S ARMY TRANSPORTATION RESEARCH COMMAND
FORT EUSTIS, VIRGINIA 23604

This report has been reviewed by this command and is considered to be technically sound. It is published for the exchange of information and the stimulation of ideas.

NOTE

On 1 March 1965, *after this report had been prepared,* the name of this command was changed from U. S. Army Transportation Research Command to:

U.S. ARMY AVIATION MATERIEL LABORATORIES

Task 1P125901A14602
Contract DA 44-177-TC-735
USAAML Technical Report 65-5
May 1965

A STUDY OF ROUGH-TERRAIN-INDUCED STRUCTURAL LANDING LOADS

Phase III

Simulated Landings of an OV-1 Aircraft Over Rough Terrain and Comparison of Experimental Loads With Theoretical Predictions

Prepared by
Douglas Aircraft Co., Inc.
Aircraft Division
Long Beach, California

for
U. S. ARMY AVIATION MATERIEL LABORATORIES
FORT EUSTIS, VIRGINIA

SUMMARY

This report describes the third phase of a project directed toward the establishment of aircraft design criteria for rough terrain landing operations.

The report presents the results of moving drop tests in which an OV-1 main landing gear was made to traverse simulated terrain irregularities of various sizes and shapes during landing impact. Test results for several cases are compared with the results of dynamic loads calculations performed on a digital computer. Recommendations for improvement of the analysis are made based on this comparison.

FOREWORD

This report presents the results of the third phase of a project sponsored by the U.S. Army Transportation Research Command to assist in the formulation of design criteria for aircraft which operate in and out of unprepared areas. The instrumentation, analytical work and report preparation were accomplished by the Douglas Aircraft Company at its Aircraft Division, Long Beach, California. The test work was accomplished by the National Aeronautics and Space Administration at its Landing Loads Test Facility, Langley Field, Virginia.

This project was conducted at Douglas under the supervision of Mr. F. C. Allen, with Mr. L. B. Mosby acting as Chief Technical Investigator. Mr. U. P. Joyner and Mr. R. C. Dreher of NASA directed the test work. Mr. J. E. Yeates of USATRECOM was the technical monitor.

CONTENTS

CONTENTS (Cont)

ILLUSTRATIONS

ILLUSTRATIONS (Cont)

ILLUSTRATIONS (Cont)

ILLUSTRATIONS (Cont)

TABLES

SYMBOLS

C	tire deflection, inches
D	drag load at the axle, pounds
K_1 through K_9	strain gauge calibration constants
μ_S	ground coefficient of sliding friction
μ_R	ground coefficient of rolling friction
R_o	radius of undeflected tire, inches
S	side load at the ground, pounds
V	vertical load at the axle, pounds
V_E	air volume in oleo strut extended, cubic inches
V_H	horizontal velocity at touchdown, FPS
V_V	vertical velocity at touchdown, FPS
W	drop weight, pounds
$X_{\mathbb{Q}}$	distance of touchdown ahead of bump centerline, feet
$(\delta/\Delta)_V$, $(\delta/\Delta)_D$, $(\delta/\Delta)_S$	strain gauge response measuring vertical, drag and side loads
W_L	wing lift, g's

INTRODUCTION

This report presents the results of the third phase of a project whose purpose is to assist in the establishment of design criteria for Army aircraft whose mission requires operation in and out of unprepared areas.

The need for the establishment of new structural criteria arises from the fact that Army aircraft are designed to meet Air Force, Navy or Federal Aviation Agency requirements. These requirements have not, generally, included adequate provisions for rough terrain landing and taxiing.

Phases I and II of this project consisted of an analytical investigation of the loads induced in an OV-1 Army observation airplane during landings on terrain of varying degrees of roughness. Weight increases caused by the rough-terrain-induced load increments were computed, and the effect of these weight increments on the range of the aircraft was determined. Ground roughness design criteria were then established on the assumption that an STOL aircraft should not be required to land on terrain whose roughness was sufficient to make the performance of the STOL airplane less than that of a VTOL aircraft of equal size. This portion of the project is reported in Reference 1.

In the above investigation, the variation in loads of the OV-1 airplane with terrain roughness was determined from an IBM 7094 computing program which simulated the operational characteristics of the gear and the elastic properties of the gear and airplane structure. Since this set of calculations was a key feature in the investigation, it was considered desirable to check the method by correlation with test data. Accordingly, a test program on the OV-1 main gear was established, and tests were run using the moving drop test facility of the National Aeronautics and Space Administration (NASA) at Langley Field, Virginia. In these tests, the gear was dropped on surfaces containing protuberances of various sizes and shapes. The present report describes this test program, presents the results and shows a comparison of test and calculated loads.

THE TEST PROGRAM

DESCRIPTION OF TEST ARTICLE

The landing gear used for these tests was the main gear of the OV-1 Mohawk airplane. The line diagram presented in Figure 1 shows that the gear has a side brace, is cantilevered with respect to fore and aft loads, has a centrally located wheel mounted on a half fork, and utilizes conventional torque links. The gear was equipped with an 8.50-10, type III tire. The normal tire inflation pressure of 90 psi was used throughout the test.

The shock strut (Figure 1) was of the conventional hydropneumatic type with a metering pin and orifice. The air volume in the extended position was 194.9 cubic inches. The stroke from fully extended to fully compressed was 15 inches.

The gear was designed for 20.8 feet per second ultimate sinking speed at an airplane weight of 10,715 pounds. The normal drop weight would ordinarily be half the airplane gross weight, but inasmuch as the unballasted weight of the drop carriage plus gear was 6618 pounds, this value was of necessity used in all tests.

The load limits for the gear, derived from technical data supplied by the aircraft manufacturer, are shown in Figure 2.

All tests were made with the axis of the strut inclined 5° 45' wheel forward as viewed from the side and 2° 13' wheel to the right as viewed from the back.

INSTRUMENTATION

A complete description of the instrumentation and calibration procedure is contained in Reference 2. For the reader's convenience, the following brief description is included herewith.

The landing gear instrumentation and recording apparatus was typical of flight test instrumentation developed in connection with Navy aircraft carrier qualification tests. The following items were measured:

(a) Strut vertical, drag and side forces at the axle

(b) Vertical, drag and side acceleration at the axle

(c) Piston position (stroke)

(d) Piston velocity

(e) Metering chamber (oil) pressure

(f) Air chamber pressure

(g) Wheel angular position

(h) Side brace load

(i) Tire deflection

Forces on the gear at the axle were obtained from strain gauges mounted on the axle and fork. Ground loads were obtained by adding to the measured axle loads the inertia forces of the wheel and tire which were determined from the accelerometers mounted in the axle.

Piston position, or stroke, was measured by a slide wire device designed by Douglas Aircraft Company, and piston velocity was measured by the output of a velocity generator mounted on the cylinder and driven by a rod attached to the fork. Wheel angular position was determined by recording the signal induced by the passage of metal studs on the wheel past a magnetic pickup mounted on the brake flange.

For convenience, the production side brace was replaced by a steel tube with compatible end fittings, and side brace loads were obtained from a conventional strain gauge installation mounted thereon.

The response of all gear instrumentation, including the recording apparatus, was within ±5 percent up to, or exceeding, 100 cps and within ±10 percent up to, or exceeding, 200 cps.

In addition to the landing gear instrumentation, the landing track facility provided instrumentation for measuring vertical velocity of the drop carriage and horizontal speed. A method was available for obtaining the magnitude of the lift applied to the drop carriage at the time of impact. The estimated accuracy of these items is as follows: Vertical velocity, ±0.5 fps; horizontal velocity, ±2.0 knots; lift force, ±5 percent.

CALIBRATION

The only instrumentation requiring special calibration techniques was the strain gauge installations measuring vertical, drag and side loads at the axle. By the use of brittle lacquer, the strain gauges were located at points on the fork or axle so that they responded primarily to one component or the other of the applied load. Interaction could not be completely eliminated, hence, the results were obtained in the form:

$$V = K_1 (\delta/\Delta)_V + K_2 (\delta/\Delta)_D + K_3 (\delta/\Delta)_S$$

$$D = K_4 (\delta/\Delta)_V + K_5 (\delta/\Delta)_D + K_6 (\delta/\Delta)_S$$

$$S = K_7 (\delta/\Delta)_V + K_8 (\delta/\Delta)_D + K_9 (\delta/\Delta)_S$$

where

V, D and S	=	vertical, drag and side loads on the gear,
$(\delta/\Delta)_V$	=	response of the strain gauge measuring predominantly vertical loads,
$(\delta/\Delta)_D$	=	response of the strain gauge measuring predominantly drag loads,
$(\delta/\Delta)_S$	=	response of the strain gauge measuring predominantly side forces, and
K_1 through K_9	=	experimentally determined constants.

To allow for the possibility of strain gauge failure, three vertical, three drag and two side gauges were installed and equations derived for all possible combinations.

The calibration was essentially a static calibration. However, laboratory drop tests were made with the strut vertical and no wheel prerotation to check dynamically the vertical load equations against the vertical load measured on a ground reaction platform. The constants for the vertical load equations were then adjusted so that agreement was obtained between the vertical load measured by the strain gauges and the vertical load measured by the platform. Thus, the vertical equations are corrected for dynamics whereas the drag and side equations are based purely on a static calibration. The reason for not correcting the drag and side equations for dynamic effects was that the load platform itself did not have good dynamic response characteristics in those directions.

The final constants obtained from the calibration tests appear in Table I.

TEST FACILITY

The tests were carried out by making moving drop tests at the NASA landing loads track. The basic elements of this facility are shown schematically in Figure 3. The large main carriage is shown in its starting position in Figure 4. The cart "A" is propelled down its track by a water jet emanating from the stationary nozzle at "B."

The landing gear is attached to the drop carriage located within the main carriage (Figure 3). This carriage is constrained to move only in the vertical direction. After the main carriage is accelerated to the proper horizontal speed, the drop carriage is released and permitted to fall through a distance sufficient to give it the desired vertical velocity. After the landing impact, the main carriage is stopped by an arresting gear.

A mechanism is provided for the application of a lift force to the drop carriage at or near the time of initial touchdown. Instrumentation is provided within the carriage for measuring the vertical speed of the drop carriage. A cab in the main carriage houses the recording apparatus for the landing gear instrumentation.

Horizontal speed is determined by measuring the time required for the main carriage to travel known distances along the track. Three such measurements are made on each run. The times are recorded in the control room.

TERRAIN CONTOURS

The surface irregularities upon which the gear was dropped are shown on Figures 5 through 11. The 1-cosine bumps were made of cast aluminum alloy and their contours were accurate within ±1/32 inch of the theoretical value. In order to provide strength in these bumps at the leading and trailing edges (i.e., to avoid feather edges), they were cast with an additional 3/4-inch of material along the bottom. A 3/4-inch steel plate was laid in front of these bumps to provide a smooth transition from the level runway to the bump.

The cylindrical and spherical protuberances were made of welded steel. All surface irregularities were equipped with angles by which they were attached to the runway.

The sand pad was 8 inches deep and was constructed of clean mortar sand with a density at the time of test equal to 96.4 pounds per cubic foot.

Photographs of the landing area with various protuberances in place are presented in Figures 12 through 16.

SCHEDULE OF TEST CONDITIONS

A list of all tests that provided complete and valid data is contained in Table II.

METHOD OF ANALYSIS

The method of calculating the landing gear loads is described in Reference 1. Briefly, the method consisted of a computing program designed for the IBM 7094 machine which used numerical integration with a predict-correct feature. The gear and airplane were considered as mutually interacting dynamic systems in which the gear operating characteristics and structural deformations were considered. The equations of motion are repeated herewith in the Appendix in order that the changes and revisions may be more conveniently described.

In comparing the test data with the output of the computing program, the intent was to establish the validity of the calculations performed in Phases I and II of this project. Hence, comparisons of test and calculated results are shown which contain no alterations to the computing program from that used in Phases I and II other than those made necessary by the peculiarities of the test conditions. Subsequently, efforts were made to improve the correlation. These efforts and the results thereof are described on page 14.

Those revisions made necessary by the peculiarities of the test conditions are as follows:

(1) Since the landing loads track was used for drop testing, airplane structural deflections were removed from the program. It was assumed that the drop carriage was a rigid body.

(2) The angle of the strut to the ground, the weight of the drop carriage, the wing lift, and the sinking speed were made equal to those existing in the tests.

(3) The initial air volume V_E was reduced from 207.3 cubic inches to 194.94 cubic inches since in the servicing of the strut prior to testing more oil was added than had been assumed in the previous analysis.

(4) The ground contour in certain tests contained, in addition to the 1-cosine shapes, a 3/4-inch by 24-inch ramp leading up to the plate in front of the first bump and 3/4-inch steps on the leading and trailing edges of the second and third bumps (see Figure 10). When these conditions prevailed, the original program would not function for technical reasons, and it was found necessary to eliminate an iteration loop in the computing program. Check

cases were run to determine differences in the standard cases with and without the iteration loop, and they were found to be negligible (less than 0.1 percent, for example, on the ground loads). It became obvious that the iteration loop is influential only when the computing interval is much larger than the 0.0001 second used in these calculations. In any event, the actual contour of the landing surface existing in the tests was used in the calculations.

TEST RESULTS AND CORRELATION WITH ANALYSIS

CONDITIONS PLOTTED AND CALCULATED

Table III lists the conditions for which data are presented and those conditions which have been correlated with analytical results. The scope of the project and the capabilities of the computing program defined the conditions to be calculated. The bumps at 45°, the semi-circular cylinder, and the hemisphere were not investigated analytically because of lack of capability in the computing program or because of lack of input data. They were included in the test program to provide additional information concerning rough terrain loads and to supply data for future investigations.

TEST RESULTS

The comparison of measured loads and calculated loads is shown in Figures 17 through 34. The calculated loads at the axle and loads at the ground versus time are compared with corresponding test data for all conditions for which analysis is provided. The measured and calculated internal strut pressures, stroke, and compressing velocity are compared for typical conditions 1/31/64-4, 1/10/64-4, and 2/5/64-2.

Test data only for all other drop tests listed in Table III are shown in Figures 35 through 40.

DISCUSSION OF RESULTS

COMPARISON OF TEST AND CALCULATED RESULTS

Bump Tests

In comparing the results of test and analysis of dynamic phenomena, it is generally conceded that the calculated curves cannot hope to duplicate all the details of the test data. In a problem as complex as the one under study, differences can arise not only from inexact representation of the system by the analysis, but also from test inaccuracies resulting from instrumentation errors and lack of precision in the determination of initial conditions. It has been noted, for instance, that the measured sinking speed was accurate to within ±0.5 fps. In a 10-fps drop, a 0.5-fps error in sinking speed introduces a 10-percent error in energy. Such a discrepancy would undoubtedly produce an equivalent difference in the maximum load from a smooth field landing and have significant effects on the magnitude of the loads developed as the gear traverses a bump. It is necessary, therefore, to examine differences between test and calculated results in somewhat of a statistical manner and attribute to analytical error differences which occur with some degree of consistency.

A study of Figures 17 through 34 shows that the theory produces curves of the same general shape as the drop tests. The vertical loads at the bumps are reproduced with fair accuracy, and in other portions of the vertical load curves the theory tends to predict an average of the oscillating test line. In the multiple bump tests, the theory tends to predict the magnitude of the load of the first bump with greater accuracy than the load at the second and third bumps.

The drag loads at the axle are predicted generally with satisfactory accuracy for the first two cycles. Then, due to a difference in phasing, the loads are not comparable.

Vertical loads at the ground show somewhat the same degree of correlation as the vertical loads at the axle. Drag loads at the ground show good correlation on some areas and poor correlation on others. High frequencies in the drag load record introduced by the drag accelerometer are not, and were not intended to be, reproduced by the analytical data.

Internal pressures were predicted remarkably well (see Figures 22c and 25d). It appears that the calculated pressures are, on the average, slightly lower than the test pressures at points away from the bumps. This observation is corroborated by slightly lower strut velocities and strokes in the same regions. Because of the simpler instrumentation

involved in measuring these quantities, it is felt that the correlation shown by Figures 22c and 25d is a better measure of the accuracy of the analysis than the correlation shown by either axle or ground loads.

The load having the largest effect on the aircraft weight is the maximum vertical strut load developed when the gear traverses a bump. The vertical strut load is the load at the axle parallel to the axis of the strut. The corresponding vertical ground load which differs from the strut load by the inertia forces of the unsprung mass designs the wheel only. The following comparison shows the accuracy of the bump load calculations.

Run Number	Figure	Measured Maximum Bump Load (lbs)	Calculated Maximum Bump Load (lbs)	Difference (%)
12/11/63-3	17a	10,600	11,900	+ 12.2
12/11/63-5	18a	16,800	18,200	+ 8.4
12/12/63-2	19a	10,100	11,700	+ 16.0
12/12/63-3	20a	17,500	17,500	0
12/12/63-6	21a	14,700	17,400	+ 18.4
1/31/64-4	22a	16,500	19,000	+ 15.0
1/31/64-2	23a	14,900	13,500	- 9.4
1/8/64-2	24a	18,000	20,200	+ 12.2
1/10/64-4	25a	15,700	18,200	+ 16.0
1/16/64-2	26a	20,100	16,900	- 15.9

This comparison draws attention to test 1/16/64-2 since it runs counter to the trend of all other cases. Objective analysis of all evidence indicates that the measured sinking speed for this condition was lower than actual. Ignoring this case, the accuracy of the vertical load calculation is -9 to +18.4 percent with an average error of +10.4 percent. Thus, there is evidence that the calculations tend to overpredict the effect of the bump. This conclusion is logical since there is a tendency in the calculations not to include all structural deflections which actually exist and which tend to alleviate the loads.

In regard to the axle drag load, which has a much lower effect on the calculated weights, a less clear-cut comparison can be made. In the bump cases the drag load which coincides with the maximum vertical load will be most significant; however, the time relationship of drag and vertical load is altered by the initial spin-up phenomena, and this

in turn is affected by the coefficient of friction at the time of spin-up. In the Phase I and II investigation, the sliding coefficient of friction was varied arbitrarily, and maximum drag loads were combined with maximum vertical loads, regardless of time relationship, to compute the weight increments. Hence, critical and, probably, conservative drag loads were used.

Examination of the drag load data in Figures 17 through 34 shows that a consistent error exists in the calculated frequency of the drag load. Since magnitudes are generally correct in the first cycle or two, it is presumed that improved correlation with respect to magnitude on subsequent cycles would be obtained if the phasing could be improved. Discussion of attempts to improve this aspect of the analysis is presented on page 14.

One of the most obvious discrepancies between test and analysis is the 30- to 40-cps fluctuation of the vertical load occurring in the early part of the load history which is not predicted by analysis. It is significant that this oscillation did not appear in the original laboratory drop test data with which the analysis was correlated. It is also significant that corresponding fluctuations in the measured oil pressure curves (Figures 22c, 25d and 28c) are almost nonexistent. A check of the test data shows that these oscillations are caused by the effect of the side gauge on the vertical load. The relative size of K_3 and K_1 in Table I is indicative of the magnitude of this effect. Based on the evidence of the pressure measurements and the previous laboratory drop tests, one is forced to conclude that this calibration overemphasizes the effect of the side load on the vertical and that the actual vertical load fluctuations are much lower than shown. On the other hand, it is believed that the analysis underestimates this effect and could be improved in this area.

Sand Tests

The comparison of test and calculated data for drops on sand (Figures 27 and 28) shows a somewhat lesser degree of correlation than is evident in the bump cases. Analysis consistently underestimates the magnitude of both vertical and drag loads. There are two known reasons for this result. First, since the wing lift applied in the tests was 0.85W, additional energy is introduced into the test system as the gear sinks through the sand. Improved correlation could probably be obtained if this additional energy were included in the analysis either as an effective increase in sinking speed or in mass. Secondly, the sand rut profile (Figure 41) shows that the gear is effectively landing on a slope. This has been shown (Reference 1) to be equivalent to landing at a higher sinking speed. It is believed that the proper approach to the problem of load computation for landings on soft soil requires the

development of a mathematical representation of the soil (a soil model) and its incorporation as part of the dynamic system into the computing program.

The measured coefficients of friction developed in the sand tests are of interest. These are shown in Figure 42, where it can be seen that the sliding coefficient of friction reaches 1.6 and the rolling friction averages 0.15 to 0.2 with a maximum of 0.3.

DATA FROM BUMPS ORIENTED 45° TO THE RUNWAY

The primary purpose of running tests with the bump oriented obliquely to the line of motion was to investigate the side loads developed under such conditions. Data from two drops on this type of contour are presented in Figures 35 and 36. The side loads developed were of approximately the same magnitude as the side loads measured near the time of initial impact. These loads are substantially lower than would be derived by the elementary procedure of multiplying the vertical load by the maximum contour slope in the side direction. This paradox can be attributed not only to inertia effects but also to the fact that the maximum vertical gear load is developed at a point beyond the point of maximum slope of the contour. (See Figure 28 of Reference 1.)

DATA FROM THE HALF-CIRCULAR CYLINDER AND THE HEMISPHERE

Figures 37 through 40 show the results of tests in which drops were made on contours consisting of a 3-inch (radius) half-cylinder and a 3-inch (radius) hemisphere. A unique feature of these results is that more often than not the vertical bump load contained a double peak.

One of the factors which these data were intended to resolve was whether or not the tire spring rate is the same when it is impressed on a surface of large curvature and on objects of small radius of curvature. To that end, additional tests were made in which the strut was blocked against compression by means of a spacer. The results of these tests are summarized as follows:

Test Number	Ground Load Increment 3-Inch (1-cosine) Bump	Test Number	Ground Load Increment 3-Inch Half-Cylinder Bump
1/17/64-2	7000 pounds	1/17/64-4	5500 pounds

It is concluded that the tire spring rate for the tire impressed on the half-cylinder is less than that for the tire impressed on the 3-inch,

1-cosine bump. From the magnitude of the vertical bump load increment induced by the hemisphere (Figures 39 and 40), it appears that the tire spring rate for this contour is even lower than for the half-cylinder.

REVISIONS NECESSARY TO IMPROVE CORRELATION

Investigations were made to improve the correlation of test and computed data. These were largely directed toward the improvement of the spin-up representation and the drag load phasing. Only one such change involved a revision to the computing program; the others involved changes to the input. The changes are described below:

(a) Spring Constant for the Gear in the Fore and Aft Direction:

The original spring constant for the gear was obtained by calculation. Vibration tests were made with the gear in place in the drop carriage and the spring constant was computed from the resonant frequency data. Figure 43 shows the spring constant as originally used and as subsequently derived.

(b) Tire Load-Deflection Curve:

Data from the drop tests permitted a rough determination of the tire load-deflection characteristics. Figure 44 presents these data and compares them with the assumed curve. Figure 45 compares the original curve with one derived from the average of the test data. Differences are quite substantial and cannot be explained. The comparison points up the need for research into the dynamics of tires.

(c) Polar Moment of Inertia of the Tire and Wheel:

Reference 3 states that the polar moment of a tire may be increased substantially because of the centrifugal forces and resulting tire deflections caused by high speed rotation. A 10-percent increase in the polar moment of inertia was estimated based on the data of Reference 3.

(d) Revision to Computer Program Equation:

The equation for wheel angular acceleration on page 30 uses the term $R_o - C/2$ to define the moment arm of the drag force at the ground about the axle centerline. "R_o" is the original tire radius and "C" is the tire deflection. The factor of 1/2 applied to C is illogical and erroneous; it is evidently a holdover from a previous program in which an average tire deflection was used. In the revised calculations the 1/2 was replaced by 1.0.

Figures 46 through 48 show comparisons of test results, and of calculations in which the foregoing modifications were made. In addition, starting times were shifted slightly so that test and calculated curves were initiated simultaneously. These time shifts are noted and varied from 0.002 second to 0.009 second. The improved correlation of test and calculated drag loads, with respect to spin-up time, magnitude and phasing, is obvious.

As a result of the tire curve change, the lowness of the calculated vertical load, which existed just prior to the bump, has been eliminated. It would appear that the tire curve has been somewhat overcorrected.

EFFECT OF ANALYSIS ACCURACY ON THE CONCLUSIONS REACHED IN THE PHASE I AND II INVESTIGATION

The conclusions reached in the Phase I and II investigation, Reference 1, can be categorized as general conclusions and specific conclusions. The former are concerned with the qualitative nature of loads, weight increments and behavior of the system, and the latter with specific magnitudes which were used to define roughness criteria. It can be said without reservation that the current test program revealed nothing which would suggest altering the general conclusions of Reference 1. It was demonstrated that the computing program gave a good representation of the operating characteristics of the gear and that the load magnitudes were qualitatively correct.

Insofar as the quantitative conclusions are concerned, it has been shown that the vertical loads calculated for the bump cases are high by 10 percent (page 10) and that the procedure used in Phases I and II produced drag loads which were also on the high side. Consequently, the rough terrain capability of the OV-1 has been underestimated by a similar amount. That is to say, the example airplane could traverse higher bumps than those computed, for a given weight increment. This would result in the establishment of larger bumps (greater ground roughness) in the design criteria.

The magnitude of the load errors is not, however, large enough to make significant difference in the design criteria when consideration is given to other less well defined areas of the problem. Two items will be used to illustrate this point. First, a design criterion has been established in this project by studying one specific airplane. Several airplanes should be investigated to arrive at a more representative set of data. Secondly, with the example airplane the design roughness for equal performance of the STOL and VTOL airplanes was dependent upon the slope and softness (resistance to forward motion) of the takeoff area. From the several values of design roughness which emerged from this study, one was chosen as being typical and was rounded off to the nearest inch for use in the design criteria. This choice would not have been influenced by a 10-percent difference in range of answers derived from the study. In summary, the accuracy of the load computation method used in the bump cases was sufficient for the purpose for which it was used. As a design tool the method has a degree of conservatism which is desirable and in accordance with structural practices.

The sand tests were directed toward the establishment of criteria for soft soil landings. In this connection the drag loads and, hence, the sliding and rolling ground coefficients of friction are important. The

ground coefficients established in the design criteria of Reference 1 were:

$\mu_{S_{(AVE)}}$ = 0.2 to 0.6 (applicable to spin-up)

$\mu_{R_{(AVE)}}$ = 0.2 to 1.0 (applicable after spin-up)

The sand tests showed:

$\mu_{S_{(MAX)}}$ = 1.60, $\mu_{S_{(AVE)}}$ = 0.7

$\mu_{R_{(MAX)}}$ = 0.3, $\mu_{R_{(AVE)}}$ = 0.2

Thus, on the basis of these tests, the criteria should be revised to increase the sliding coefficient of friction and lower the rolling coefficient of friction. It should be remembered, however, that these tests were performed on only one example of soft soil, and the conclusions may well be modified further by tests on other types of soil.

The lack of conservatism of the computing program in the sand tests (page 11) is of some concern. That unconservatism attributable to increased test energy resulting from a wing lift less than 1.0W can be ignored since wing lift during actual landings is usually close to 1.0W. The unconservatism resulting from the effective shape of the ground should be eliminated by a revision of the computing program. Such a revision should include a mathematical representation of the soil and will be quite complex. It is not within the scope of this phase of the project to prepare such a revision. Research has been initiated by the Air Force to accomplish this task (Reference 4).

CONCLUSIONS AND RECOMMENDATIONS

1. Based on the discussion of results on page 10, it is concluded that the computing program predicts with satisfactory accuracy the important loads used in the Phase I and II investigations.

2. There is evidence that the calculations predict a load at the bump which is on the average 10 percent too high.

3. The following consistent differences between calculated and measured loads were noted:

   (a) In multiple bump cases, the analysis predicted the first bump load more accurately than the second and third bump loads.

   (b) A 30- to 40-cps fluctuation in vertical load, which was not predicted by theory, occurred in tests.

   (c) The frequency of the calculated drag load was approximately 15 percent greater than the measured.

   (d) The calculated spin-up time was approximately 15 percent less than the measured.

   (e) In the sand tests, the calculations predicted vertical and drag loads which were on the average approximately 20 percent less than measured.

4. Substantial improvement in the spin-up time and the magnitude and phasing of the drag load was obtained by making rational improvements in the strut rigidity, the tire polar moment of inertia and the tire load-deflection curve. An error was discovered in one equation in the computing program. The correction contributed to the improved correlation.

5. Sand tests showed that slightly higher average sliding ground coefficients and substantially lower average rolling coefficients of friction should be specified for soft soil landings than were specified in the Phase I and II work.

6. There was evidence that the assumed tire load-deflection curve was substantially different from the one measured in these tests under dynamic conditions. There also was evidence that the tire spring rate was 25 percent lower when the gear traversed a 3-inch half-cylinder than when the gear traversed a 3-inch by 30-inch 1-cosine bump.

7. Based on the conclusions in paragraph 6, it is recommended that theoretical and test work be done which would lead to a method of predicting accurately the dynamic deflection characteristics of tires.

8. It is recommended that methods be developed for incorporating a mathematical representation of the soil in the computer program so that better results can be obtained from calculations of soft soil landings.

REFERENCES

1. Allen, F. C., Rehder, D. M., Mosby, L. B., "A Study of Rough-Terrain-Induced Structural Landing Loads, Phases I and II," Douglas Aircraft Company, Long Beach, California, TRECOM Technical Report 63-68, December 1963.

2. Jirgal, R. M., "Rough Terrain Landing Loads Tests Instrumentation," Douglas Report Number LB-31412, August 1963.

3. Smiley, R. F. and Horne, W.B., "Mechanical Properties of Pneumatic Tires with Special Reference to Modern Aircraft Tires," NACA TN 4110, January 1958.

4. Anon, "Aircraft Dynamic Loads from Sub-Standard Landing Sites," U.S. Air Force, Research and Technology Division, Air Force Systems Command, RFP No. 18070-KNA, June 1964.

DISTRIBUTION

US Army Materiel Command	1
US Army Mobility Command	3
US Army Aviation Materiel Command	6
Chief of R&D, D/A	1
US Army Aviation Materiel Laboratories	54
USAAML Liaison Officer, US Army R&D Group (Europe)	2
US Army Engineer R&D Laboratories	2
US Army Limited War Laboratory	1
Army Research Office-Durham	1
US Army Test and Evaluation Command	1
US Army Combat Developments Command, Fort Belvoir	1
US Army Combat Developments Command Aviation Agency	2
US Army Combat Developments Command Experimentation Center	1
US Army War College	1
US Army Command and General Staff College	1
US Army Transportation School	1
US Army Aviation School	1
US Army Transportation Center and Fort Eustis	1
US Army Aviation Test Board	1
US Army Aviation Test Activity	2
US Army Transportation Engineering Agency	1
US Army General Equipment Test Activity	1
Air Force Systems Command, Wright-Patterson AFB	1
Air Force Flight Test Center, Edwards AFB	1
Air Proving Ground Center, Eglin AFB	1
Air University Library, Maxwell AFB	1
Air Force Avionics Laboratory, Wright-Patterson AFB	1
Bureau of Naval Weapons	3
US Naval Postgraduate School	1
US Naval Air Station, Patuxent River	1
Commandant of the Marine Corps	1
Marine Corps Liaison Officer, US Army Transportation School	1
Ames Research Center, NASA	1
NASA-LRC, Langley Station	2
NASA Representative, Scientific and Technical Information Facility	2
Research Analysis Corporation	1
National Aviation Facilities Experimental Center	1
US Army Standardization Group, Canada	1
Canadian Liaison Officer, US Army Transportation School	1
British Army Staff, British Embassy, Washington	1
US Army Standardization Group, U. K.	2
Defense Documentation Center	20
US Government Printing Office	1

APPENDIX I

EQUATIONS OF MOTION
DYNAMIC LANDING LOADS ANALYSIS

NOTATION

Theory	Fortran	Definition	Units
$a, \dot{a}, \ddot{a}$	A	Motion at axle parallel with strut of unsprung mass of rolling assembly, positive down	in., sec.
$\bar{a}$		Distance from lower piston bearing to axle parallel to strut with strut fully extended	in.
A_0		Gross orifice area without reduction for pin	$in.^2$
A_1		Internal area of oleo piston	$in.^2$
A_2		Piston area based on i.d. of lower bearing	$in.^2$
A_p	AP	Metering pin area, function of strut stroke	$in.^2$
a_i		Slopes of line equation for pin diameter	-
$\left[A_{ij}\right]$		Aerodynamic damping coefficients	1/sec.
$\alpha, \dot{\alpha}, \ddot{\alpha}$	Alpha	Angular motion of rolling assembly	Rad., Sec.
b_i		Intercepts of line equations for pin diameter	in.
$\bar{b}$		Distance from upper to lower piston bearing parallel to strut, strut fully extended	in.
$\left[B_{ij}\right]$		Coefficients of displacements in airplane equation of motion	$1/sec.^2$

NOTATION (Cont)

Theory	Fortran	Definition	Units
C	C	Tire deflection	in.
$\bar{C}$		Damping coefficient perpendicular to strut	lb.-sec./in.
C_D		Coefficient of discharge	-
C_C		Discharge coefficient for compression	-
C_E		Discharge coefficient for extension	-
C_N		Maximum allowable tire deflection	in.
$\lvert C_i \rvert$		Coefficient of force from gear	$1/lb.sec.^2$
$\Delta, \dot{\Delta}, \ddot{\Delta}$	D	Motion at axle perpendicular to strut of unsprung mass of rolling assembly, positive aft	in., sec.
$\bar{\Delta}, \dot{\bar{\Delta}}, \ddot{\bar{\Delta}}$	BD	Motion at axle in relative coordinates	in., sec.
δ		Distance from axle to gear attach point with strut fully extended	in.
D_o	DO	Coefficient of oil damping force in oleo	$lb/sec^2/ft^2$
$\lvert D_i \rvert$		Coefficient of moment from gear	$1/ft.lb.sec.^2$
$\bar{e}$		Distance from axle to strut $\mathcal{C}_L$ normal to strut, positive for axle forward	in.
$\lvert E_i \rvert$		Vector column of constants	$1/sec.^2$
		Angle of strut with vertical, positive for strut forward of gear attach point	
F_A	FA	Load on axle parallel to strut, positive down	lb.

NOTATION (Cont)

Theory	Fortran	Definition	Units
$F_{\perp}$	FP	Load on axle $\perp$ to strut, positive aft	lb.
F_H	FH	Load on airplane from gear, $\perp$ to reference plane, positive down	lb.
F_1	F1	Normal force on upper piston bearing, positive aft	lb.
F_2	F2	Normal force on lower piston bearing, positive aft	lb.
g		Gravitational constant	in./sec.^{2}
$\lvert G_i \rvert$		Coefficient of moment from gear	
$\lvert H_i \rvert$		Coefficient of force from gear	
I_R		Mass moment of inertia of rolling assembly	lb.in.sec.^{2}
K_1		Strut influence coefficient, deflection forward due to force acting down parallel to strut	in./lb.
K_{32}, K_{33}		$K_{32} + SK_{33}$ is deflection aft due to force acting aft perpendicular to strut	lb./in., lb./in.^{2}
k_1, k_2		Coefficients of gear force for horizontal accelerations	-
λ		Instantaneous skidding velocity	ft./sec.
λ/V_L	SR	Slip ratio	-
l_i		Intercepts in lines for tire load	lb.
m_i		Slopes in lines for tire load versus deflection	lb./in.
n		Polytropic exponent for strut air load	-
o		Subscript to denote initial conditions	-

NOTATION (Cont)

Theory	Fortran	Definition	Units
P_A	PA	Strut air load	lb.
P_D	PD	Drag load in horizontal plane	lb.
P_E	PE	Airload in oleo with strut extended	lb.
P_F	PF	Bearing friction force on strut	lb.
P_O	PO	Strut oil load	lb.
$P_\perp$	PP	Force at axle (relative co-ordinates) perpendicular to strut positive forward	lb.
P_T	PT	Tire load	lb.
P_V	PV	Vertical ground reaction load	lb.
$\lvert P \rvert$		Coefficient of generalized displacement	ft. or in.
$Q, \dot{Q}, \ddot{Q}$	A	Airplane motion, generalized coordinates	-, 1/sec., $1/sec.^2$
ρ_o		Mass density of hydraulic fluid	$lb.sec.^2/in.^4$
R_o		Radius of undeflected tire	in.
R	R	Instantaneous rolling radius of tire	in.
$\lvert R \rvert$		Coefficients of generalized acceleration	-
$S, \dot{S}, \ddot{S}$	S	Strut motion measured from full extension	in., sec.
S_c		Maximum strut stroke	in.
S_i		Values of S associated with pin constants	in.
$\lvert S \rvert$		Coefficients of Q in equation for airplane loads	-

NOTATION (Cont)

Theory	Fortran	Definition	Units
t		Time	sec.
Δt		Interval of numerical integration	sec.
t_F		End of integration	sec.
$\lvert T_{Hi} \rvert$		Generalized airplane coefficients of force at gear attaching point	in./lb. sec^2
$\lvert T_{\alpha_i} \rvert$		Generalized coefficients of moments at gear attaching point	1 lb./$sec.^2$
μ		Coefficient of friction identified (numerically) by its subscript	-
μ_1		Bearing coefficients friction befcre strut moves - static friction	-
μ_2		Bearing coefficients after strut moves	-
μ_s	GRMU	Ground coefficient sliding friction	-
μ_R	GRMU	Ground coefficient rolling friction	-
$\lvert u \rvert$		Arbitrary constants in equation for loads on airplane	-
V_E		Air volume in oleo strut extended	$in.^3$
V_L		Forward velocity of airplane	in./sec.
$\lvert V \rvert$		Coefficients of generalized velocities	in. or ft.
W_U		Unsprung weight of gear	lb.
W_N		Airplane net weight supported by gear	lb.
X	X	Horizontal coordinate of ground contact point for rough terrain function	in.

NOTATION (Cont)

Theory	Fortran	Definition	Units
X_i		Arguments in table of terrain roughness, $0 = i = 700$	in.
X_A	XA	Axle coordinate, horizontal displacement along terrain roughness	in.
X_1, X_2, X_3, X_4		Coordinates used to define terrain	in.
X_o		Initial (starting value) of X	in.
$Y_B, \dot{Y}_B, \ddot{Y}_B$	YB	Motion at top of strut	in., sec.
Z	Z	Vertical coordinate of ground contact point for rough terrain function	in.
Z_A	ZA	Axle displacement from touchdown, positive down	in.
Z_o		Initial (starting value) of Z	in.
θ		Ground slope	Rad.
TAN θ	TAN	Printed for instantaneous value of ground slope	-
A, B, C, D		Amplitudes of terrain roughness entered in X-table, positive down	in.
M_α	AM	Moment from gear, positive airplane nose up	ft. lb.
p		Multiple of Δt at which printing of program output takes place	-
	VA	Vertical accelerations	
	PA	Pitching acceleration	

NOTATION (Cont)

Theory	Fortran	Definition	Units
	SH	Shear	
	BM	Bending moment	
	TQ	Torque	
	AA	Airplane angle of attack	
	AV	Airplane pitching velocity	
	APA	Airplane pitching acceleration	
	VP	Airplane vertical position	
	VV	Airplane vertical velocity	
	AVA	Airplane vertical acceleration	
	HA	Airplane horizontal acceleration	

EQUATIONS OF MOTION

GEAR EQUATIONS

$$\ddot{\Delta} = \left| -P_V \sin\phi + P_D \cos\phi - P + W_U \sin\phi \right| \div \frac{W_U}{g}$$

$$\ddot{a} = \left| -P_V \cos\phi - P_D \sin\phi + F_A + W_U \cos\phi \right| \div \frac{W_U}{g}$$

$$= \left[T_{H_i} \right] \left| \ddot{Q}_i \right| \cos\phi \quad \text{Before the strut moves}$$

$$\ddot{\alpha} = \mu P_T \left(R_o - \frac{C}{2} \right) \div I_R$$

$$F_\perp = \left| -\bar{\Delta} - K_1 F_A \right| \left[K_{32} + S K_{33} \right]$$

$$P_\perp = -F_\perp + \bar{C} \dot{\bar{\Delta}}$$

$$F_A = P_A + P_O + P_F$$

$$= \frac{W_U}{g} \ddot{a} + P_V \cos\phi + \mu P_V \sin\phi - W_U \cos\phi$$

Before the strut moves

$$F_1 = \frac{P_\perp (\bar{a} - S) - F_A (\bar{e} - \bar{\Delta})}{\bar{b} + S}$$

$$F_2 = F_1 + P_\perp$$

$$P_F = \left| \mu_i F_1 \right| + \left| \mu_i F_2 \right|$$

$\dot{S} \geq 0$, P_F positive

$\dot{S} < 0$, P_F negative

$\mu_i = \mu_1$ before strut moves

$= \mu_2$ after strut moves

$$\ddot{Y}_B = \left[T_{H_i} \right] \left| \ddot{Q}_i \right|$$

$$\ddot{\bar{\Delta}} = \ddot{\Delta} - \ddot{Y}_B \sin\phi + (\delta - S) \left[T_{\alpha_i} \right] \left| \ddot{Q}_i \right|$$

$$\ddot{S} = \left[T_{H_i} \right] \left| \ddot{Q}_i \right| \cos\phi - \ddot{a}$$

AIRPLANE EQUATIONS

$$\left|\ddot{Q}_i\right| = \left[A_{ij}\right]\left|\dot{Q}_i\right| + \left[B_{ij}\right]\left|Q_i\right| + F_{H_1}\left|C_i\right|_1 + F_{H_2}\left|C_i\right|_2 + M_{\alpha_1}\left|D_i\right|_1 + M_{\alpha_2}\left|D_i\right|_2 + \left|E_i\right|$$

$$F_H = -F_A \cos\phi - F_\perp \sin\phi$$

$$M_\alpha = (\delta - S) F_\perp$$

$$\left[A_{ij}\right] = -\left[T^*MT + T^*A_1T\right]^{-1}\left[T^*A_2T\right]$$

$$\left[B_{ij}\right] = -\left[T^*MT + T^*A_1T\right]^{-1}\left[T^*KT + T^*CT + T^*A_3T\right]$$

$$\left|C_i\right| = \left[T^*MT + T^*A_1T\right]^{-1}\left|T^*_{H_i}\right|$$

$$\left|D_i\right| = \left[T^*MT + T^*A_1T\right]^{-1}\left|T_{\alpha_i}\right|$$

$$\left|E_i\right| = -\left[T^*MT + T^*A_1T\right]^{-1}\left\{W_{U_1}\left|T^*H_1\right| + W_{U_2}\left|T^*_{H_2}\right| - \delta_1 W_{U_1}\sin\phi_1\left|T^*_{\alpha_1}\right| - \delta_2 W_{U_2}\sin\phi_2\left|T^*_{\alpha_2}\right| - \left[T^*A_2T\right]\left|\dot{Q}_i\right|_{t=o}\right\} \text{ when } \left|\ddot{Q}_i\right|_{t=o} = 0$$

INTEGRATION EQUATIONS

Prediction

$$\bar{X}_{N+1} = X_N + \Delta t\dot{X}_N + .5\,\Delta t^2\ddot{X}_N$$

$$\bar{\dot{X}}_{N+1} = \dot{X}_N + 1.5\,\Delta t\ddot{X}_N - .5\,\Delta t\ddot{X}_{N-1}$$

Correction

$$X_{N+1} = X_N + \Delta t\dot{X}_N + .5\,\Delta t^2\ddot{X}_{N+1}$$

$$\dot{X}_{N+1} = \dot{X}_N + .5\,\Delta t\ddot{X}_{N+1} + .5\,\Delta t\ddot{X}_N$$

where

$X = a, \Delta, \alpha, Q$

$$P_O = D_o \dot{S} \left|\dot{S}\right| \qquad D_o = \frac{\rho_o (A_1 - A_p)^3}{2 \left[C_D (A_O - A_p)\right]^2}$$

$$A_p = \frac{\pi}{4}(a_i S + b_i)^2$$

$$C = R_o - R$$

$$P_T = \ell_i + m_i C$$

$$\lambda / V_L = 1 - \frac{\left(R_o - \frac{C}{2}\right)\dot{\alpha} + \dot{\Delta}\cos\phi}{V_L}$$

$\mu = \mu_S$ Before spin-up

$= \mu_R$ After spin-up

$$P_V = P_T \cos\theta + \mu P_T \sin\theta$$

$$P_D = - P_T \sin\theta + \mu P_T \cos\theta$$

Criterion for strut motion $F_A \geq P_E + P_F$

$$X_A = X_o + V_L t - \Delta\cos\phi + a \sin\phi$$

$$Z_A = Z_o + \Delta \sin\phi + a \cos\phi$$

$$X = X_A - R \sin\theta$$

$$Z = A \left[1 - \cos 2\pi \frac{X - X_1}{X_2 - X_1}\right] + C$$

$$\text{TAN}\,\theta = \frac{2\pi A}{X_2 - X_1} \sin 2\pi \frac{X - X_1}{X_2 - X_1} + C$$

$$R = \left[(X-X_A)^2 + (Z-Z_A)^2\right]^{1/2}$$

$$\sin\theta = \frac{TAN\ \theta}{(1 + TAN^2\theta)^{1/2}}$$

$$\cos\theta = \frac{1}{(1 + TAN^2\theta)^{1/2}}$$

EQUATIONS FOR LOADS

Accelerations $= \left|R_{ij}\right|\left|\ddot{Q}_i\right|$

Shear, Bending Moment, Torque $= \left|S_{ij}\right|\left|\ddot{Q}_i\right| + F_{H_1}\left|H_i\right|_1 + F_{H_2}\left|H_i\right|_2 + M_{\alpha_1}\left|G_i\right|_1 + M_{\alpha_2}\left|G_i\right|_2 + \left|u_i\right|$

Displace nent $= \left|P_{ij}\right|\left|Q_i\right|$

Velocities $= \left|V_{ij}\right|\left|\dot{Q}_i\right|$

Horizontal Acceleration $= (k_1 P_{D_1} + k_2 P_{D_2}) \div W_N$

DATA OUTPUT

The following were printed at time intervals of 0.001 second:

P_A	Strut air load	lb.
P_o	Strut oil load	lb.
P_F	Strut friction force	lb.
F_A	Axle load $\parallel$ strut	lb.
$F_\perp$ = FP	Axle load $\perp$ strut	lb.
$P_\perp$ = PP	Axle load $\perp$ strut in relative coordinates	lb.
F_1	Aft normal force on upper bearing	lb.
F_2	Forward normal force on lower bearing	lb.
P_T	Tire load	lb.
P_V	Vertical ground load	lb.
P_D	Horizontal drag load	lb.
F_H	Gear force on airplane	lb.
M_α = AM	Gear pitching moment on airplane	lb.
A_P	Area of metering pin	$in.^2$
D_O	Oil force damping coefficient	$lb\ sec^2/in.^2$
λ/V_L=SR	Slip ratio	-
X_A, Z_A	Coordinates of axle	in.
X, Z	Coordinates of ground contact point	in.
TAN θ	Slope of terrain at ground contact point	-
C	Tire deflection	in.

DATA OUTPUT (Cont)

R	Rolling radius of ground contact point	in.
$\mu_{R,S}$	GRMU, ground coefficients of friction	
F_T	Normal force on splines due to torque	lb.
F_{1T}	Resultant upper bearing force	lb.
F_{2T}	Resultant lower bearing force	lb.
P_S	Side load at axle	lb.
F_{PS}	Side spring force at axle	lb.
T_β	Torque on upper bearing splines	in. -lb.
M_θ	Wing bending moment	ft. -lb.
$F_{\psi re}$	Side load at ground	lb.
C_S	Side damping force	lb.
ψ	Tire yaw angle	Rad.
$S, \dot{S}, \ddot{S}$	Strut motion in strut direction	in., sec.
$a, \dot{a}, \ddot{a}$	Axle motion in strut direction	in., sec.
$\Delta, \dot{\Delta}, \ddot{\Delta}$	Axle motion $\perp$ strut	in., sec.
$\Delta, \dot{\Delta}, \ddot{\Delta}$	Axle motion $\perp$ strut in relative coordinates	in., sec.
$Y_B, \dot{Y}_B, \ddot{Y}_B$	Motion at top of strut	in., sec.
$\alpha, \dot{\alpha}, \ddot{\alpha}$	Angular motion of rolling assembly	Rad., sec.
$Y_2, \dot{Y}_2, \ddot{Y}_2$	Lateral motion of unsprung mass	in., sec.
$\beta, \dot{\beta}, \ddot{\beta}$	Torsional motion of upsprung mass	in., sec.

DATA OUTPUT (Cont)

The following data are general:

t	Time	sec.
$Q, \dot{Q}, \ddot{Q}$	Airplane response vectors	-

APPENDIX II

TABLES AND FIGURES

TABLE 1

STRAIN GAUGE CALIBRATION CONSTANTS

$$V = K_1 (\delta/\Delta)_V + K_2 (\delta/\Delta)_D + K_3 (\delta/\Delta)_S$$

$$D = K_4 (\delta/\Delta)_V + K_5 (\delta/\Delta)_D + K_6 (\delta/\Delta)_S$$

$$S = K_7 (\delta/\Delta)_V + K_8 (\delta/\Delta)_D + K_9 (\delta/\Delta)_S$$

$K_1 = 16315$
$K_2 = -236$
$K_3 = 8496$
$K_4 = 131$
$K_5 = 3467$
$K_6 = 17$
$K_7 = 122$
$K_8 = -315$
$K_9 = 3340$

TABLE 2

SCHEDULE OF CONDITIONS

Drop Number	Contour Descriptions	Reference Figure	V_H (fps)	V_V (fps)	Touchdown Ahead of Bump Centerline (feet, XC_L)
12/2/63-1	2-inch 1-cosine	5a	130	6.7	37.0
12/10/63-2	2-inch 1-cosine	5a	146	8.0	15.3
12/10/63-3	2-inch 1-cosine	5a	140	8.1	41.2
12/10/63-5	2-inch 1-cosine	5a	136	9.2	38.0
12/11/63-1	2-inch 1-cosine	5a	136	8.0	17.3
12/11/63-2	2-inch 1-cosine	5a	131	9.8	25.9
12/11/63-3*	2-inch 1-cosine	5a	139	7.7	22.1
12/11/63-4	2-inch 1-cosine	5a	140	9.0	25.2
12/11/63-5*	2-inch 1-cosine	5a	142	9.4	15.7
12/11/63-6	2-inch undulations	6a	140	5.8	1.1
12/12/63-2*	2-inch undulations	6a	135	6.6	14.1
12/12/63-3*	2-inch undulations	6a	142	8.1	27.0
12/12/63-5	3-inch 1-cosine	5b	140	6.2	20.5
12/12/63-6*	3-inch 1-cosine	5b	140	8.8	24.9

*Comparison condition.

TABLE 2 (Continued)

Drop Number	Contour Descriptions	Reference Figure	V_H (fps)	V_V (fps)	Touchdown Ahead of Bump Centerline (feet, XC_L)
12/12/63-7	3-inch 1-cosine	5b	143	6.9	32.9
1/30/64-2	3-inch 1-cosine	5b	132	9.4	47.8
1/31/64-4*	3-inch 1-cosine	5b	148	9.8	23.4
1/31/64-5	3-inch 1-cosine	5b	135	9.3	40.6
1/8/64-2*	3-inch undulations	6b	129	9.3	15.5
1/8/64-3	3-inch undulations	6b	131	10.0	33.0
1/31/64-1	3-inch undulations	6b	143	5.9	24.0
1/31/64-2*	3-inch undulations	6b	150	6.0	33.9
1/10/64-4*	3-inch spaced 108 o.c.	10	141	7.5	27.4
1/16/64-2*	3-inch spaced 108 o.c.	10	150	8.0	21.3
1/6/64-5	3-inch half-cylinder	8	132	9.1	34.7
2/3/64-2①	3-inch half-cylinder	8	140	7.6	24.5
2/3/64-3①	3-inch half-cylinder	8	140	7.5	44.8
2/3/64-4	3-inch half-cylinder	8	138	6.6	7.0

*Comparison condition.

①Plotted condition.

TABLE 2 (Continued)

Drop Number	Contour Descriptions	Reference Figure	V_H (fps)	V_V (fps)	Touchdown Ahead of Bump Centerline (feet, XC_L)
2/4/64-4	2-inch 1-cosine at 45°	7a	148	8.2	12.0
2/4/64-5	2-inch 1-cosine at 45°	7a	146	9.5	13.7
12/18/63-2①	3-inch 1-cosine at 45°	7b	138	8.1	29.4
12/18/63-3	3-inch 1-cosine at 45°	7b	137	8.9	38.0
12/18/64-3①	3-inch hemisphere	9	135	7.9	9.2
1/6/64-4①	3-inch hemisphere	9	138	9.5	31.8
12/18/63-5	level terrain	-	134	5.5	-
1/17/64-2	1-cosine gear blocked	5b	133	1.5	275
1/17/64-4	half-cylinder gear blocked	8	128	1.5	275
1/29/64-1	10° yaw	-	130	5.2	-
1/29/64-2	5° yaw	-	148	4.5	-
2/5/64-1*	sand	11	148	6.8	-
2/5/64-2*	sand	11	148	9.0	-

*Comparison condition.

①Plotted condition.

TABLE 3

CALCULATED AND PLOTTED CONDITIONS

Drop Number	Contour Descriptions	Reference Figure	V_H (fps)	V_V (fps)	$X_{\mathbb{C}}$ feet	WL g's	μ_s
12/11/63-3	2-inch 1-cosine	5a	139	7.7	22.1	.886	.639
12/11/63-5	2-inch 1-cosine	5a	142	9.4	15.7	.85	.2
12/12/63-2	2-inch undulations	6a	135	6.1	14.1	.85	.497
12/12/63-3	2-inch undulations	6a	142	8.1	27.0	.85	.264
12/12/63-6	3-inch 1-cosine	5b	140	8.8	25.0	.827	.401
1/31/64-4	3-inch 1-cosine	5b	148	9.8	23.4	.855	.487
1/31/64-2	3-inch undulations	6b	150	6.0	34.0	.92	.64
1/8/64-2	3-inch undulations	6b	129	9.3	15.5	.92	.239
1/10/64-4	3-inch spaced 108 o.c.	10	141	7.5	27.4	.784	.457

TABLE 3 (Continued)

Drop Number	Contour Descriptions	Reference Figure	V_H (fps)	V_V (fps)	$X_{\mathcal{L}}$ feet	WL g's	μ_s
1/16/64-2	3-inch spaced 108 o.c.	10	150	8.0	21.3	.948	.445
2/5/64-1	sand	11	148	6.8	-	.78	.667
2/5/64-2	sand	11	148	9.0	-	.85	.70
12/18/63-2	3-inch 1-cosine at 45°	7b	138	8.1	30.6	-	-
12/18/63-3	3-inch 1-cosine at 45°	7b	137	8.6	39.1	-	-
2/3/64-2	3-inch half-cylinder	8	140	7.7	24.5	-	-
2/3/64-3	3-inch half-cylinder	8	140	7.5	44.8	-	-
12/12/63-4	3-inch hemisphere	9	135	7.9	9.2	-	-
1/6/64-4	3-inch hemisphere	9	138	9.5	31.9	-	-

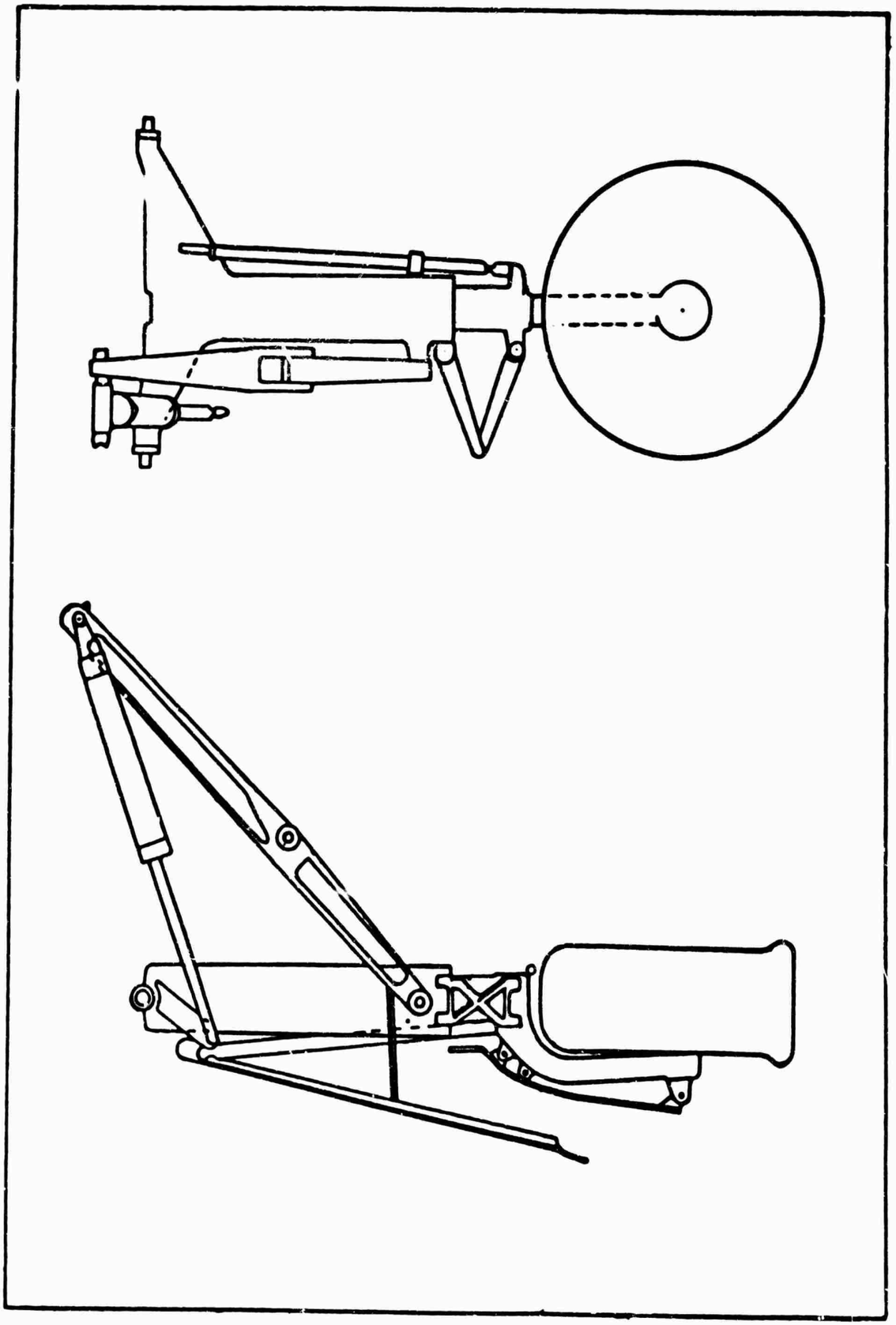

Figure 1. OV-1 Main Gear.

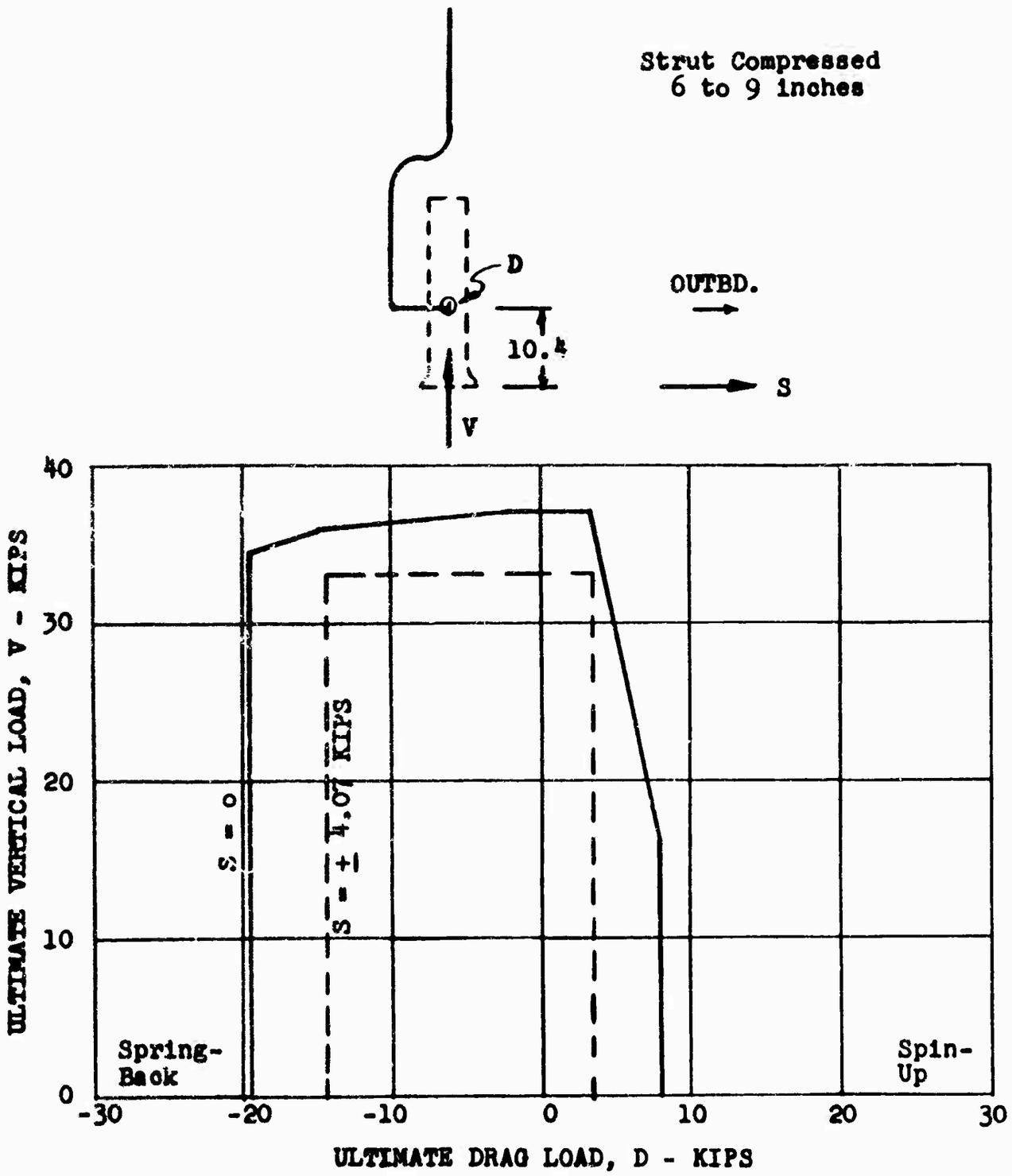

Figure 2. OV-1 Main Gear Strength Envelope.

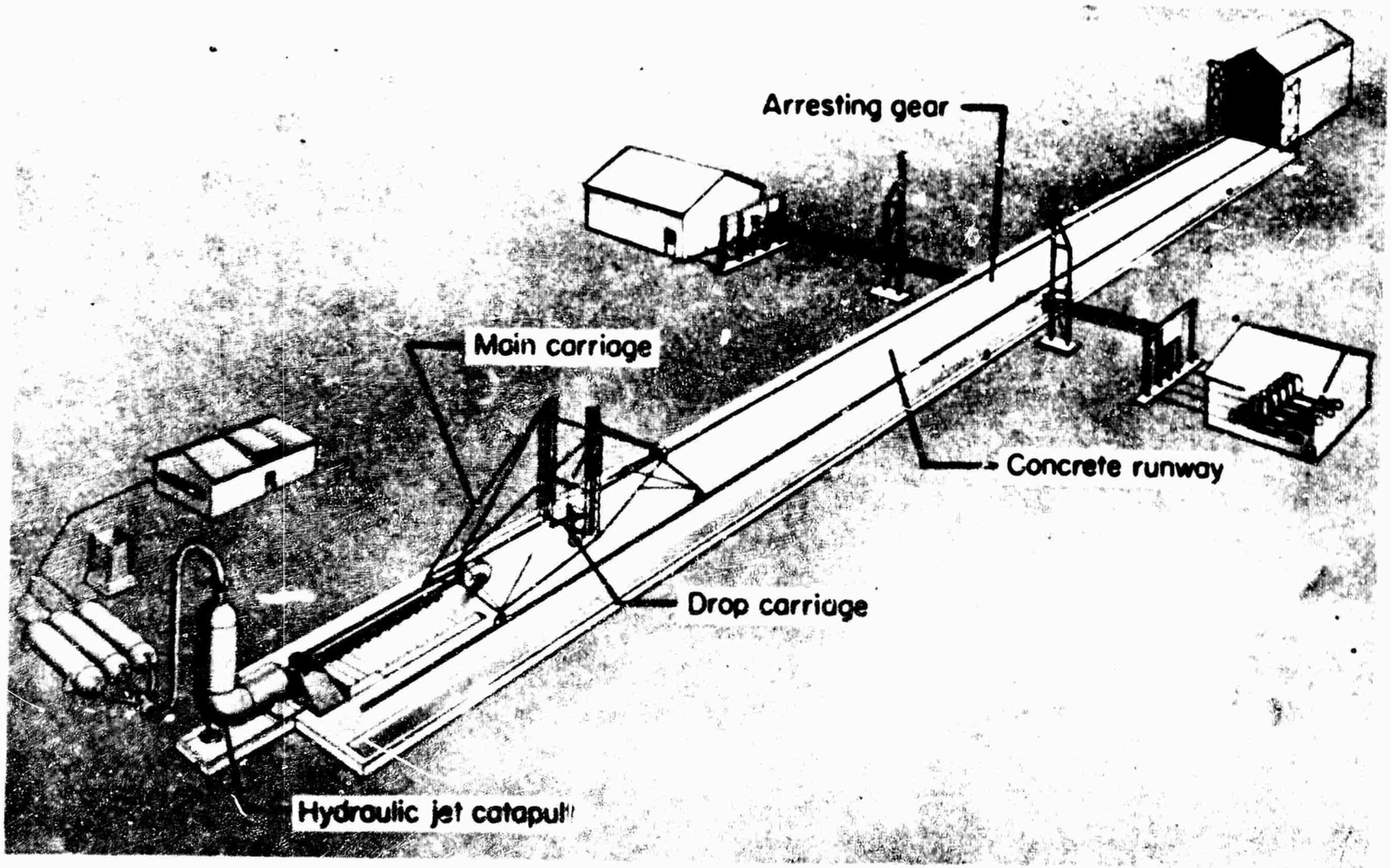

Figure 3. Schematic Drawing of Langley Landing Loads Track.

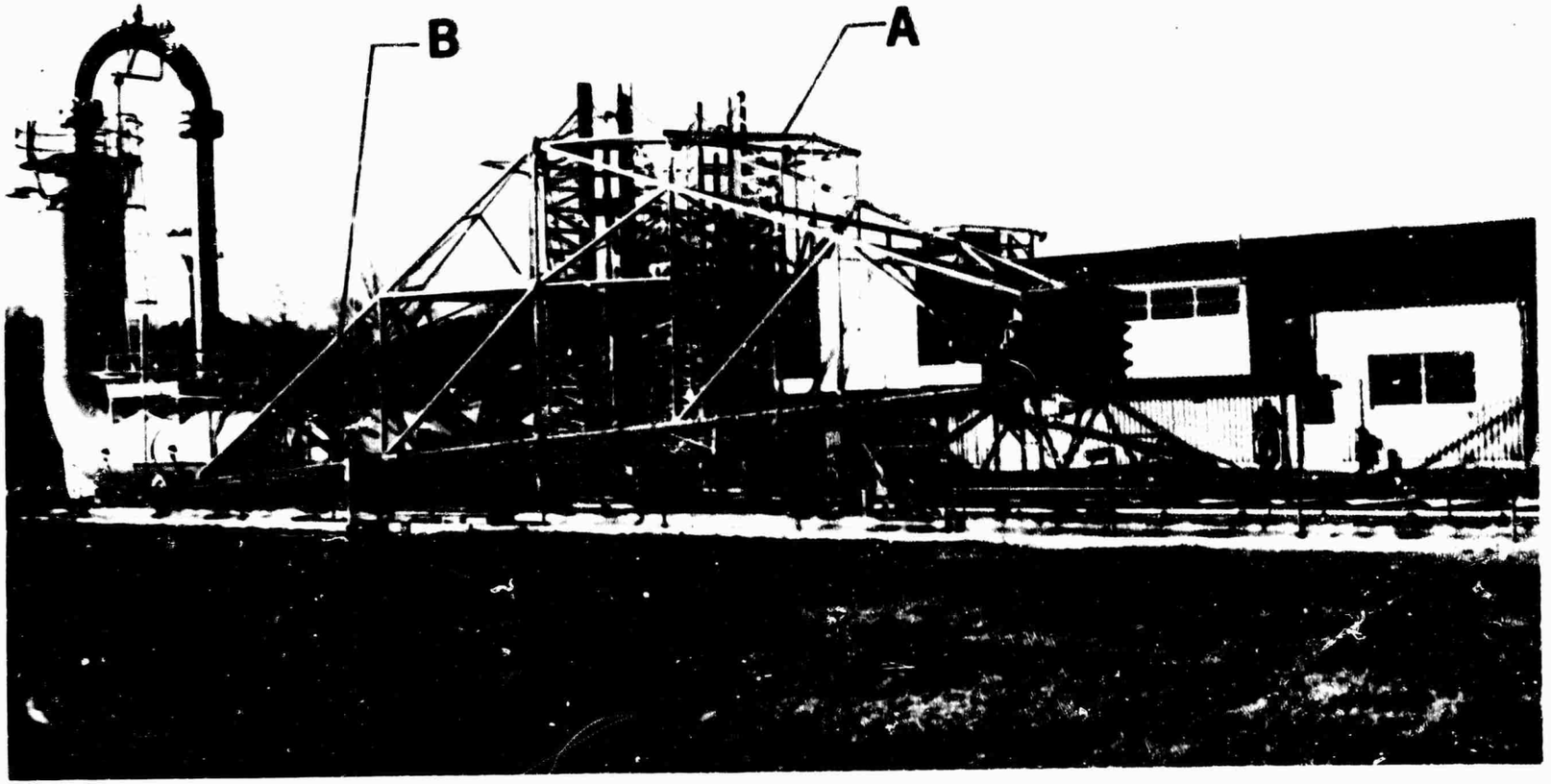

Figure 4. Moving Drop Test Rig

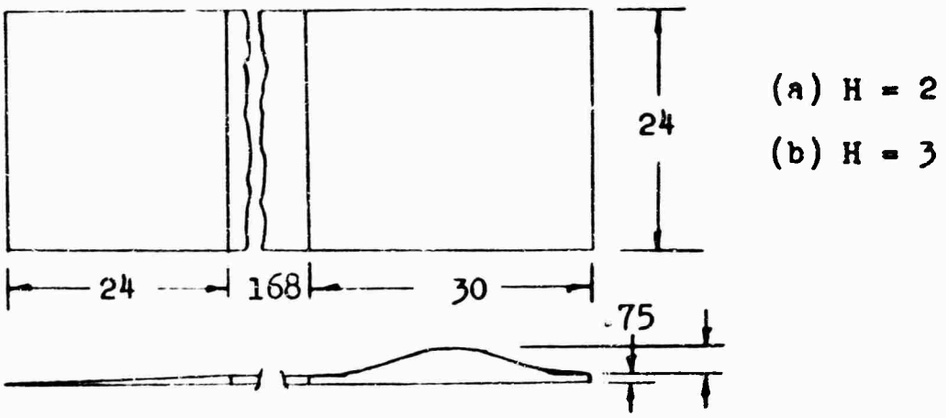

Figure 5. Single 1-Cosine Bump.

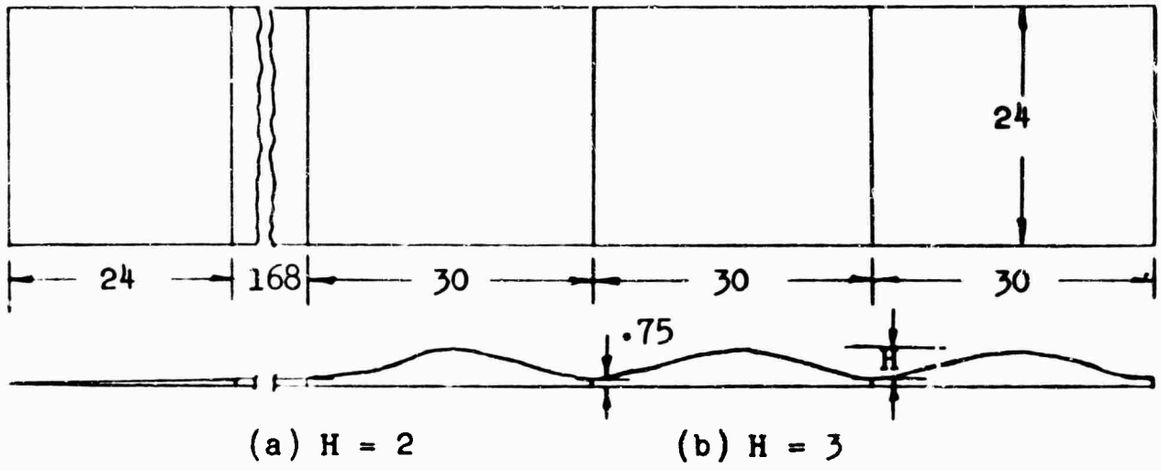

Figure 6. Three Continuous 1-Cosine Bumps.

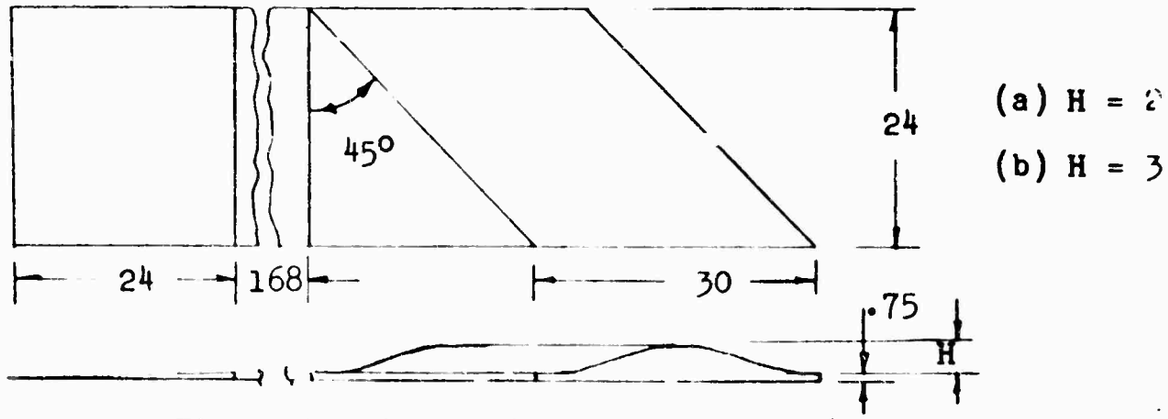

Figure 7. Single 1-Cosine Bump at 45 Degrees.

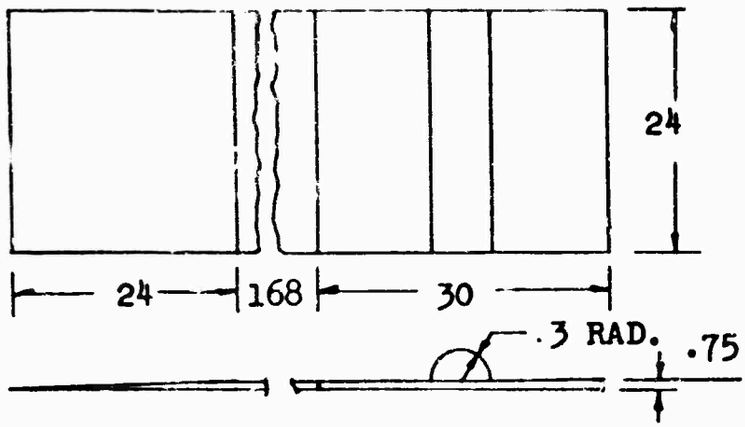

Figure 8. Three-Inch Half Cylinder.

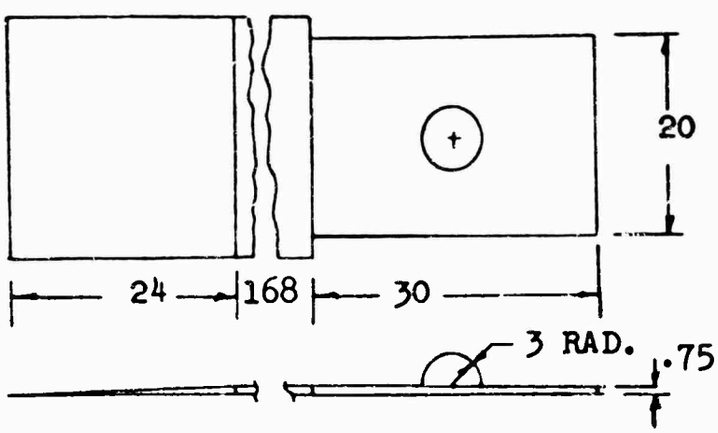

Figure 9. Three-Inch Hemisphere.

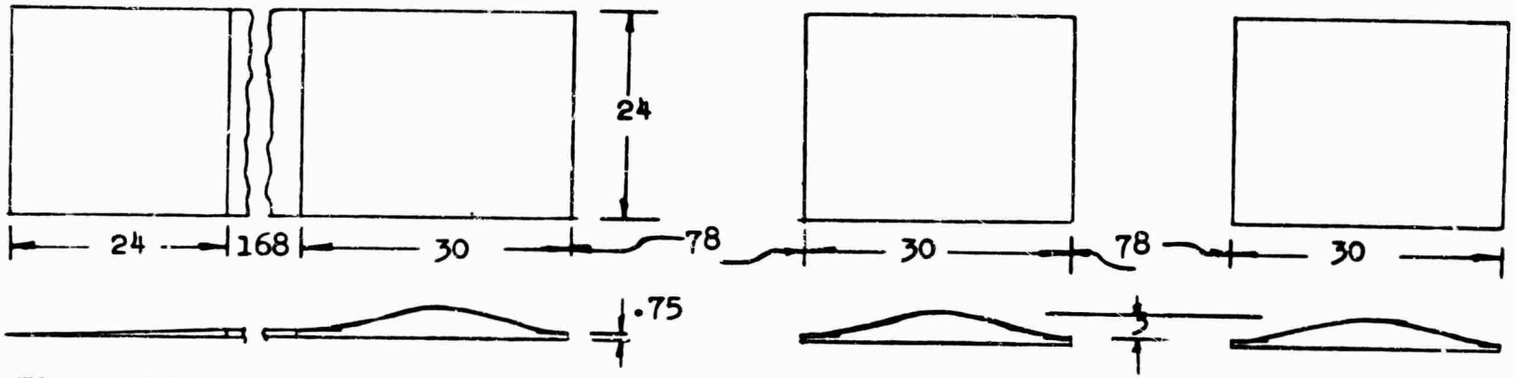

Figure 10. Three 1-Cosine Bumps Spaced 108 Inches between Centerline .

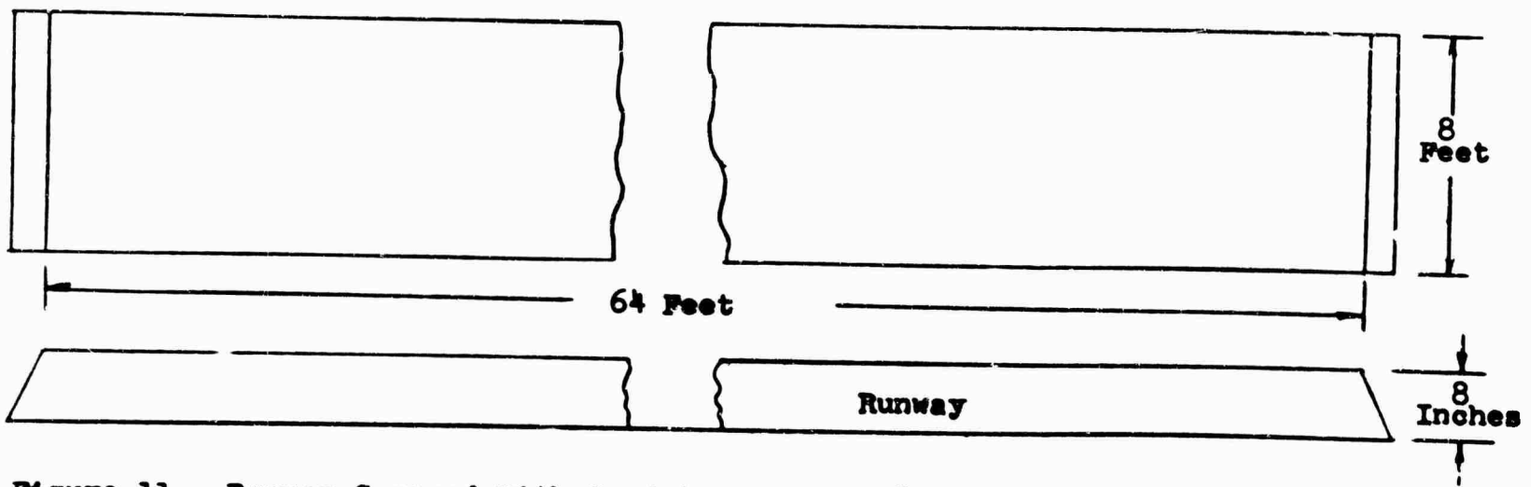

Figure 11. Runway Covered With Sand to Depth of 8 Inches.

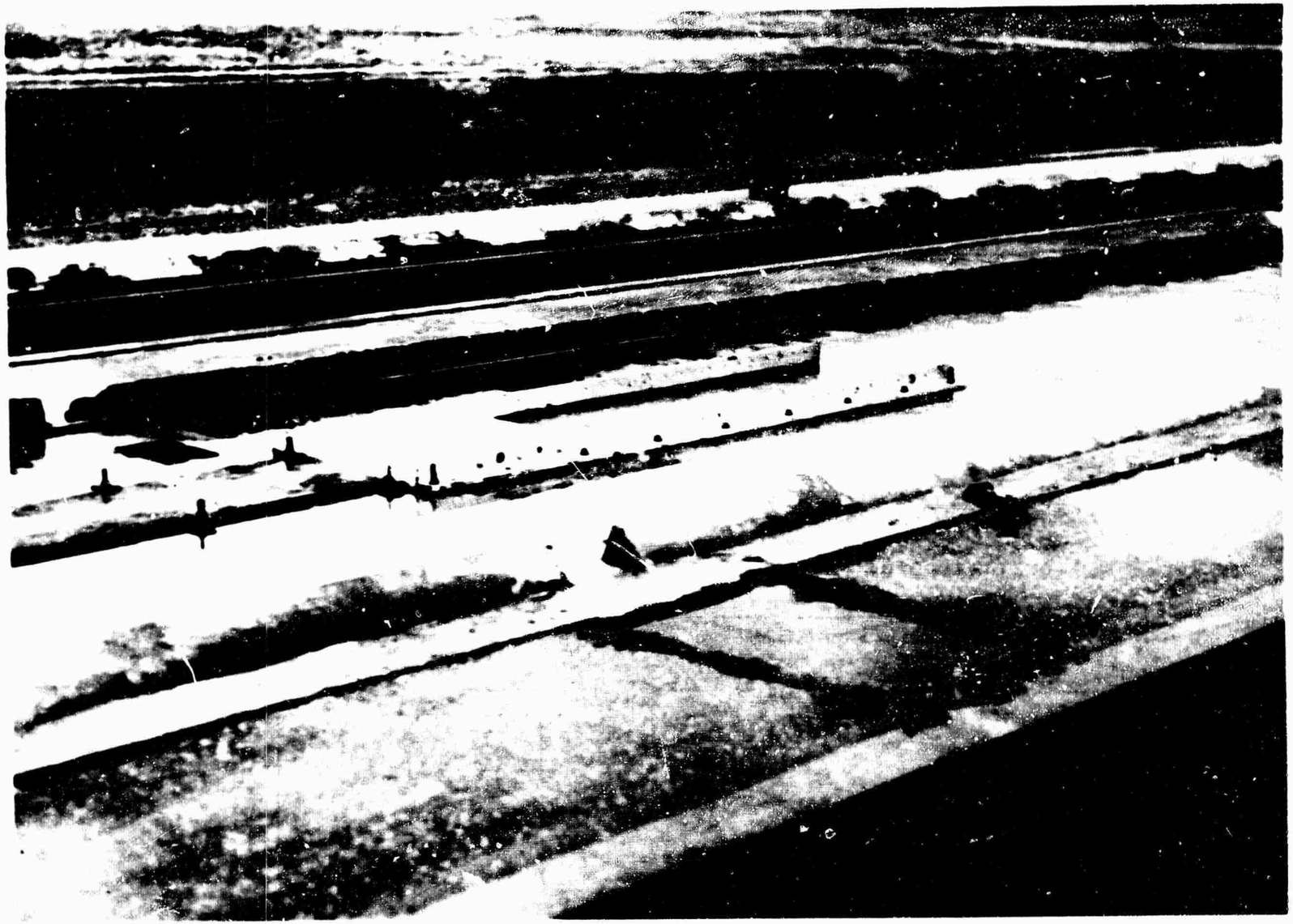

Figure 12. Runway Setup for Drop on 1-Cosine Bump

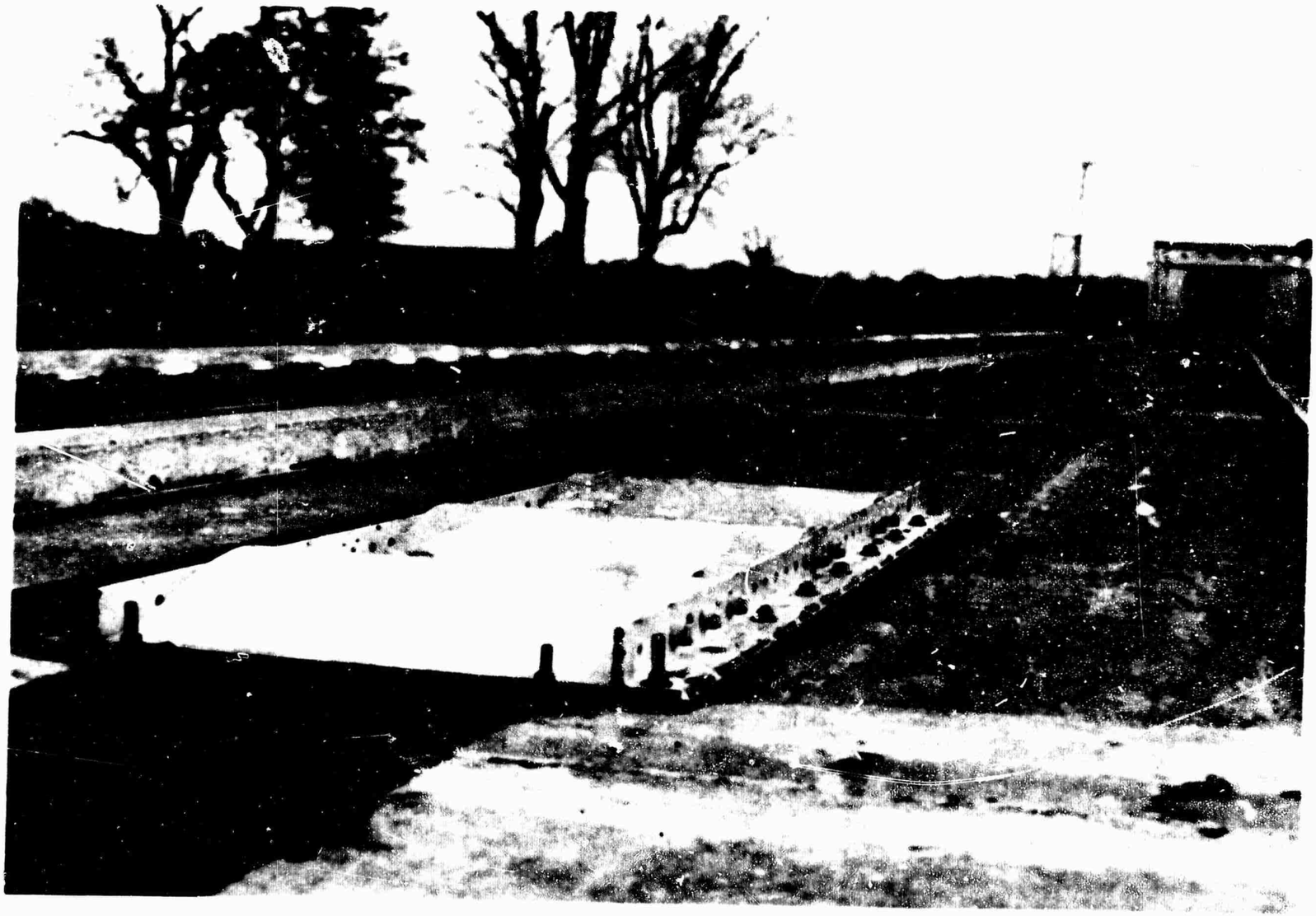

Figure 13. Runway Setup for Drop Tests on Three 1-Cosine Bumps

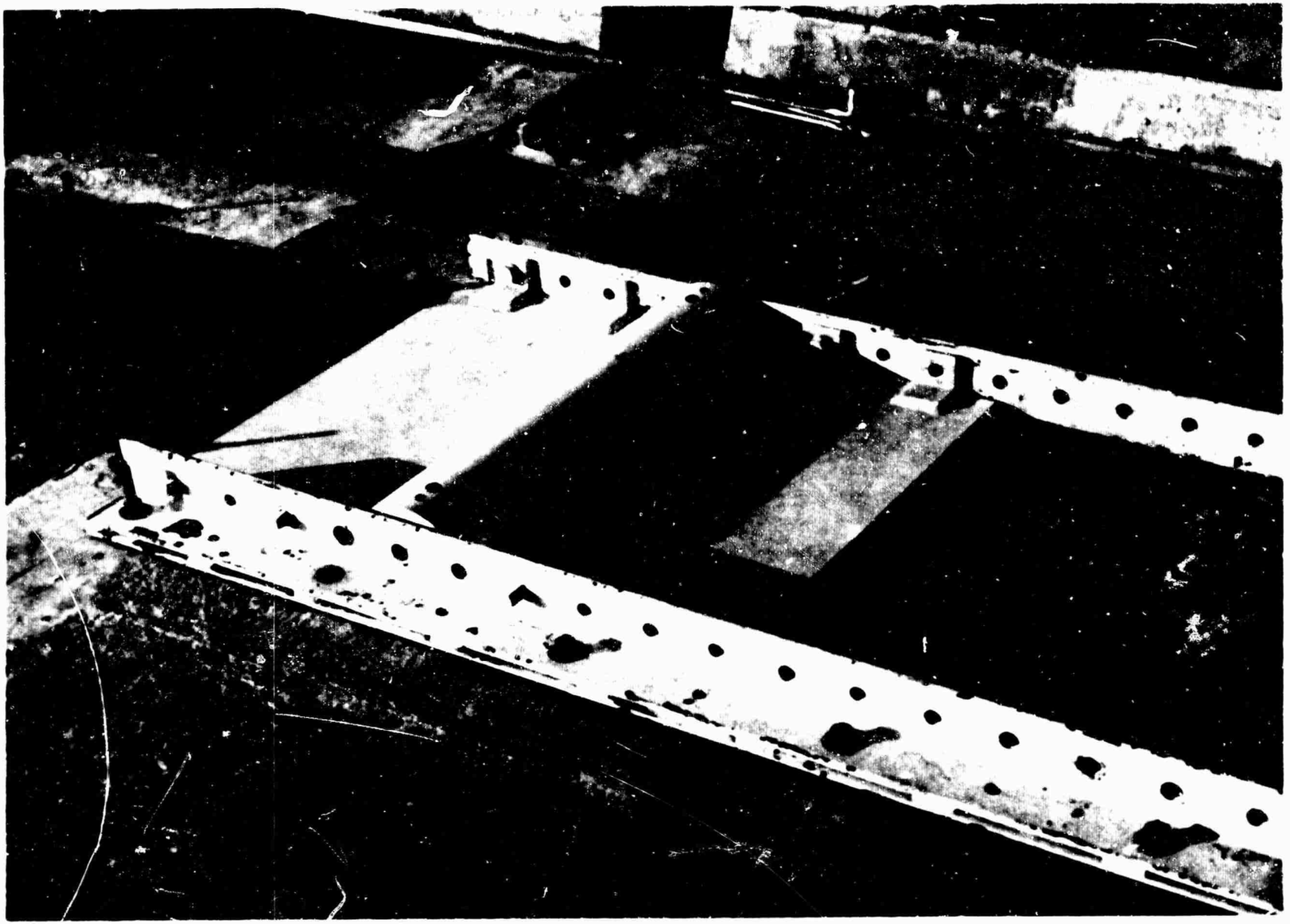

Figure 14. Runway Setup for Drop Tests on 3-Inch Half-Cylinder

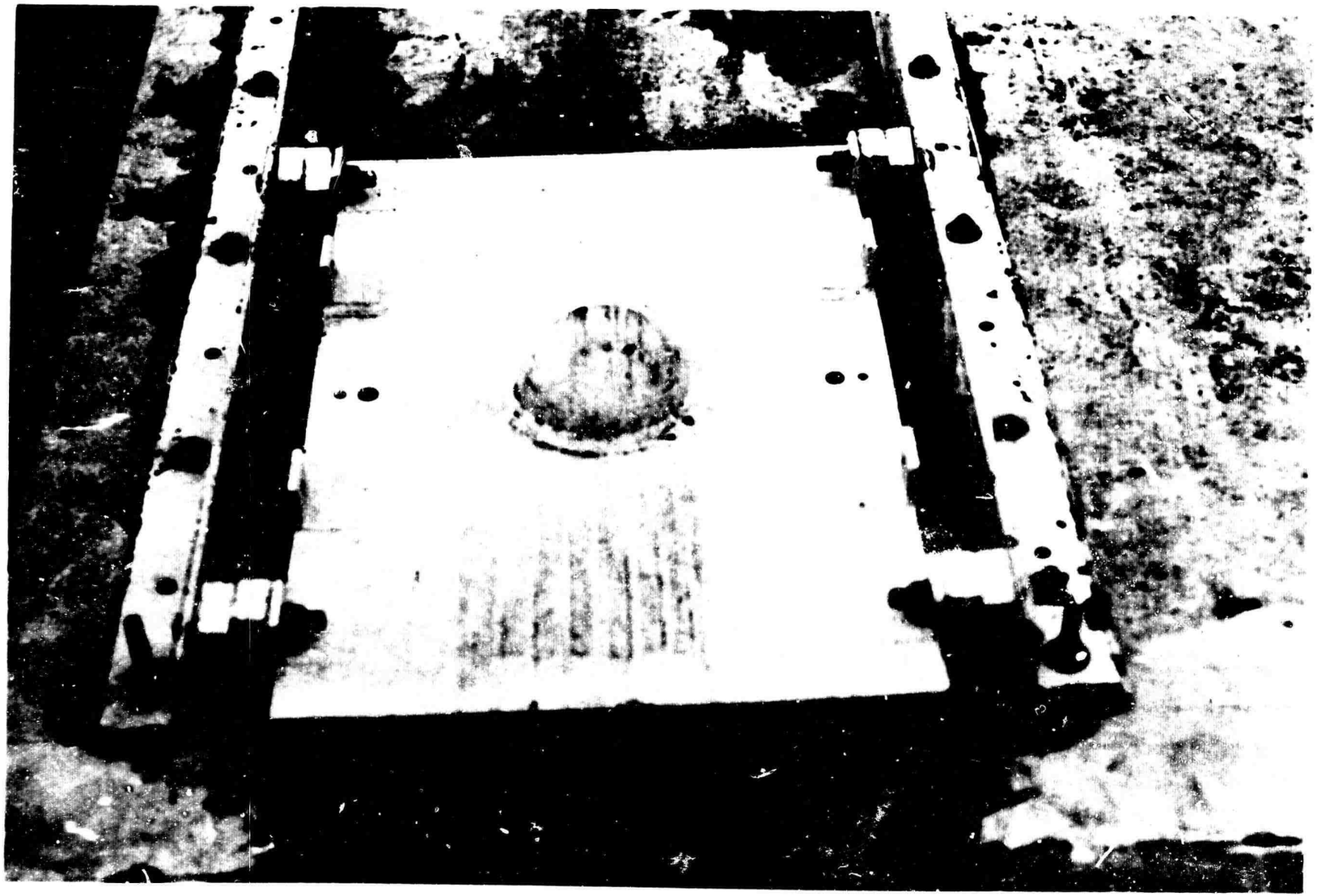

Figure 15. Runway Setup for Drop Tests on 3-inch Hemisphere

Figure 16. Runway Setup for Drop Tests on Sand

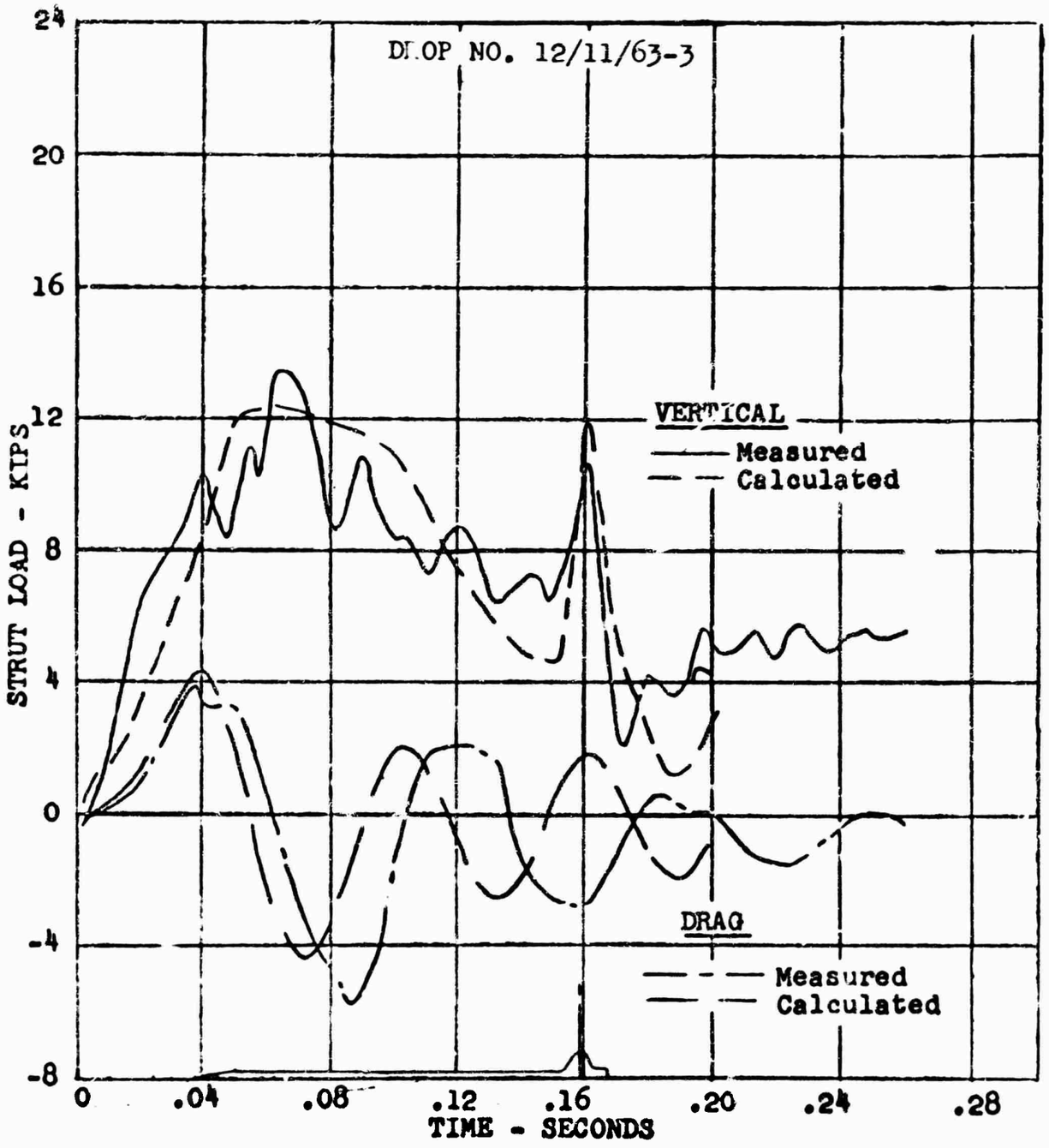

(a) Comparison of Loads at Axle.

Figure 17. Comparison of Measured and Calculated Loads for a 7.7 FPS Drop on a 2-Inch by 30-Inch 1-Cosine Bump.

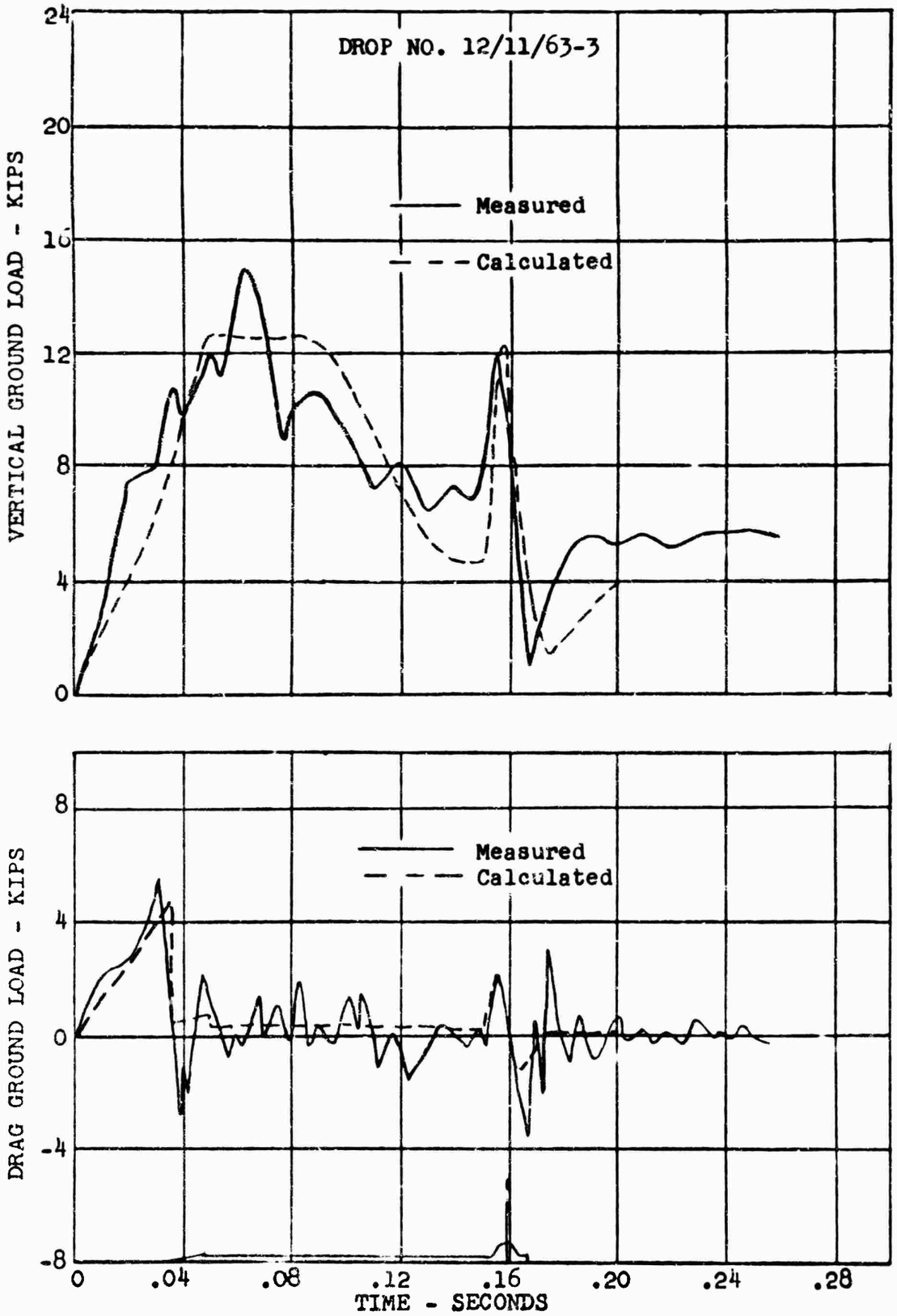

(b) Comparison of Loads at Ground.

Figure 17. Concluded.

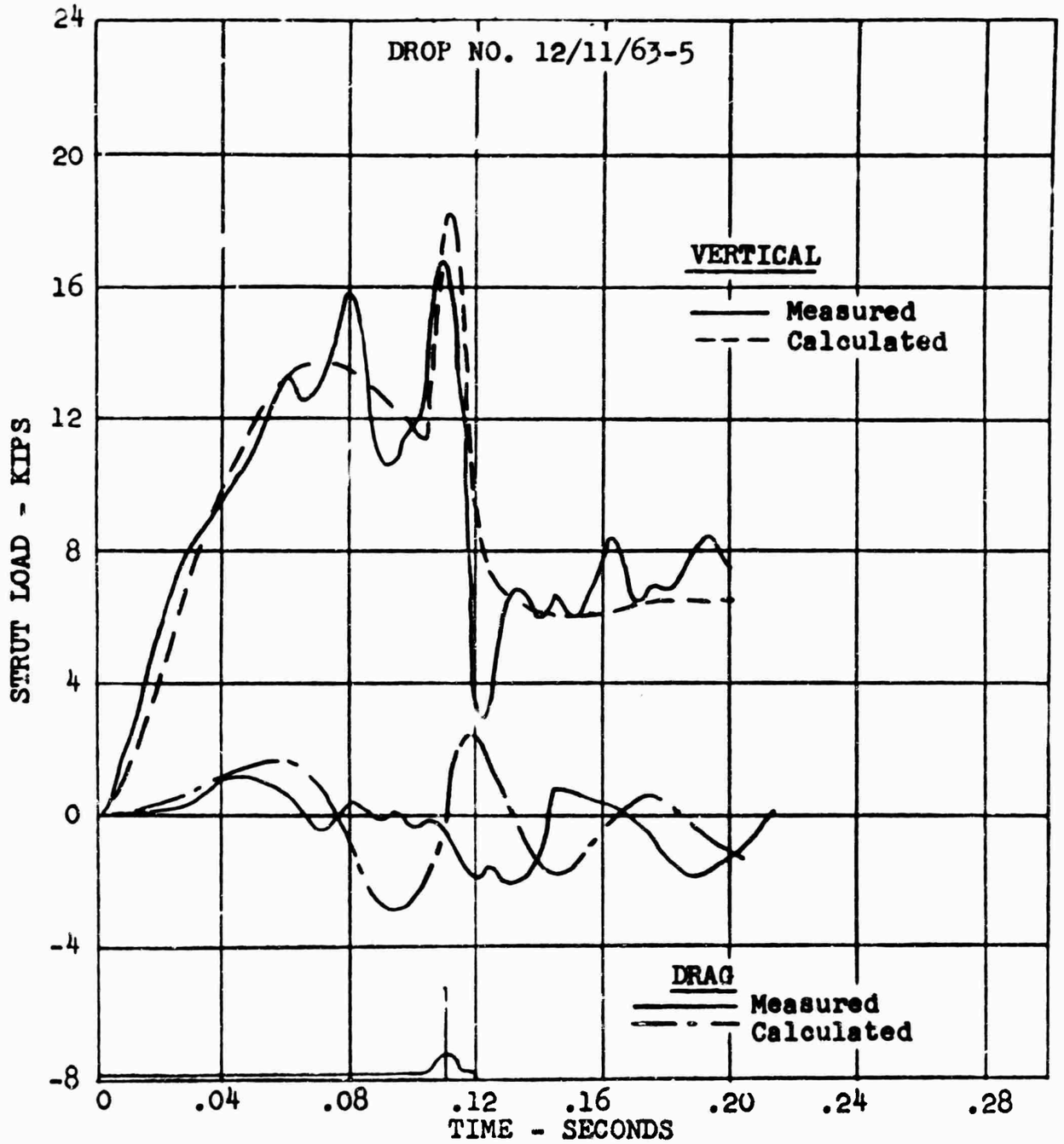

(a) Comparison of Loads at Axle.

Figure 18. Comparison of Measured and Calculated Loads for a 9.4 FPS Drop on a 2-Inch by 30-Inch 1-Cosine Bump.

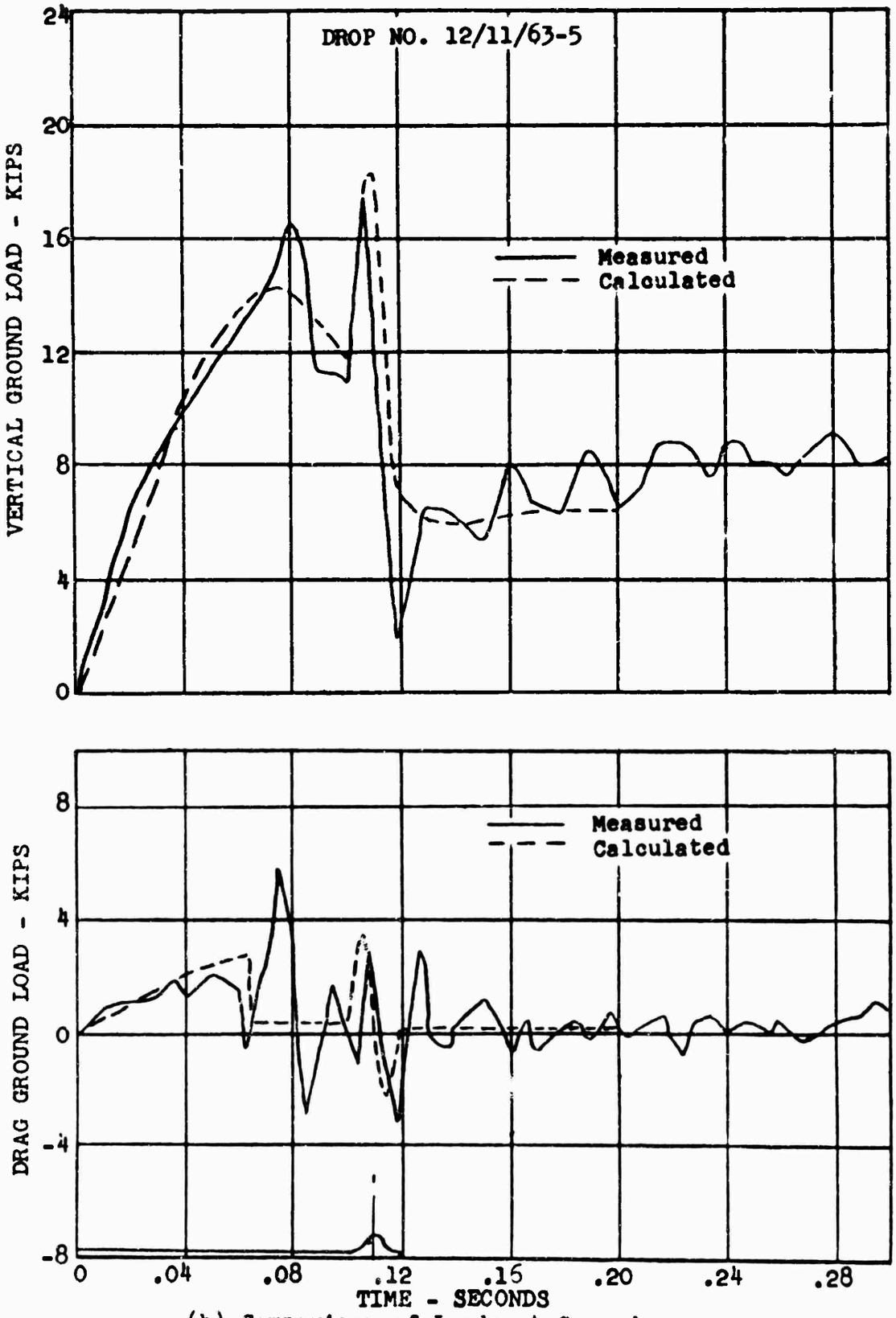

(b) Comparison of Loads at Ground.

Figure 18. Concluded

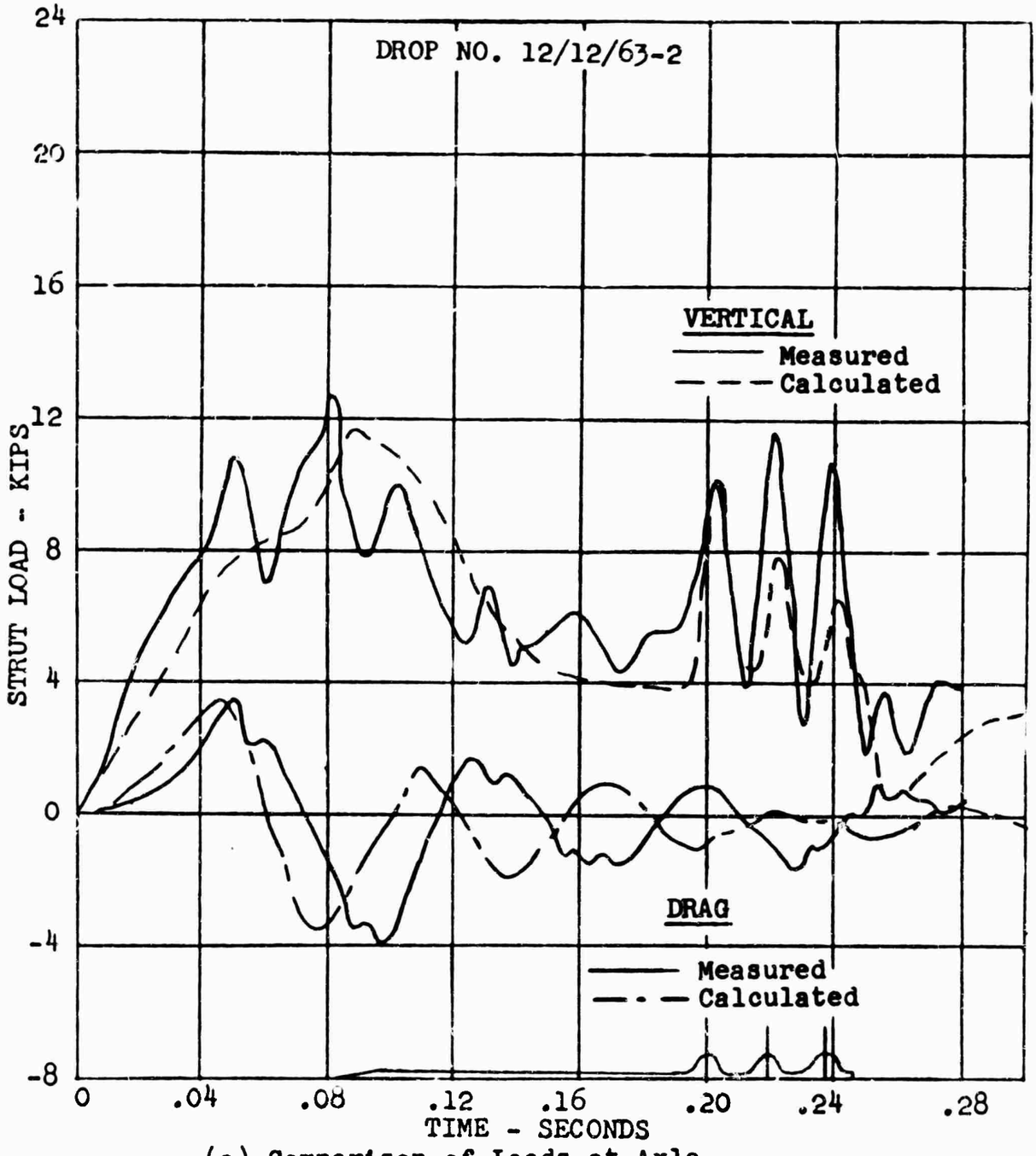

(a) Comparison of Loads at Axle.

Figure 19. Comparison of Measured and Calculated Loads for a 6.1 FPS Drop on Three 2-Inch by 30-Inch 1-Cosine Continuous Undulations.

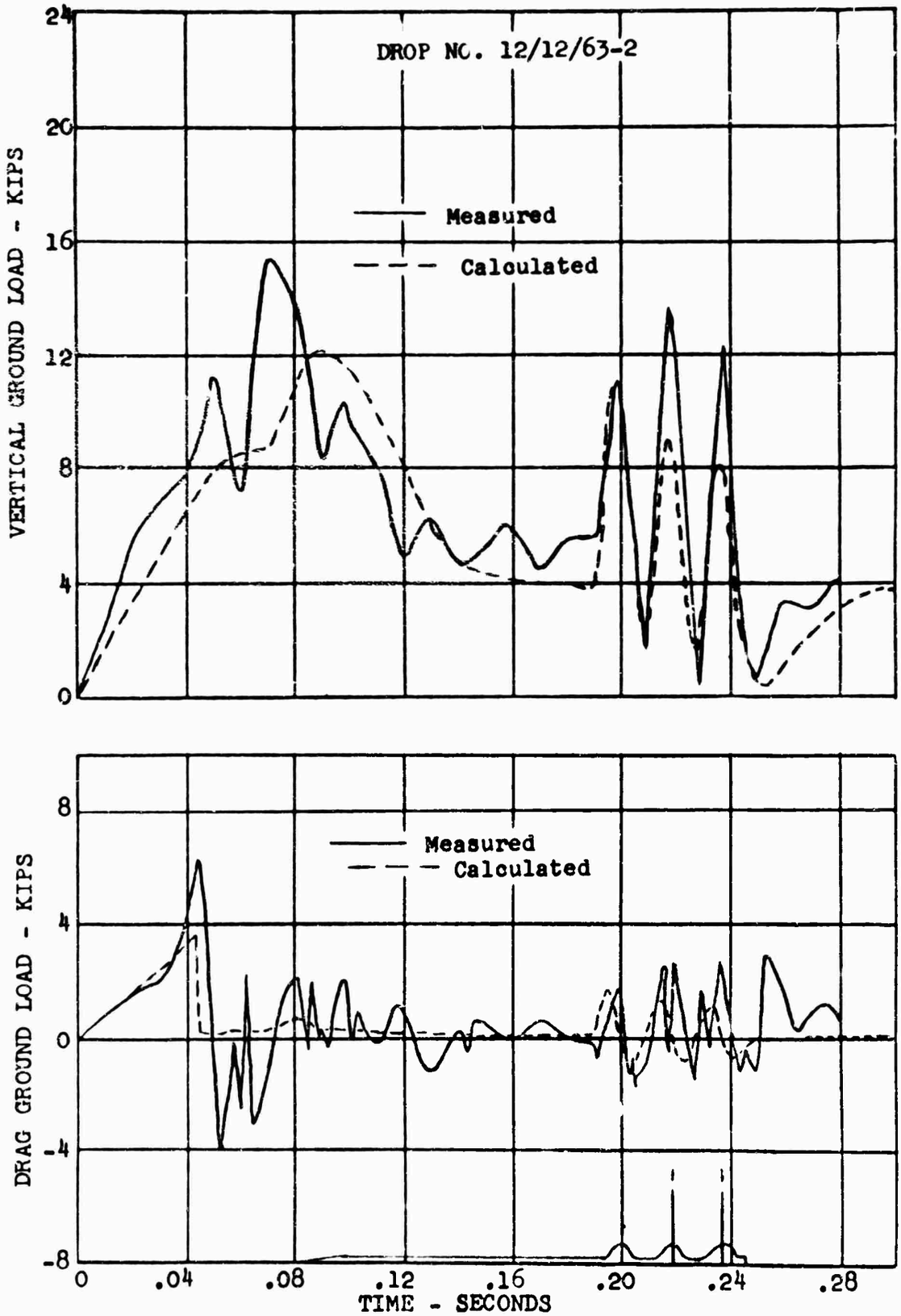

(b) Comparison of Loads at Ground.

Figure 19. Concluded.

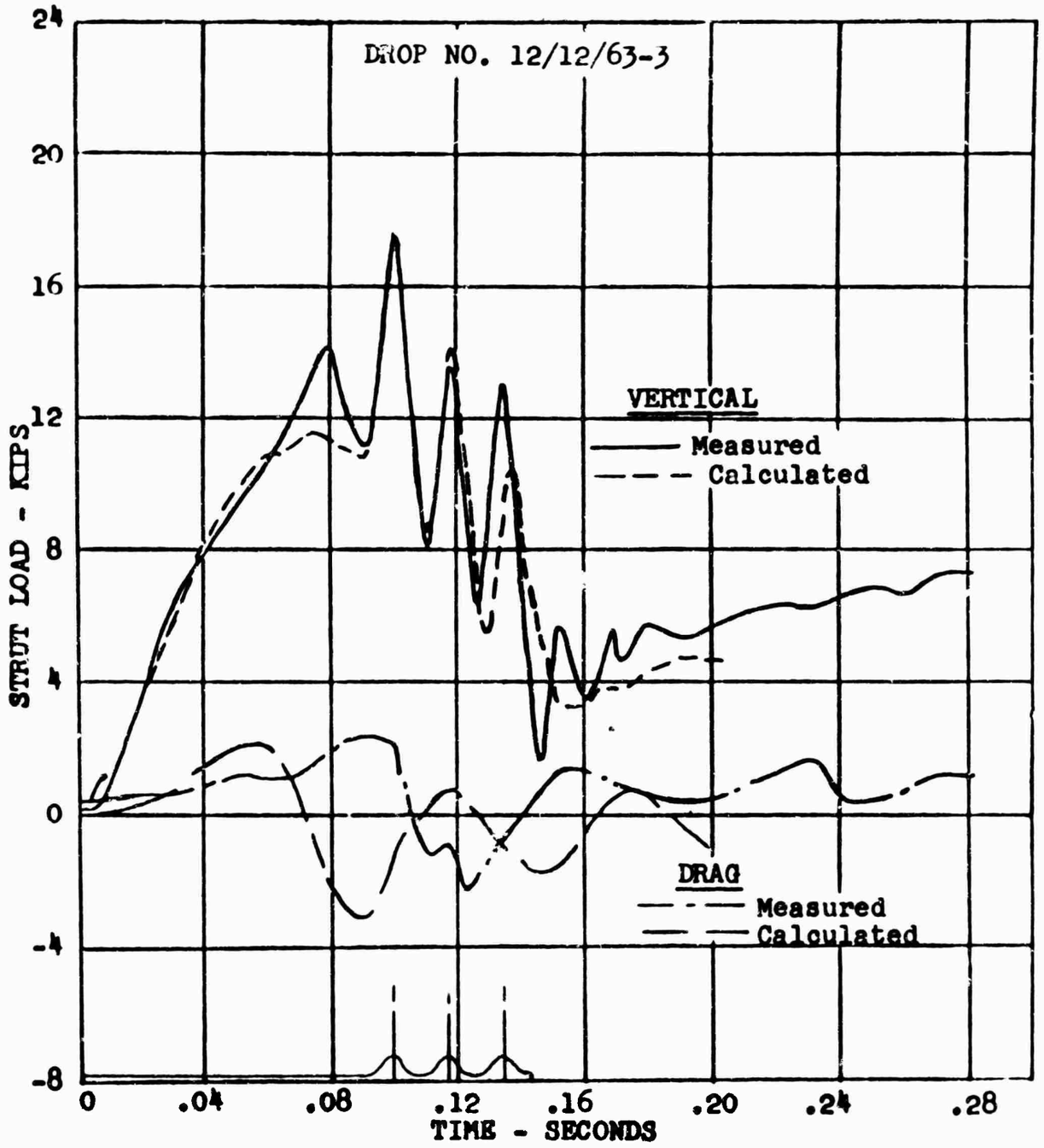

(a) Comparison of Loads at Axle.

Figure 20. Comparison of Measured and Calculated Loads for an 8.1 FPS Drop on Three 2-Inch by 30-Inch 1-Cosine Continuous Undulations.

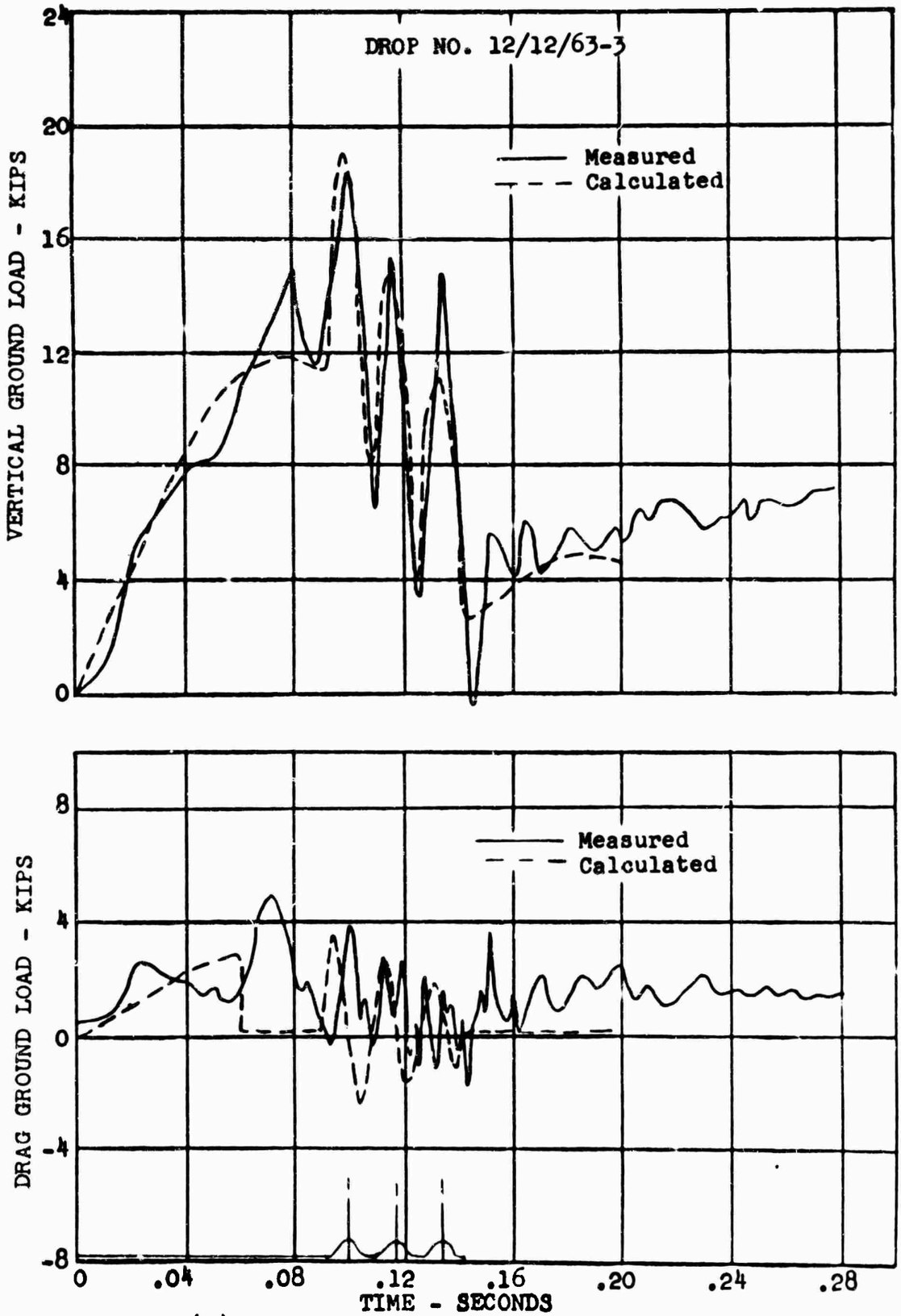

(b) Comparison of Loads at Ground.

Figure 20. Concluded

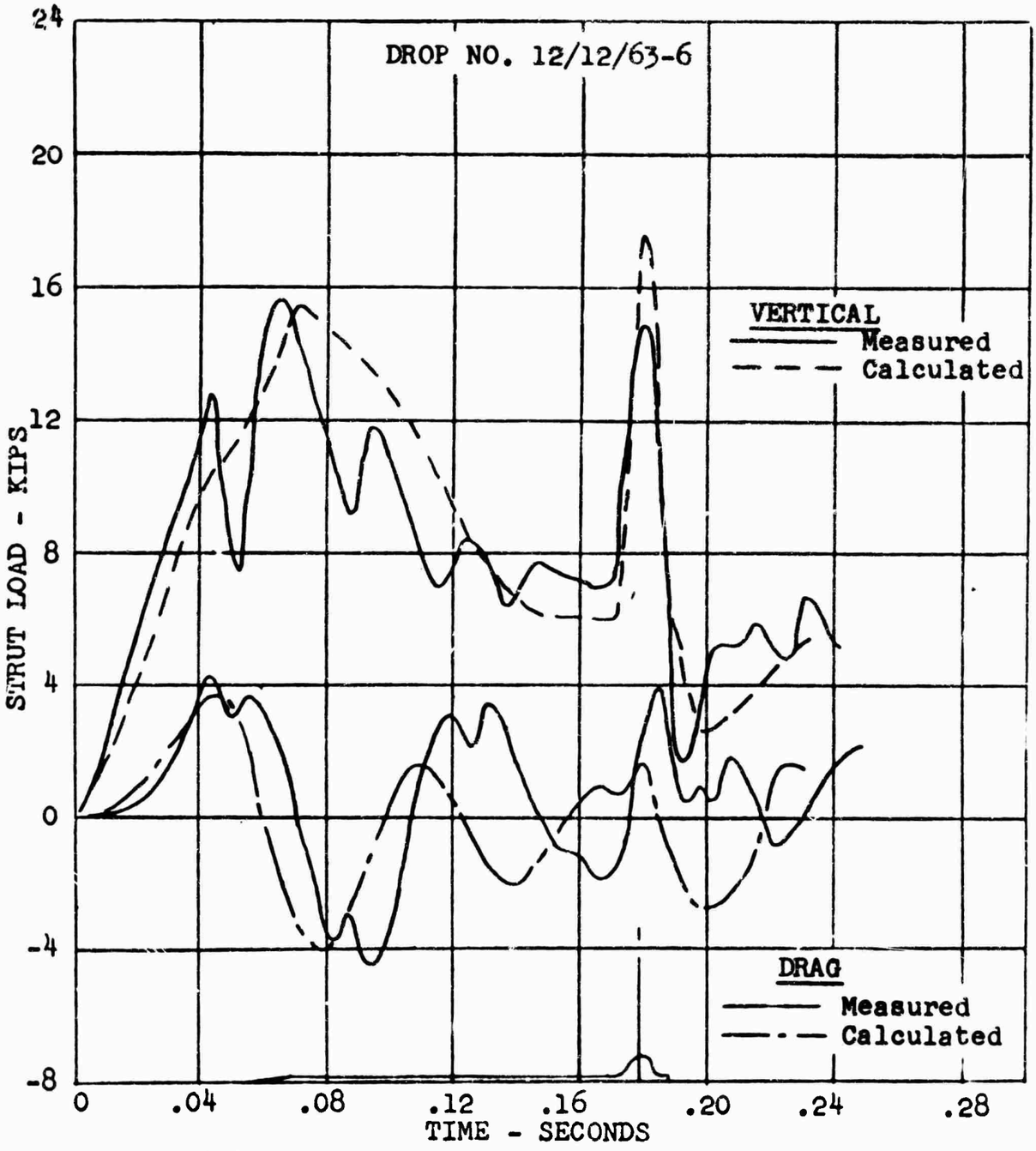

(a) Comparison of Loads at Axle.

Figure 21. Comparison of Measured and Calculated Loads for 8.8 FPS Drop on a 3-Inch by 30-Inch 1-Cosine Bump.

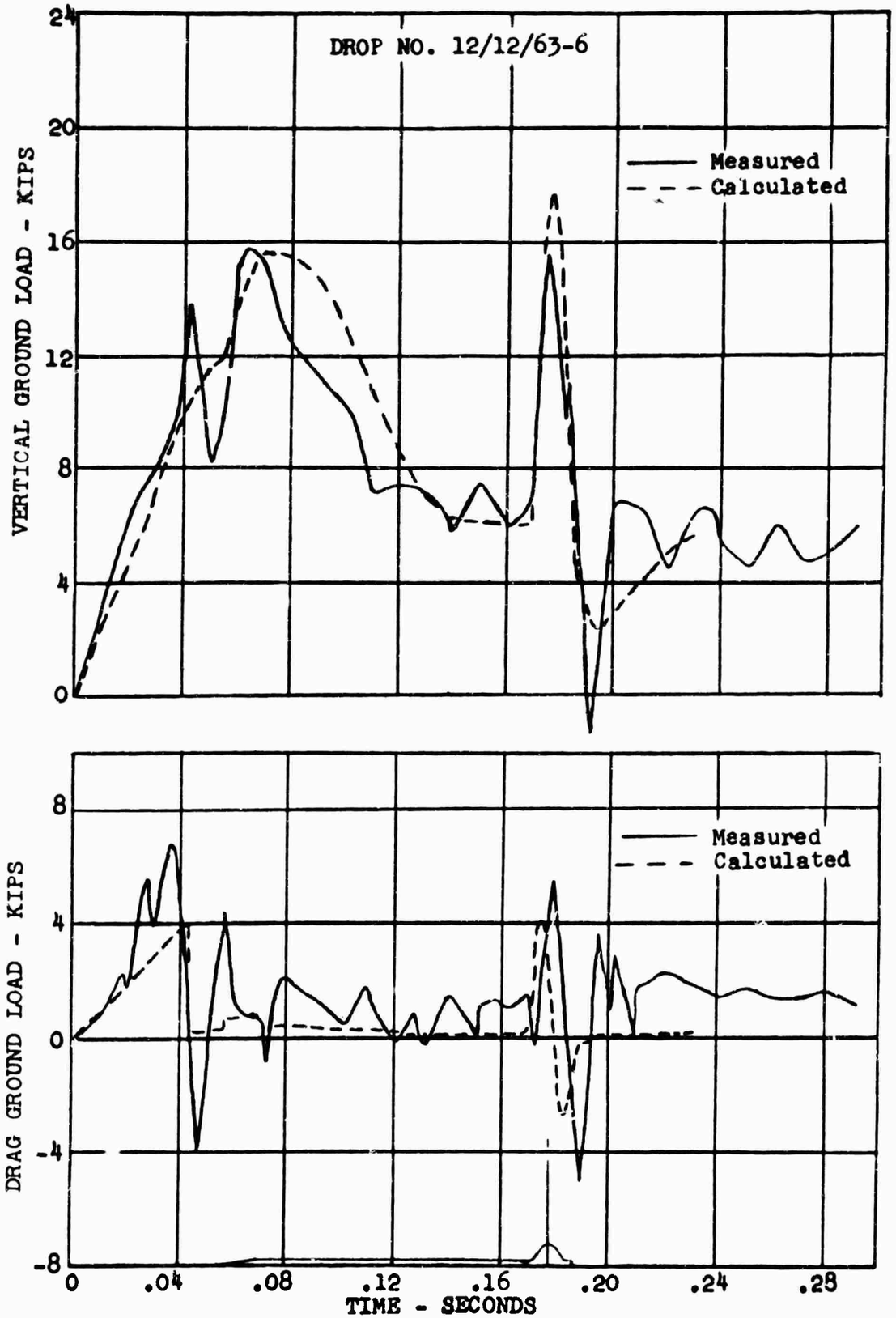

(b) Comparison of Loads at Ground.

Figure 21. Concluded

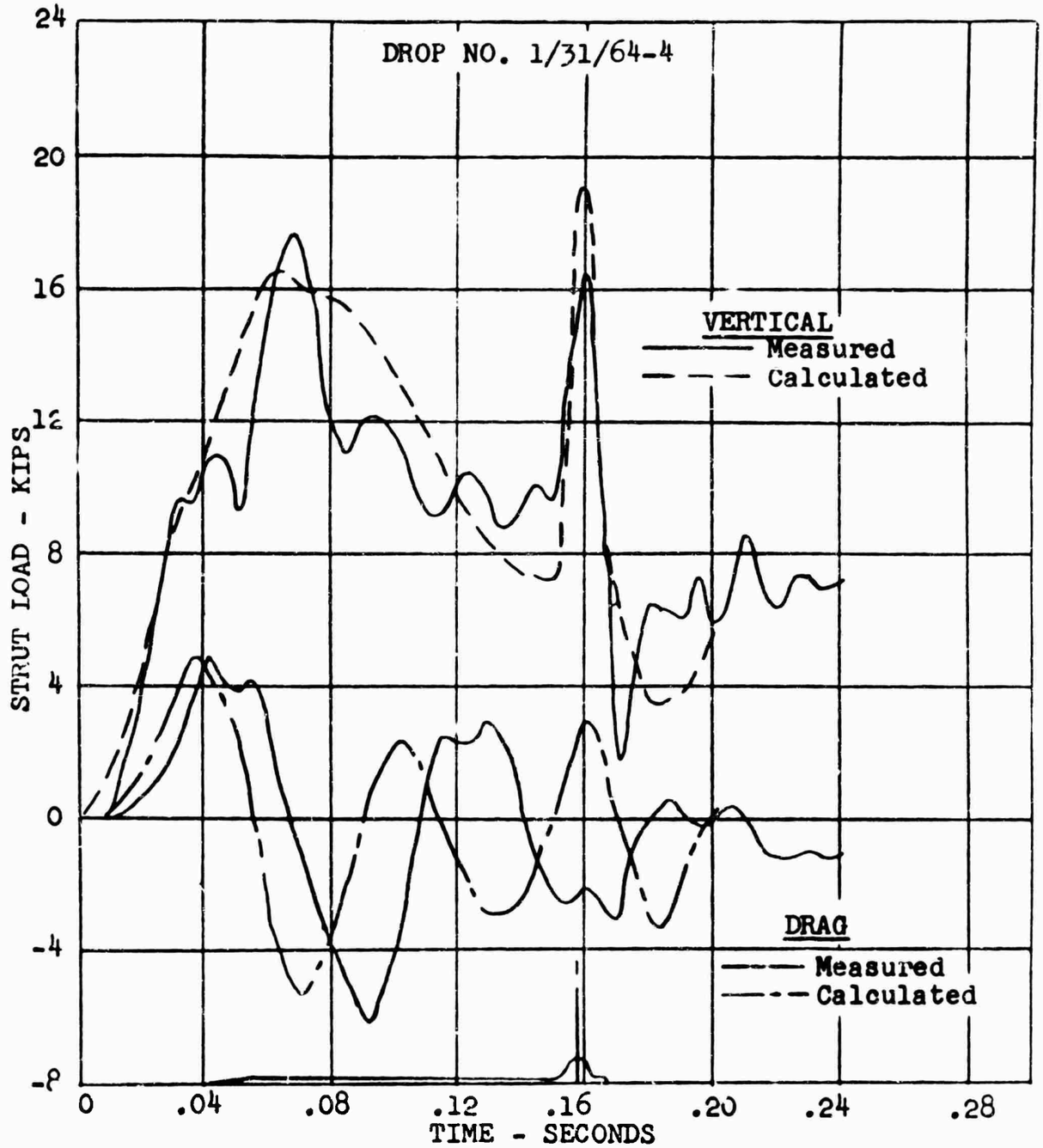

(a) Comparison of Loads at Axle.

Figure 22. Comparison of Measured and Calculated Loads, Pressures and Axle Motion for a 9.8 FPS Drop on a 3-Inch by 30-Inch 1-Cosine Bump.

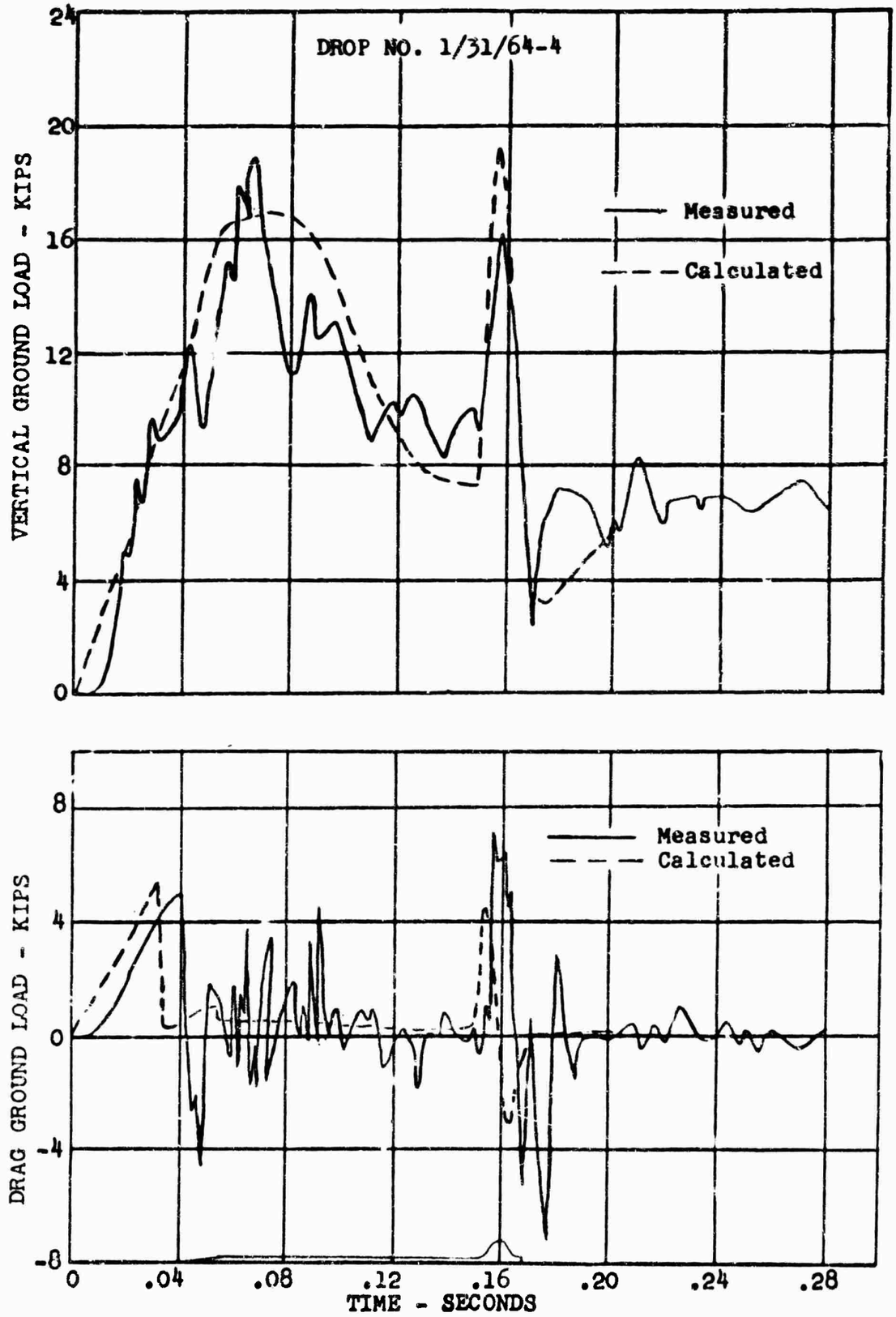

(b) Comparison of Loads at Ground.

Figure 22. Continued.

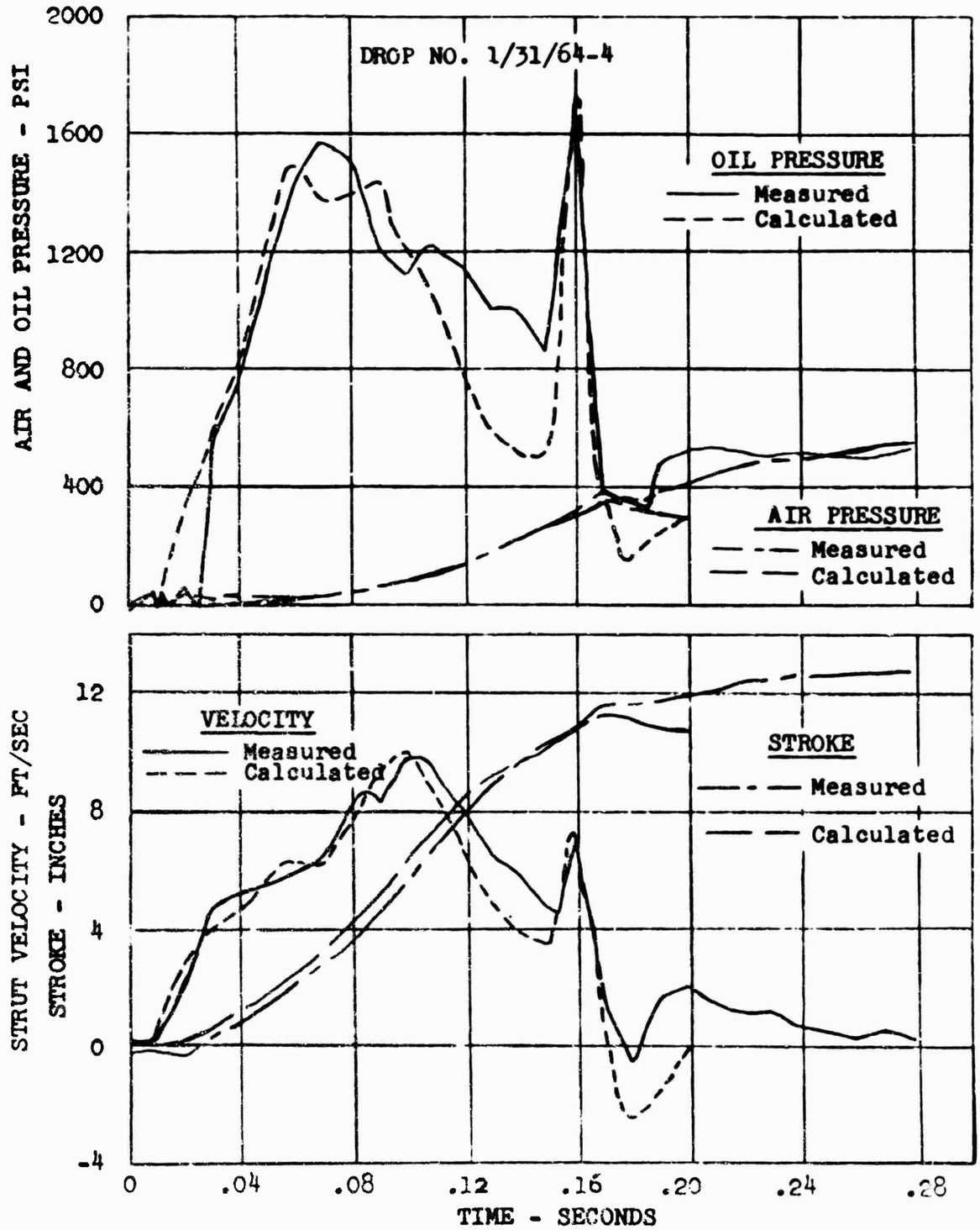

(c) Comparison of Strut Pressures and Comparison of Strut Stroke and Velocity.

Figure 22. Concluded.

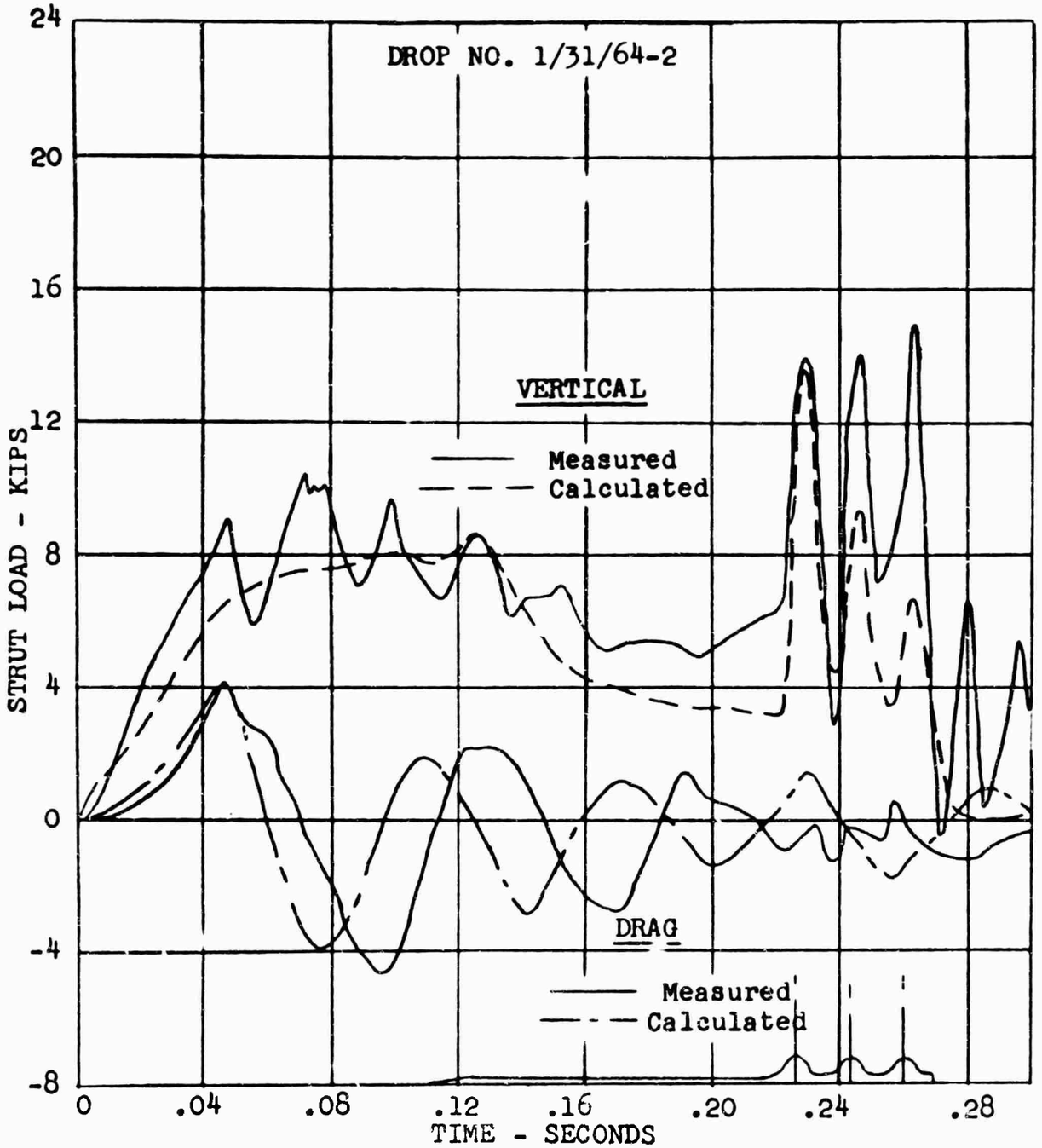

(a) Comparison of Loads at Axle.

Figure 23. Comparison of Measured and Calculated Loads for a 6.0 FPS Drop on Three 3-Inch by 30-Inch 1-Cosine Continuous Undulations.

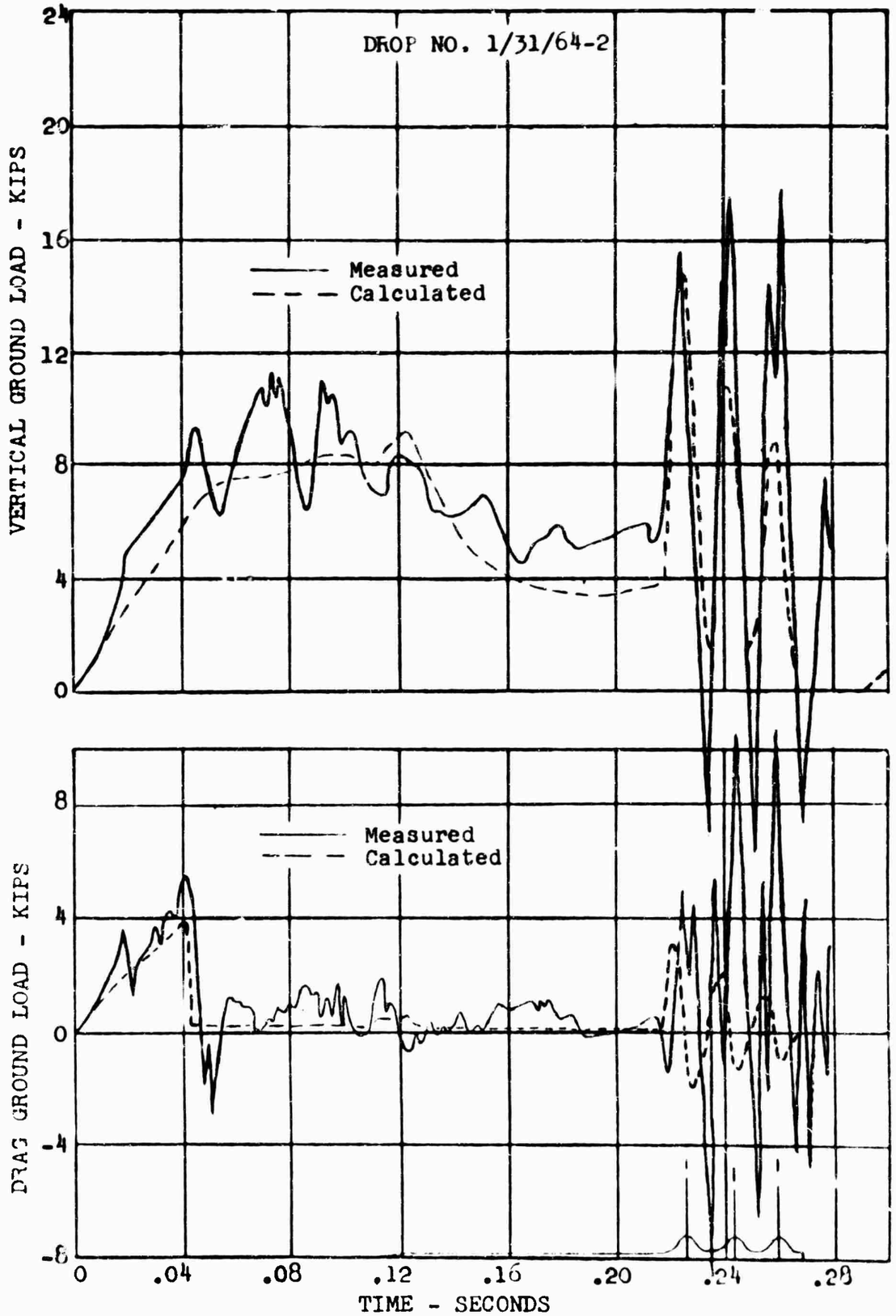

(b) Comparison of Loads at Ground.

Figure 23. Concluded.

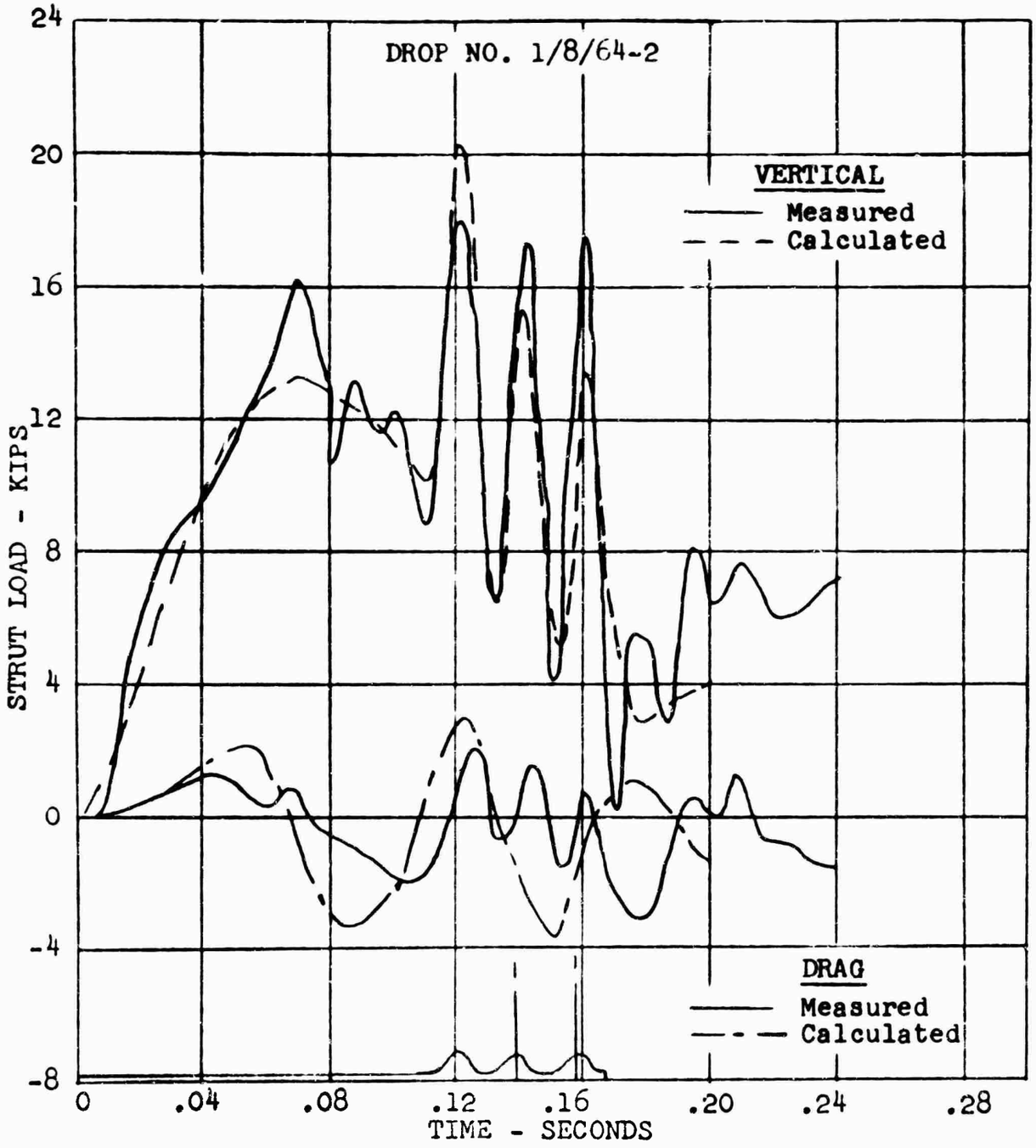

(a) Comparison of Loads at Axle.

Figure 24. Comparison of Measured and Calculated Loads for a 9.3 FPS Drop on Three 3-Inch by 30-Inch 1-Cosine Continuous Undulations.

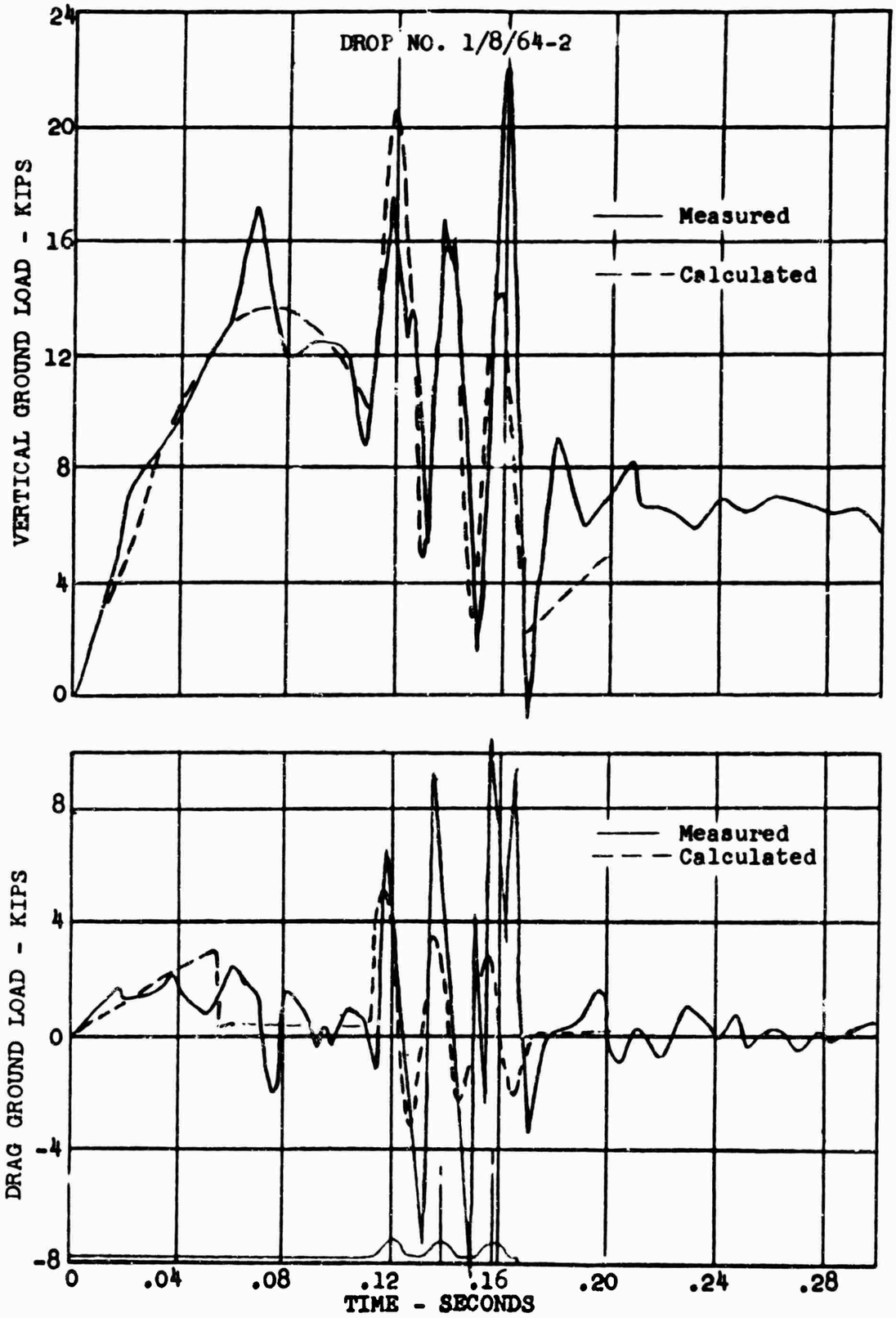

(b) Comparison of Loads at Ground.

Figure 24. Concluded.

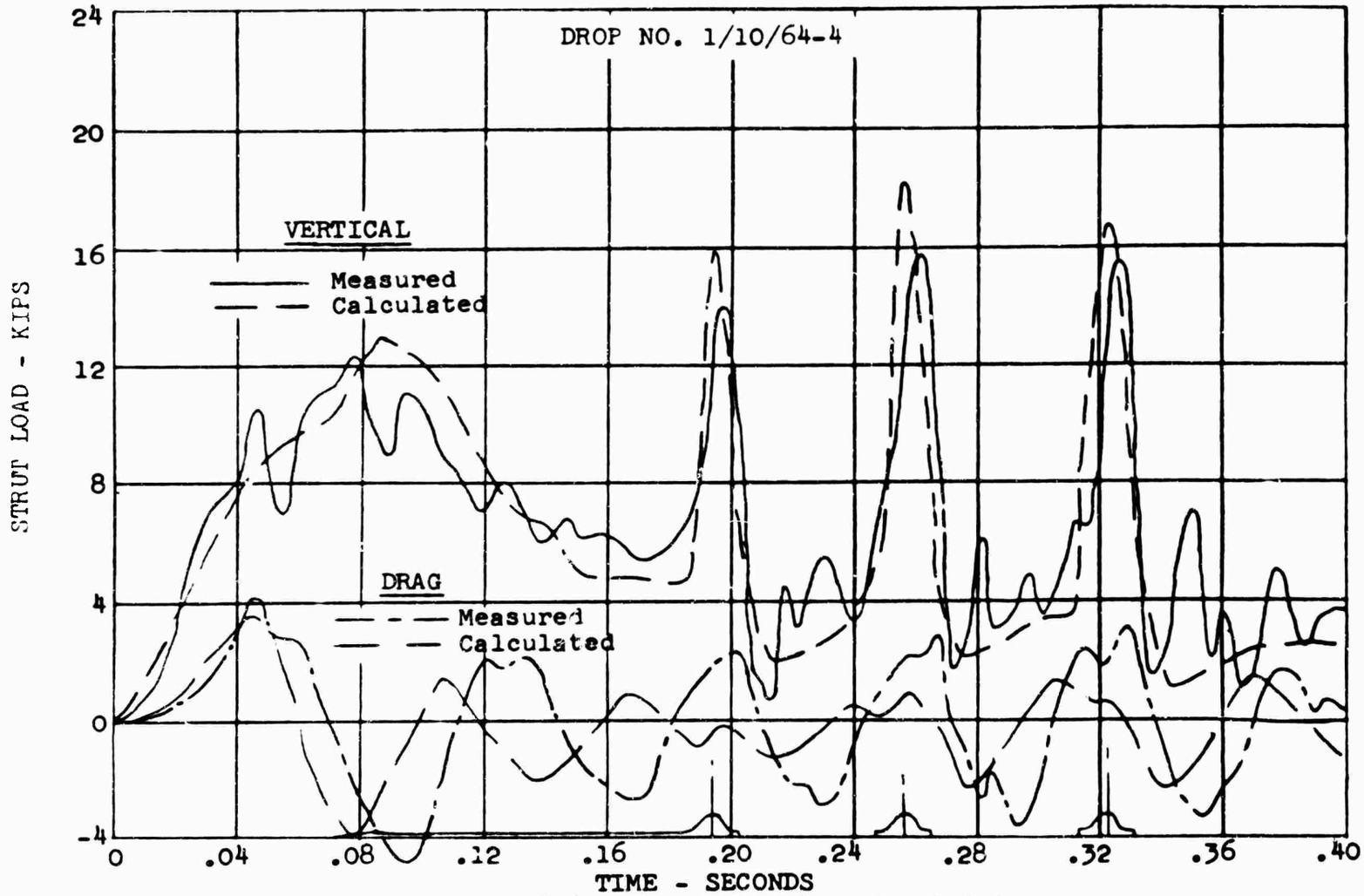

(a) Comparison of Loads at Axle.

Figure 25. Comparison of Measured and Calculated Loads, Pressures and Axle Motion for a 7.5-FPS Drop on Three 3-Inch by 30-Inch 1-Cosine Bumps Spaced 108 Inches Apart.

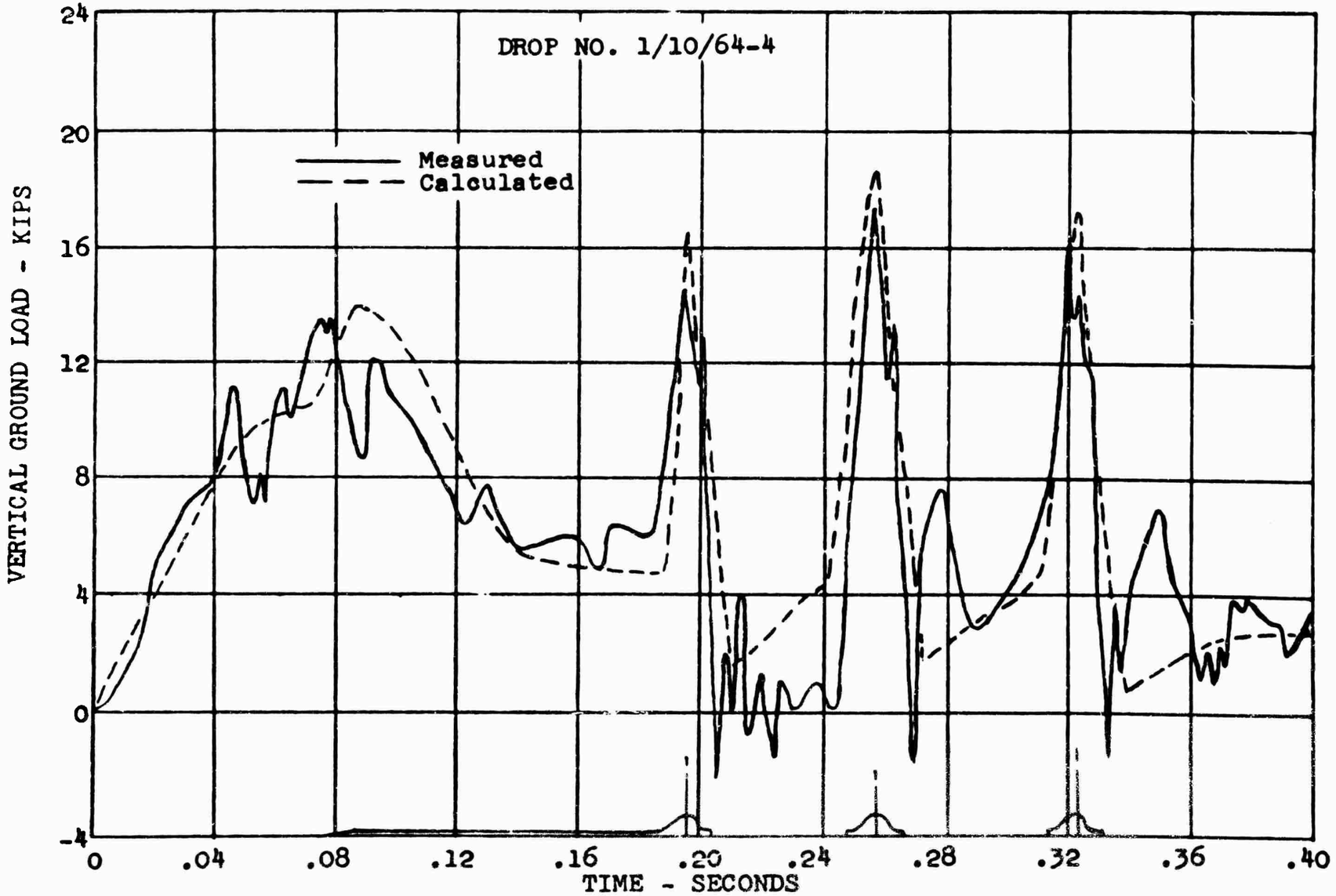

(b) Comparison of Vertical Loads at Ground.

Figure 25. Continued.

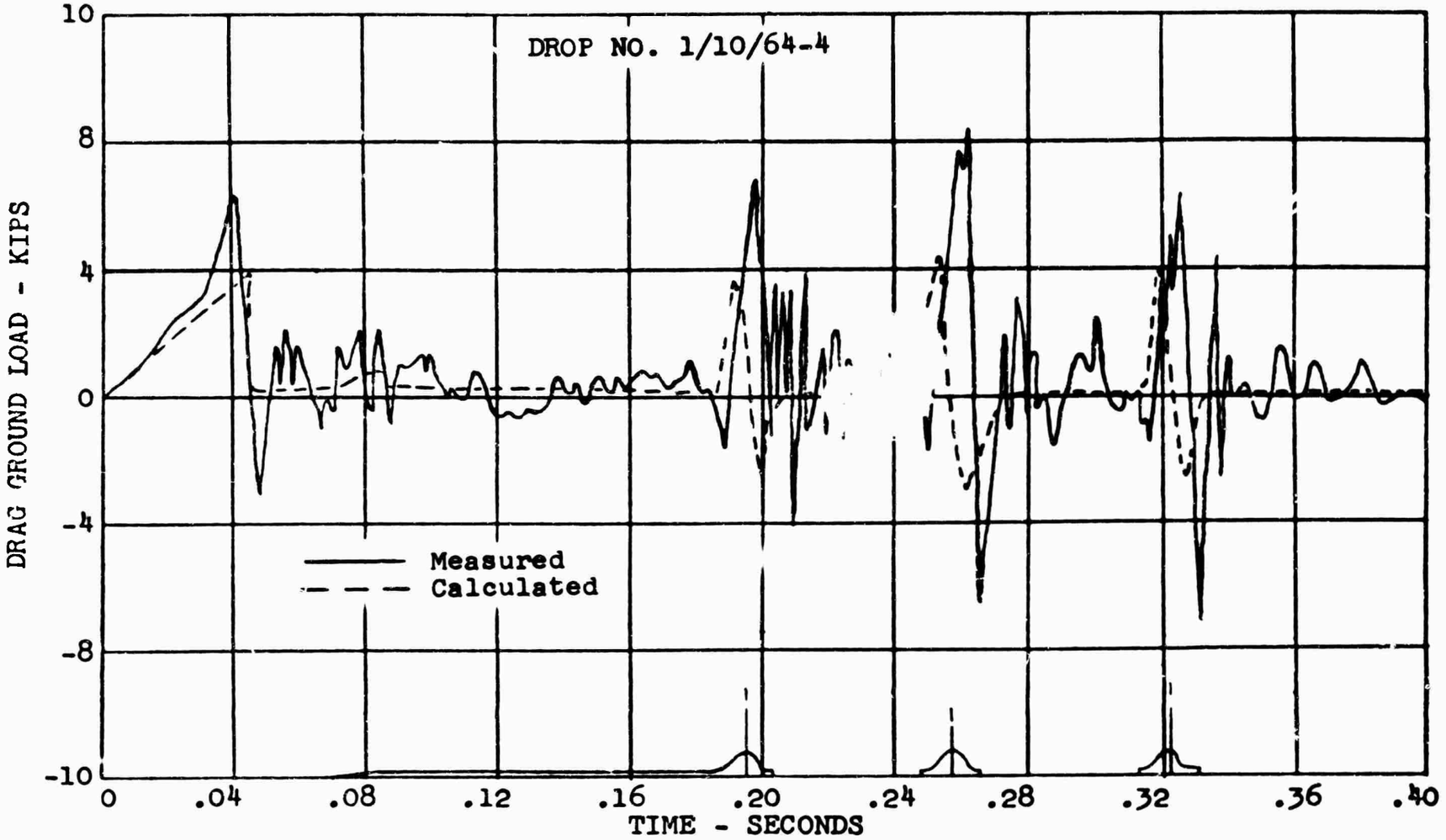

(c) Comparison of Horizontal Loads at Ground

Figure 25. Continued.

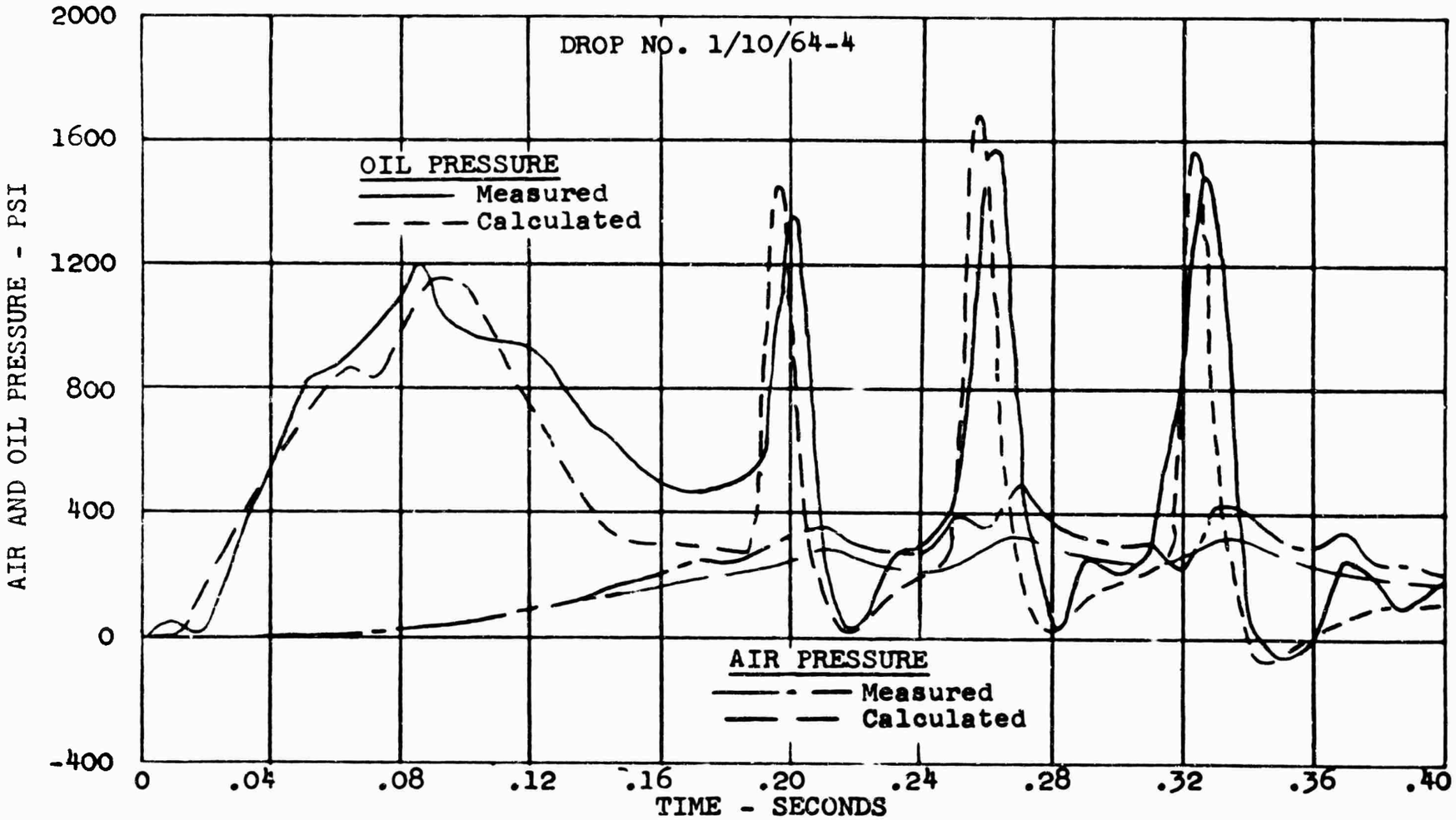

(d) Comparison of Strut Pressures.

Figure 25. Continued.

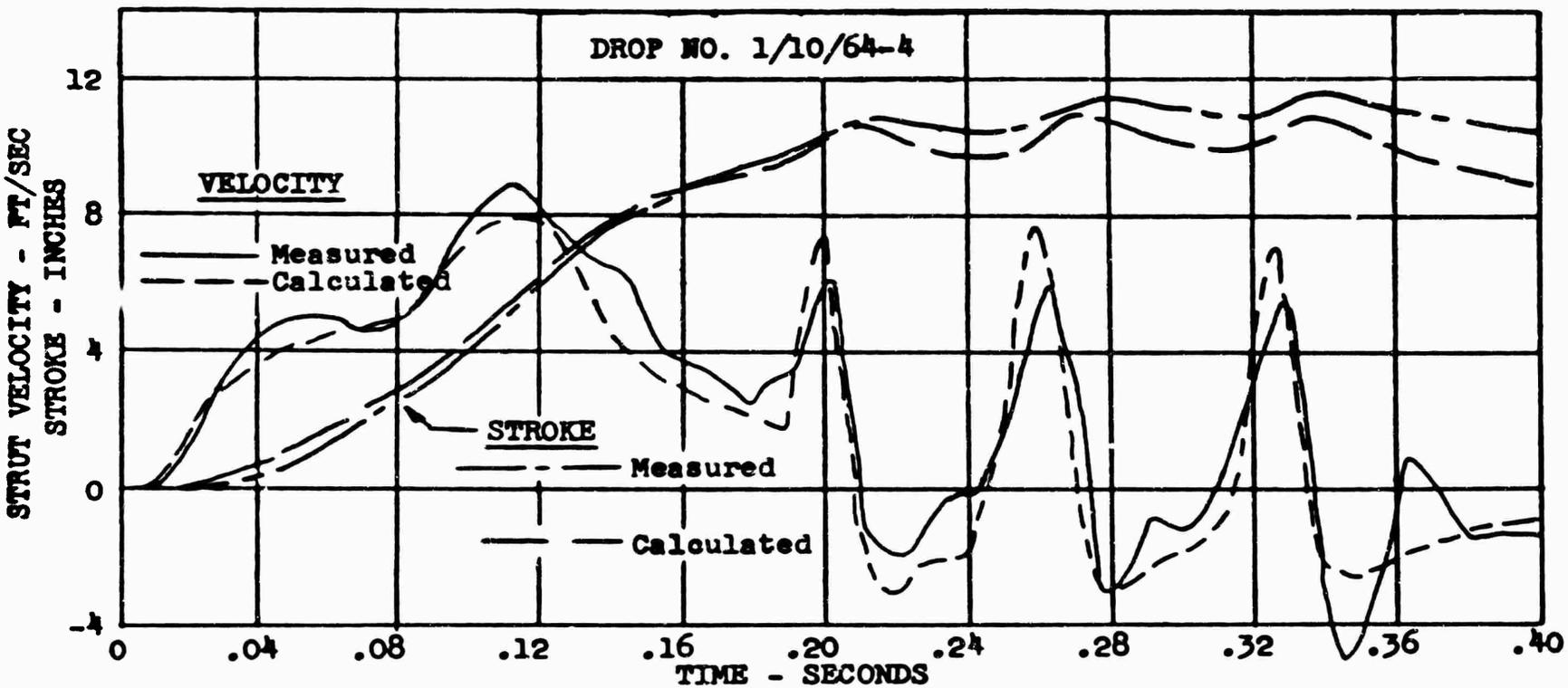

(e) Comparison of Strut Stroke and Velocity.

Figure 25. Concluded.

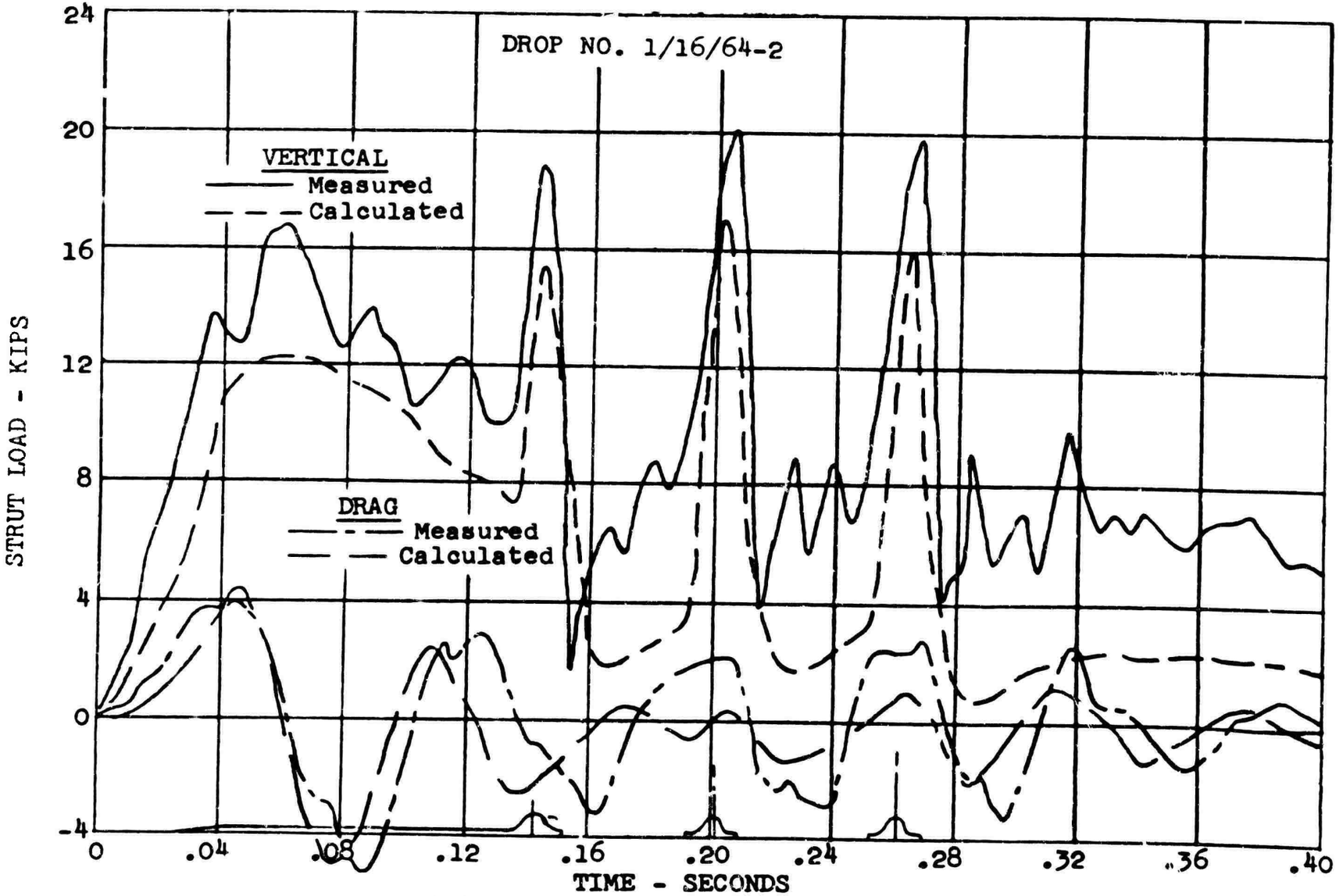

(a) Comparison of Loads at Axle.

Figure 26. Comparison of Measured and Calculated Loads for an 8.0-FPS Drop on Three 3-Inch by 30-Inch 1-Cosine Bumps Spaced 108 Inches Apart.

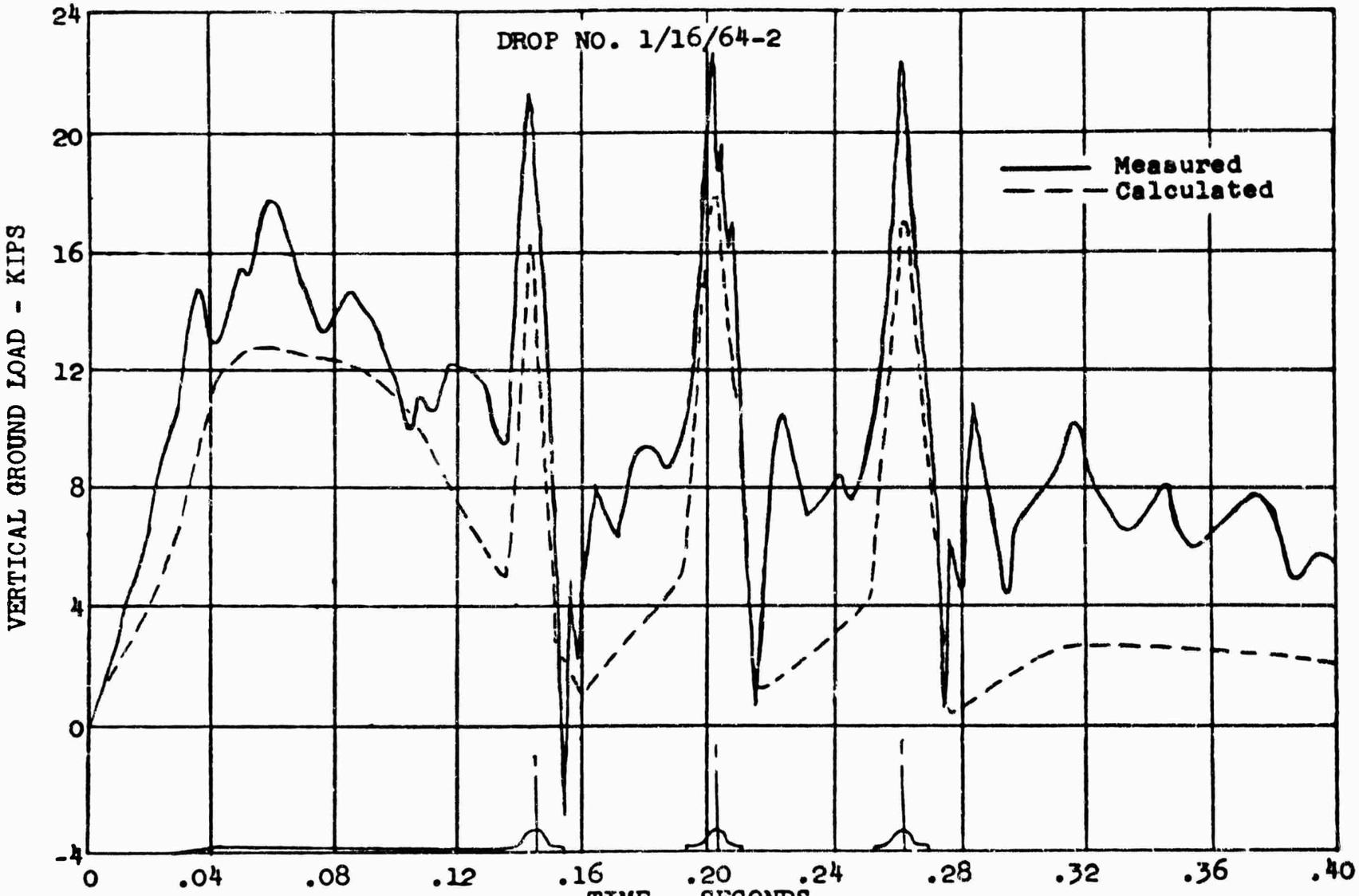

(b) Comparison of Vertical Loads at Ground,
Figure 26. Continued.

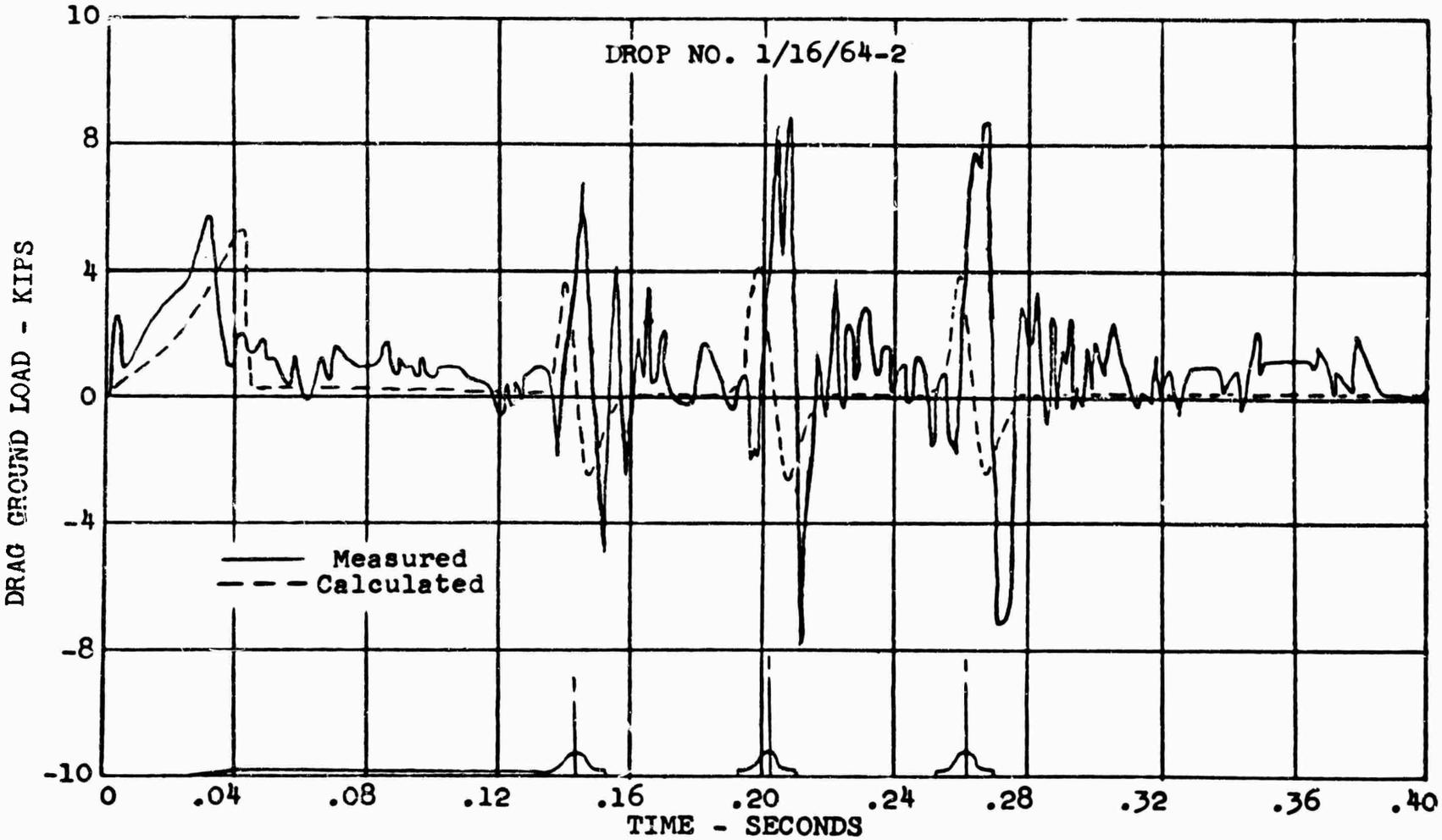

(c) Comparison of Horizontal Loads at Ground.

Figure 26. Concluded.

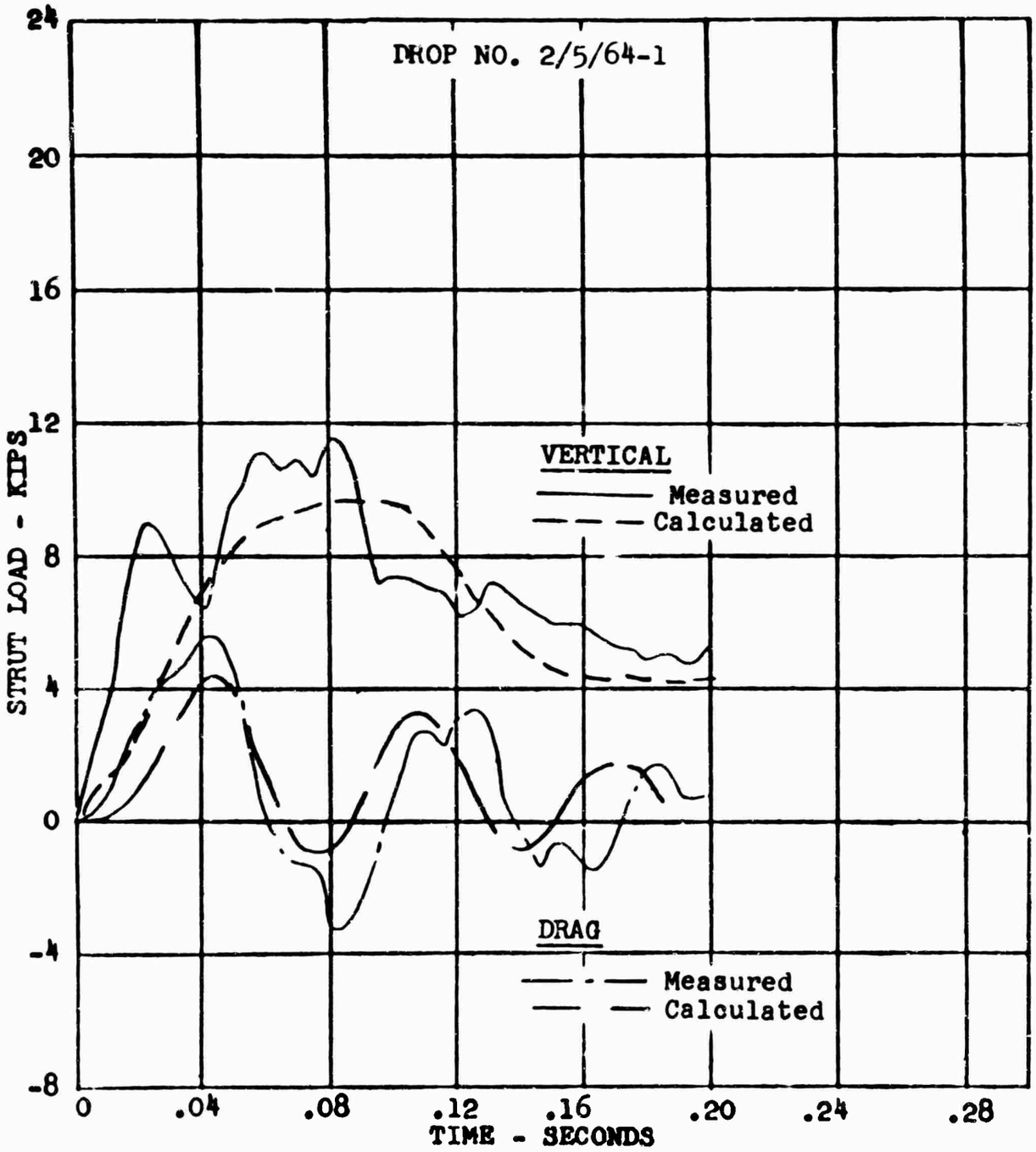

(a) Comparison of Loads at Axle.

Figure 27. Comparison of Measured and Calculated Loads for a 6.8-FPS Drop on Sand.

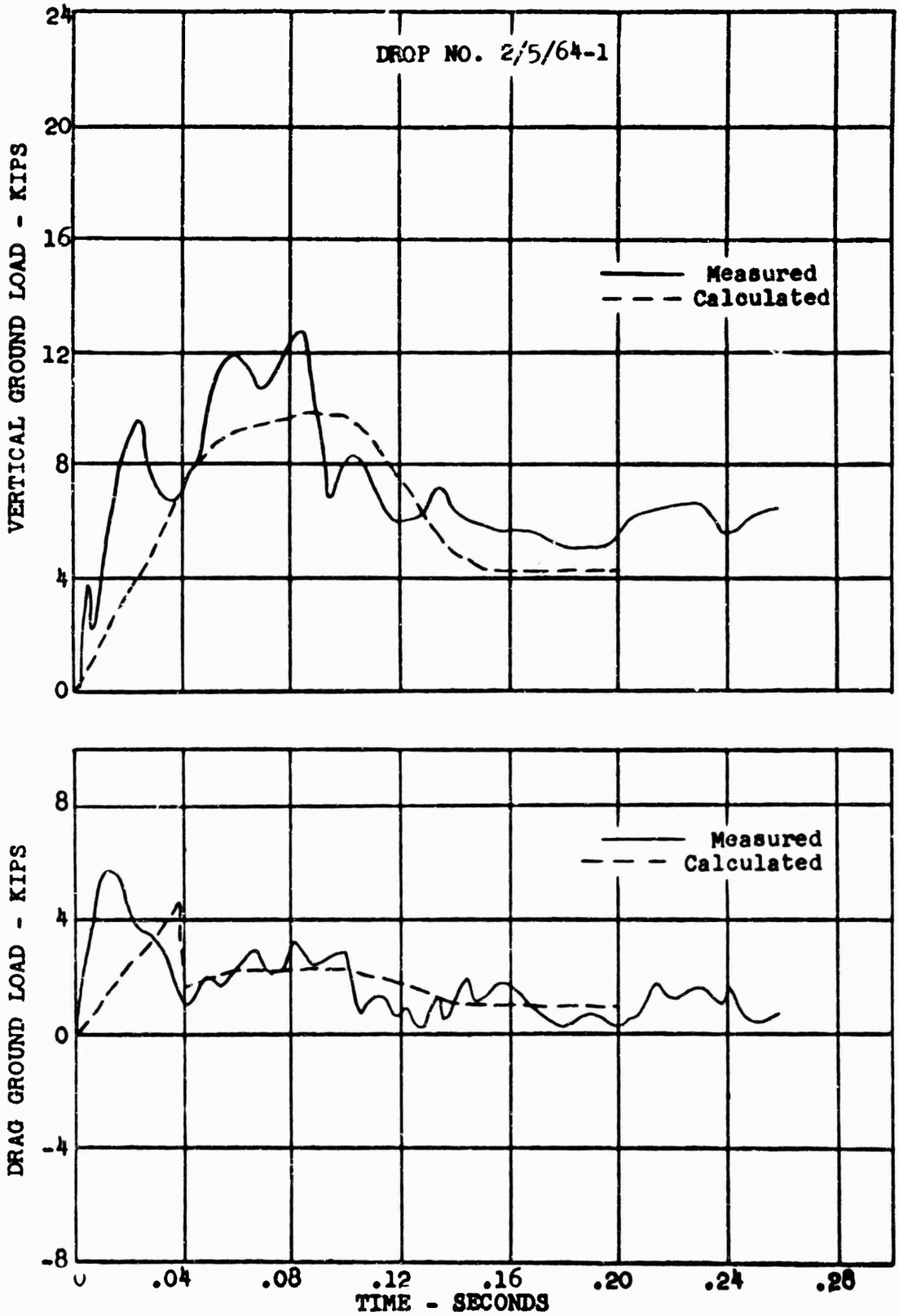

(b) Comparison of Loads at Ground.

Figure 27. Concluded.

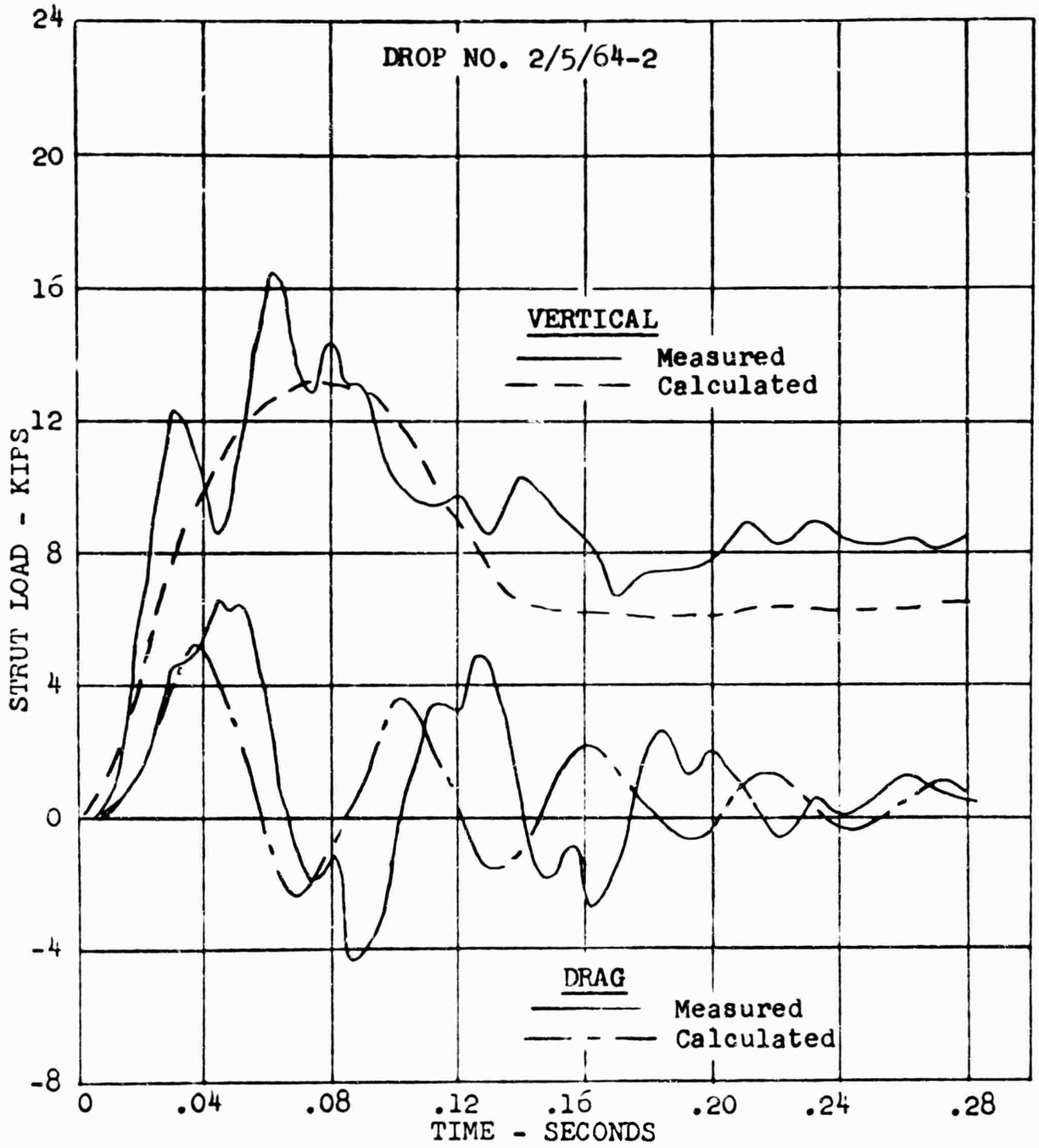

(a) Comparison of Loads at Axle.

Figure 28. Comparison of Measured and Calculated Loads, Pressures and Axle Motion for a 9.0-FPS Drop on Sand.

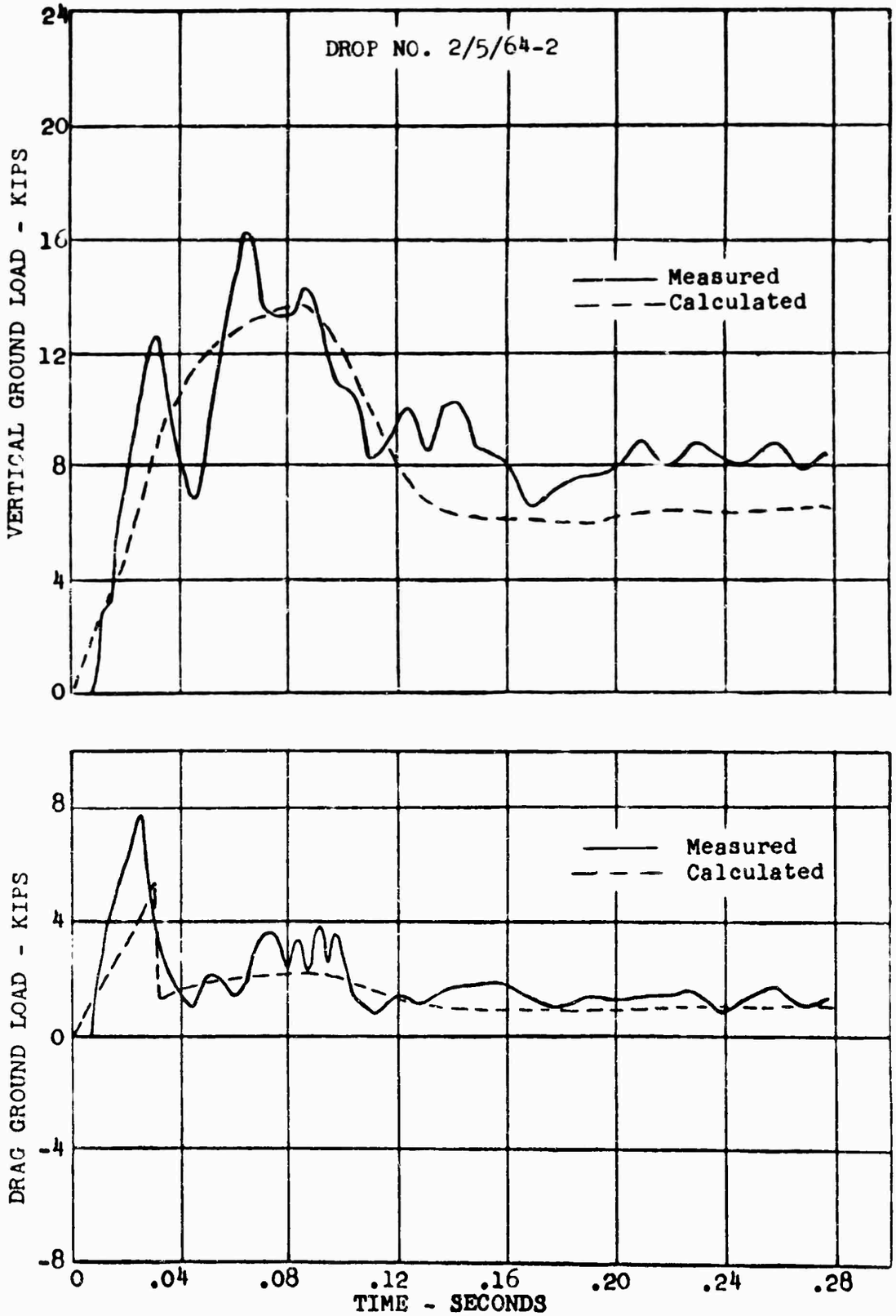

(b) Comparison of Loads at Ground.

Figure 28. Continued.

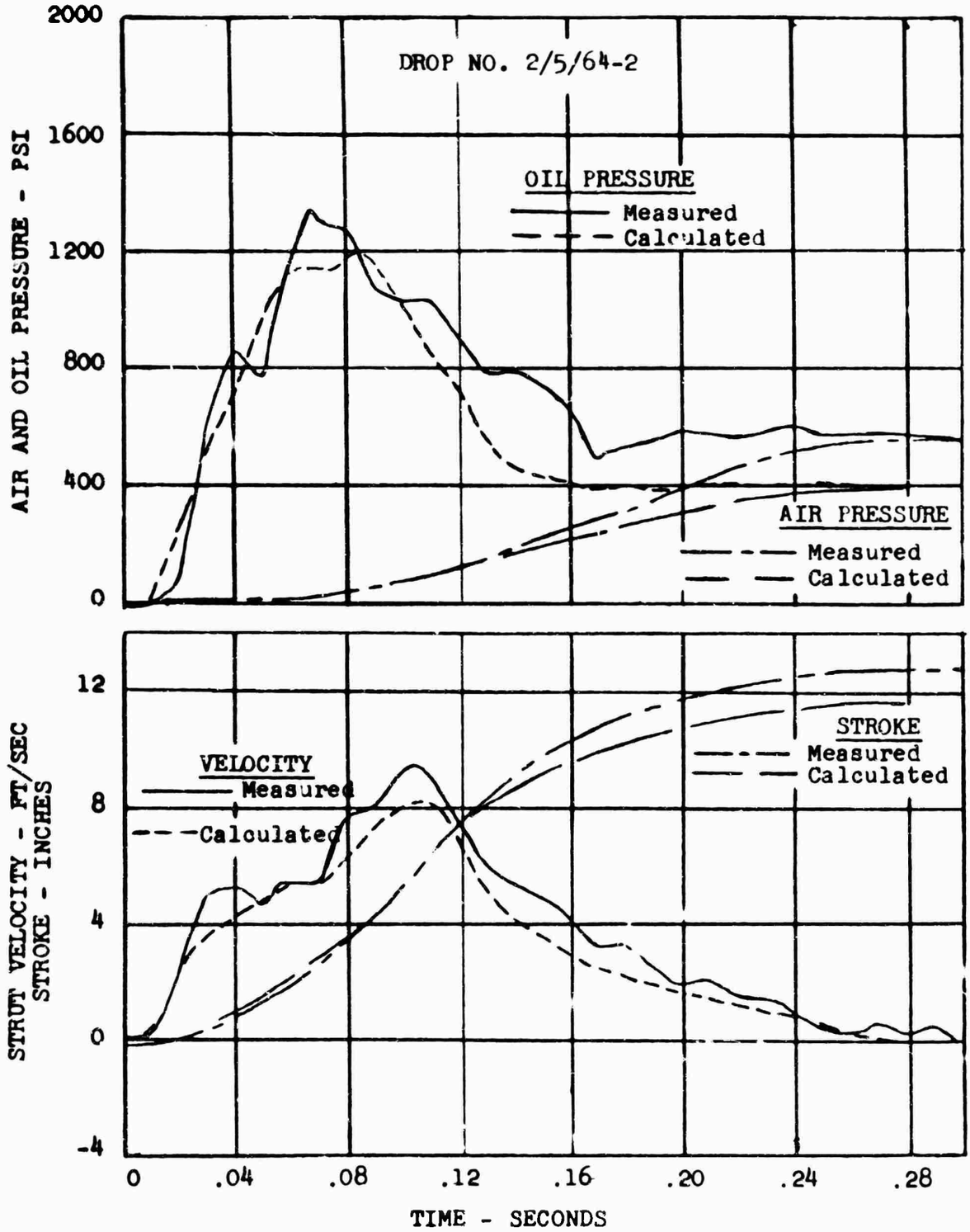

(c) Comparison of Strut Pressures and Comparison of Strut Stroke and Velocity.

Figure 28. Concluded.

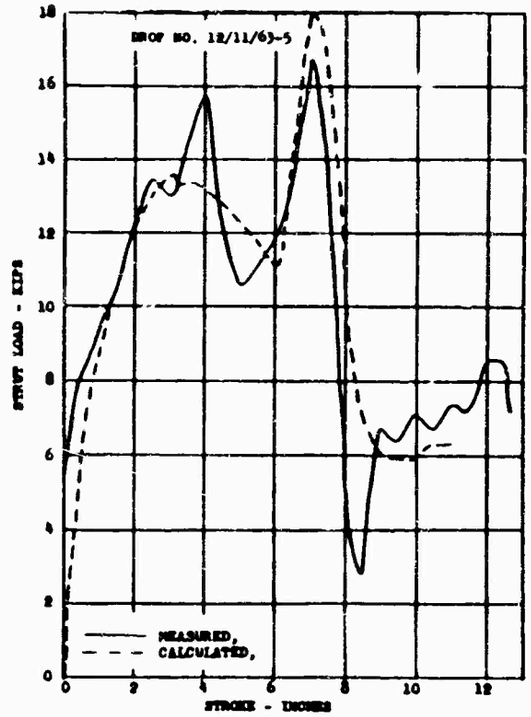

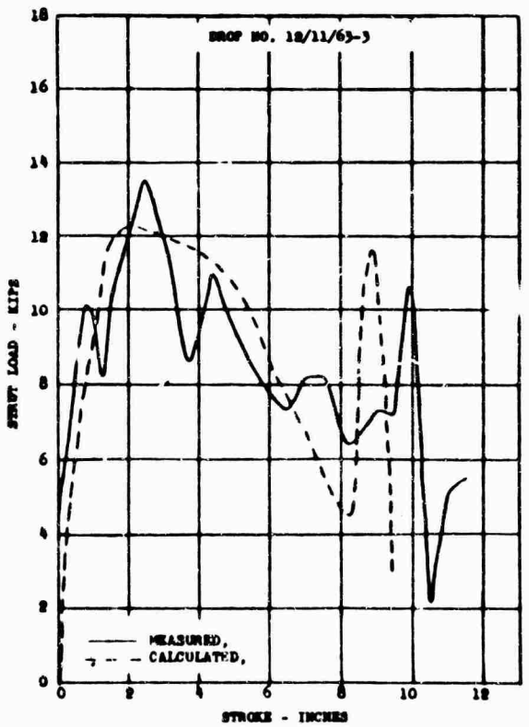

Figure 29. Comparison of Measured and Calculated Load-Stroke Curves for Drops on 2-Inch 1-Cosine Bumps.

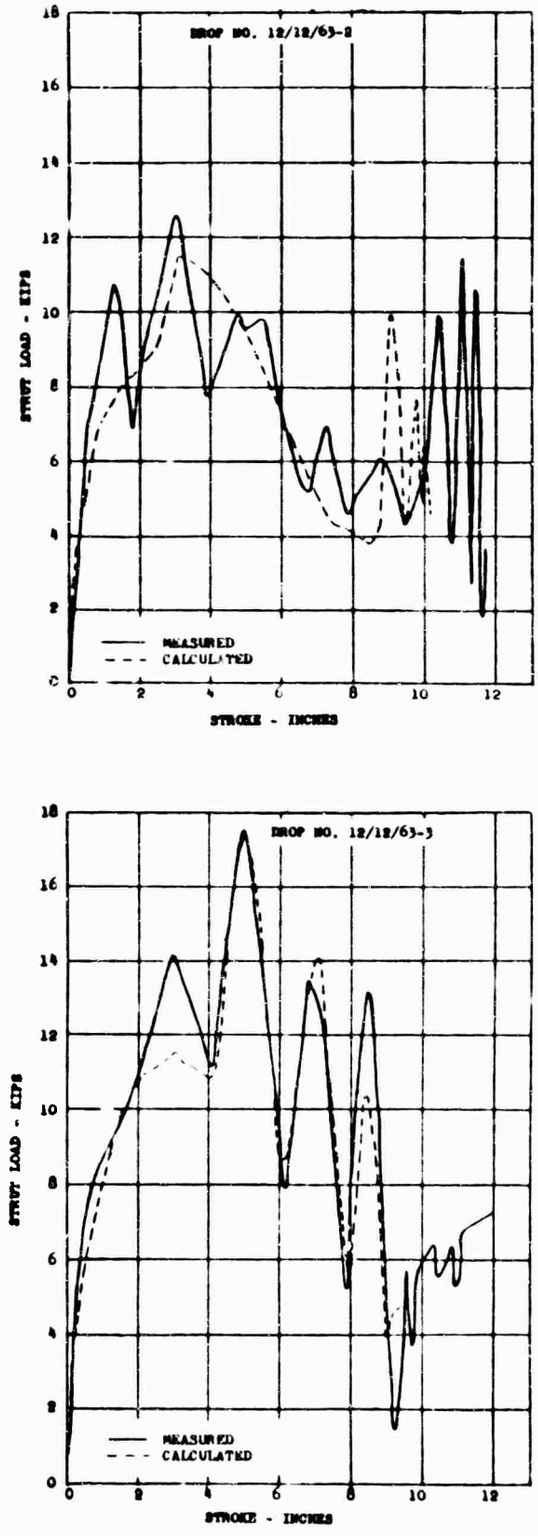

Figure 30. Comparison of Measured and Calculated Load-Stroke Curves for Drops on Three 2-Inch 1-Cosine Continuous Undulations.

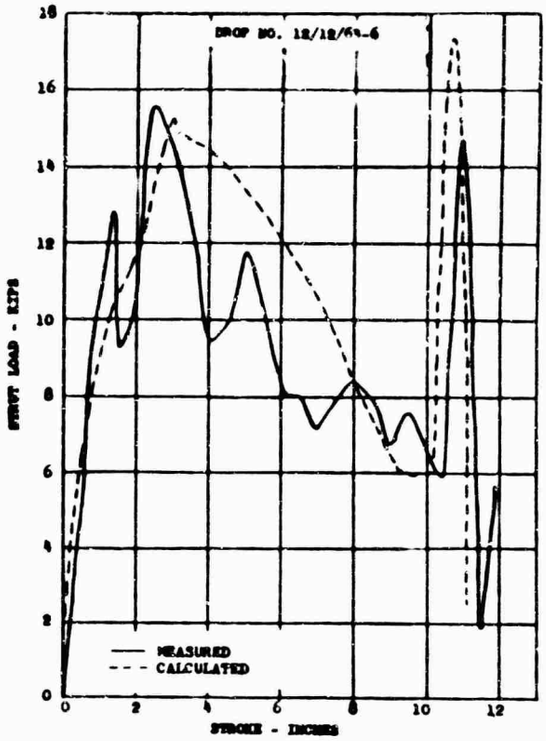

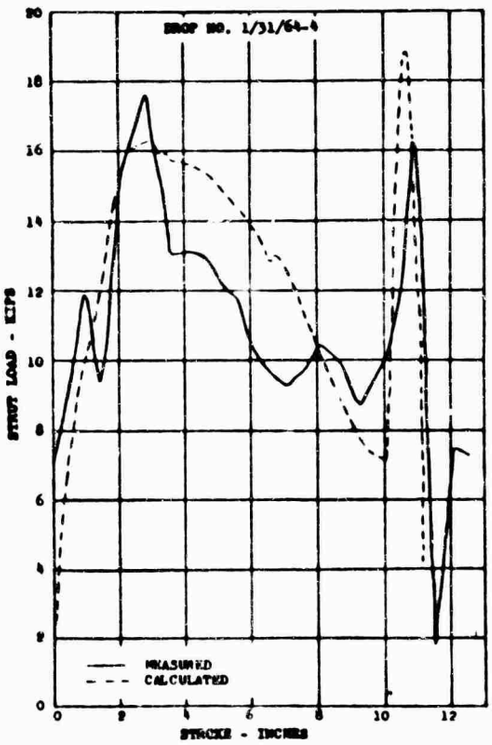

Figure 31. Comparison of Measured and Calculated Load-Stroke Curves for Drops on 3-Inch 1-Cosine Bumps.

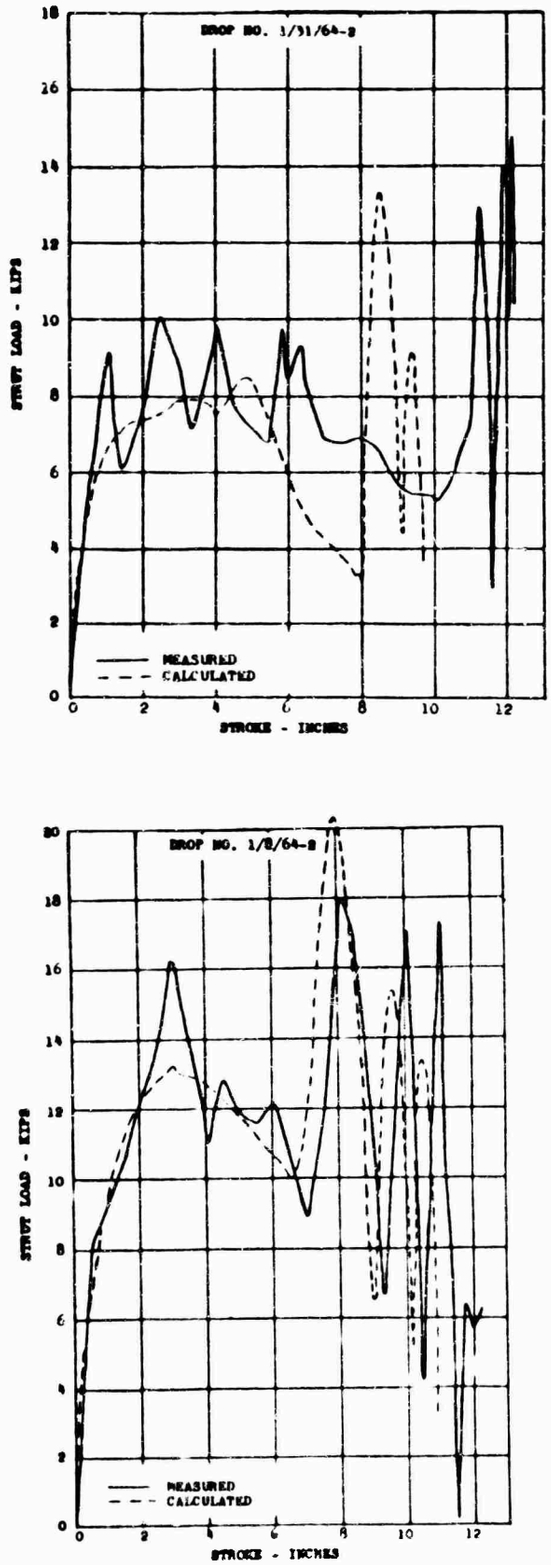

Figure 32. Comparison of Measured and Calculated Load-Stroke Curves for Drops on Three 3-Inch 1-Cosine Continuous Undulations.

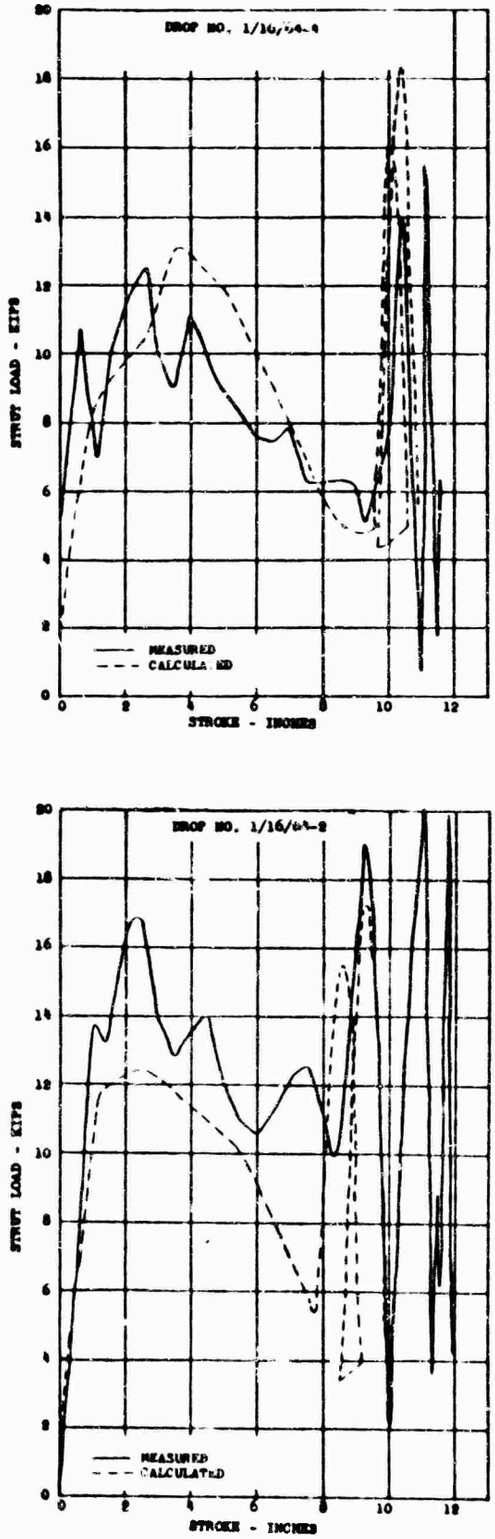

Figure 33. Comparison of Measured and Calculated Load-Stroke Curves for Drops on Three 3-Inch 1-Cosine Bumps Spaced 108 Inches Apart.

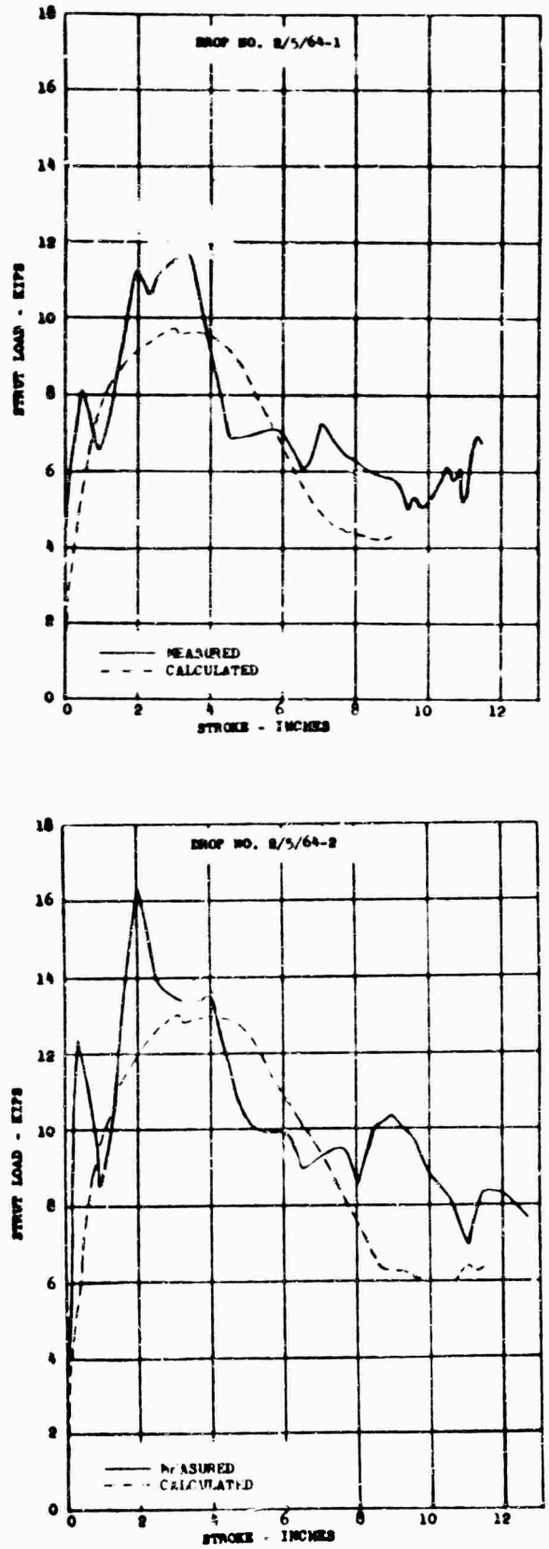

Figure 34. Comparison of Measured and Calculated Load-Stroke Curves for Drops on Sand.

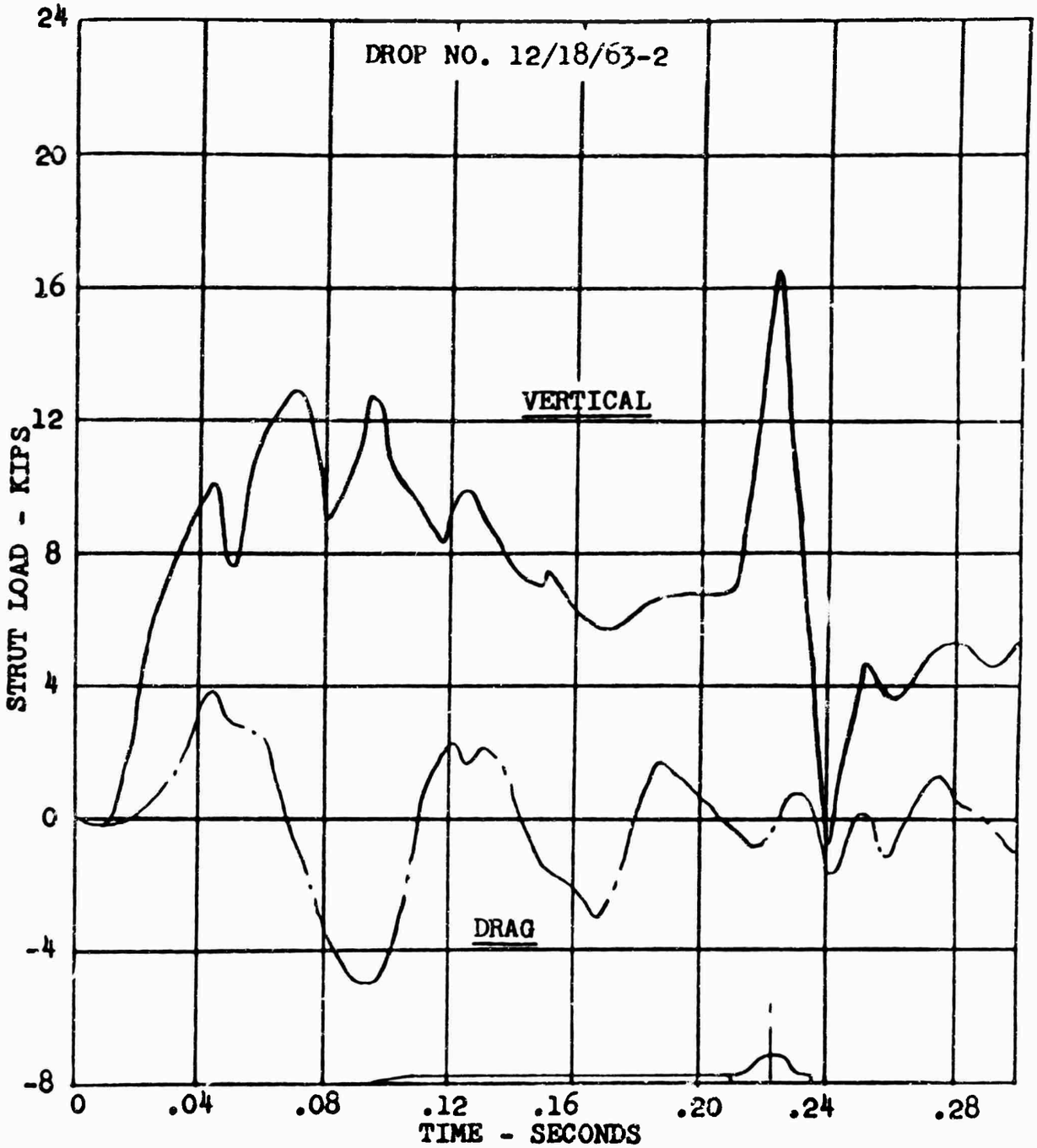

(a) Measured Loads at Axle.

Figure 35. Measured Loads, Pressures, and Axle Motion for an 8.1 FPS Drop on a 3-Inch 1-Cosine Bump Oriented at 45 Degrees to the Runway.

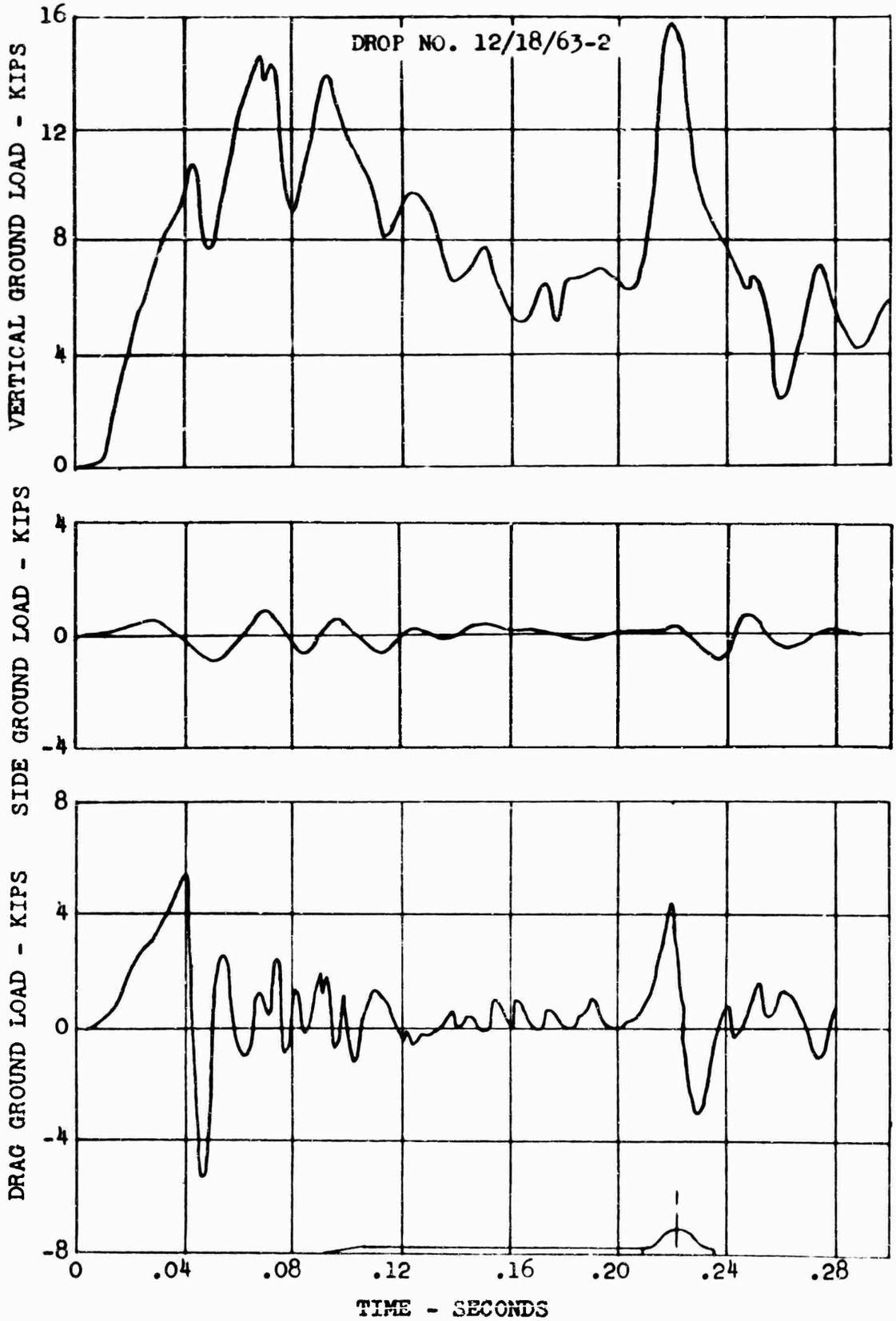

(b) Measured Loads at Ground.
Figure 35. Continued.

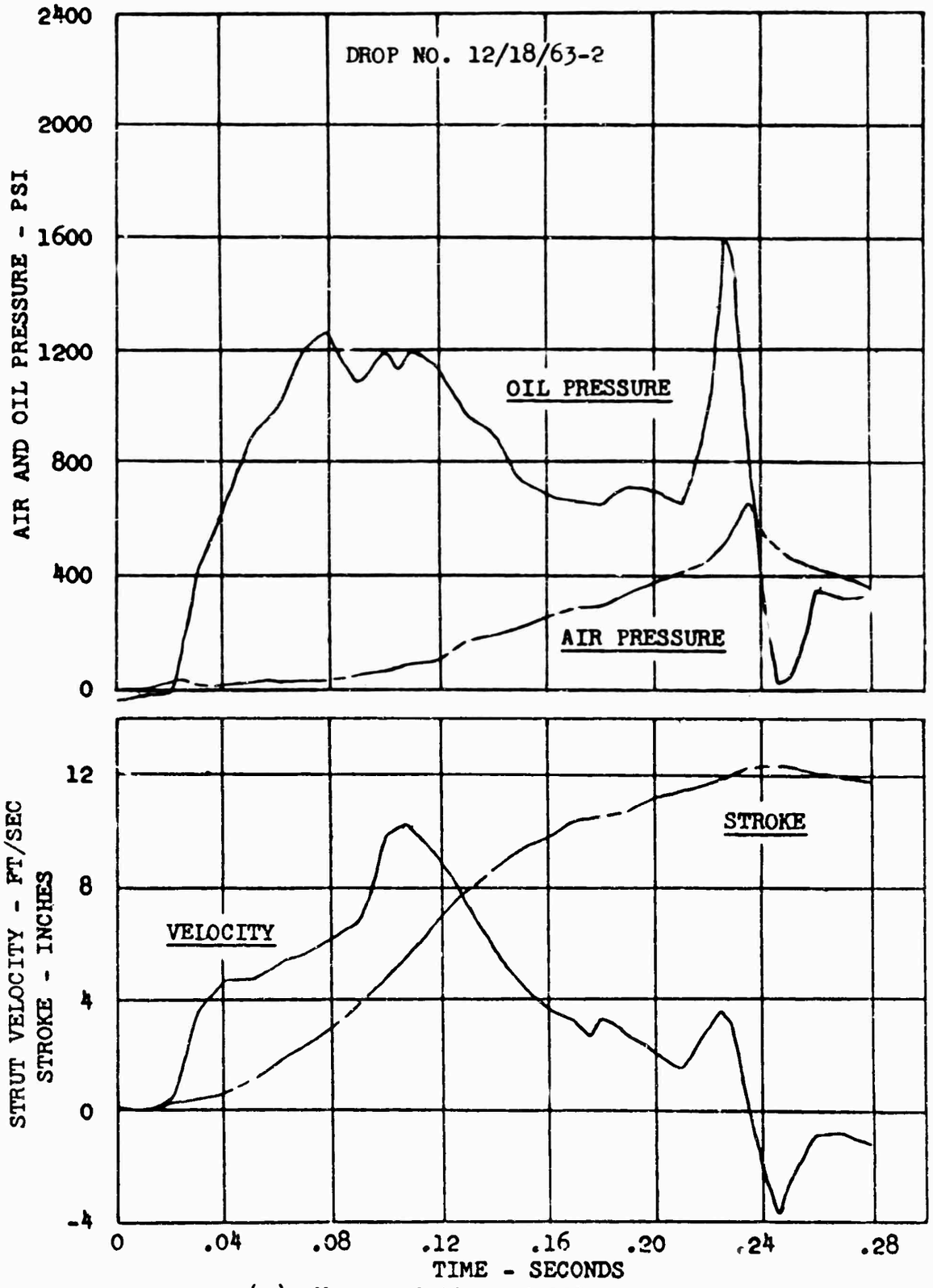

(c) Measured Air and Oil Pressures and Measured Strut Stroke and Velocity.
Figure 35. Concluded.

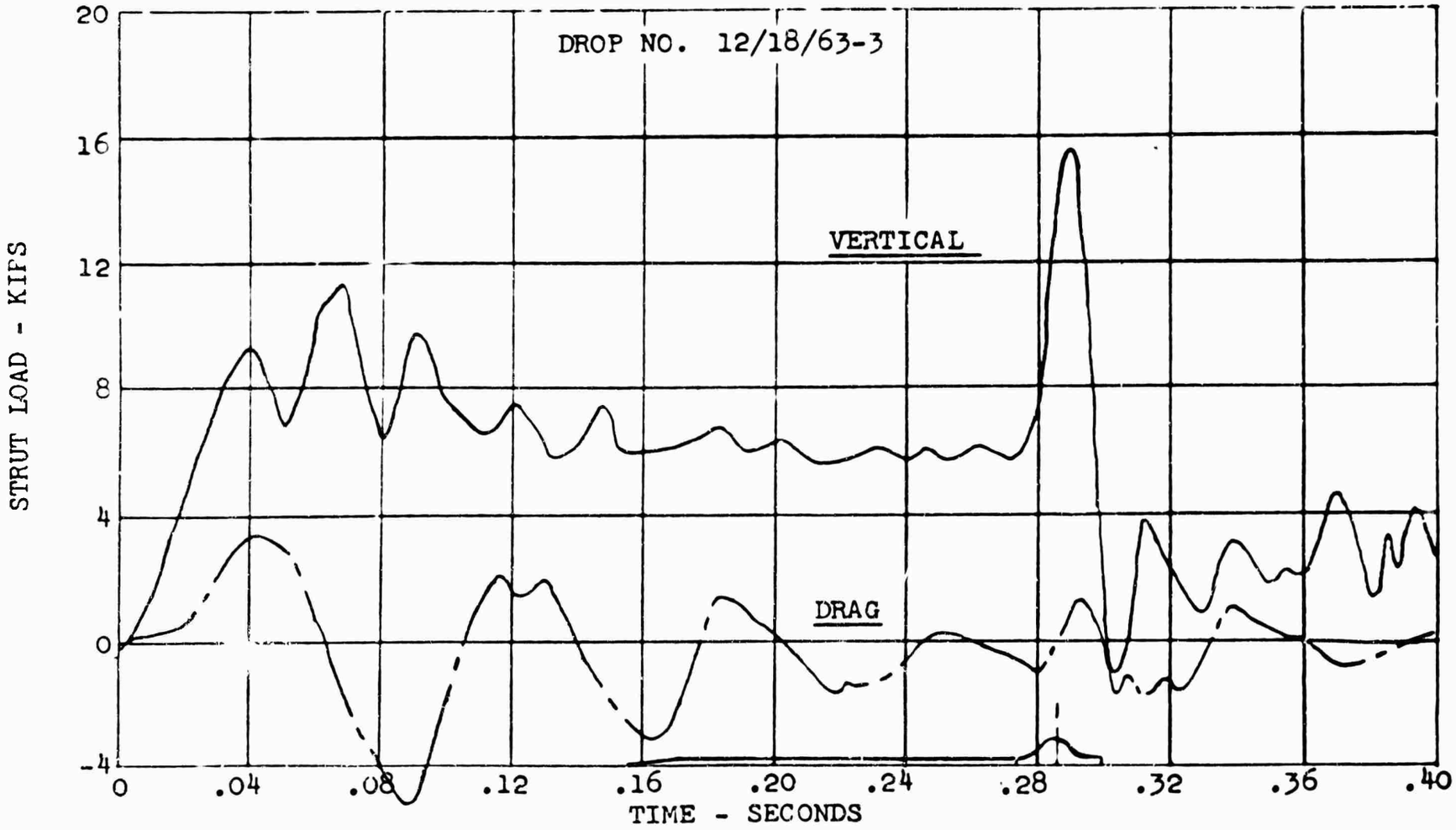

(a) Measured Loads at Axle.

Figure 36. Measured Loads, Pressures, and Axle Motion for an 8.6-FPS Drop on a 3-Inch 1-Cosine Bump Oriented at 45 Degrees to the Runway.

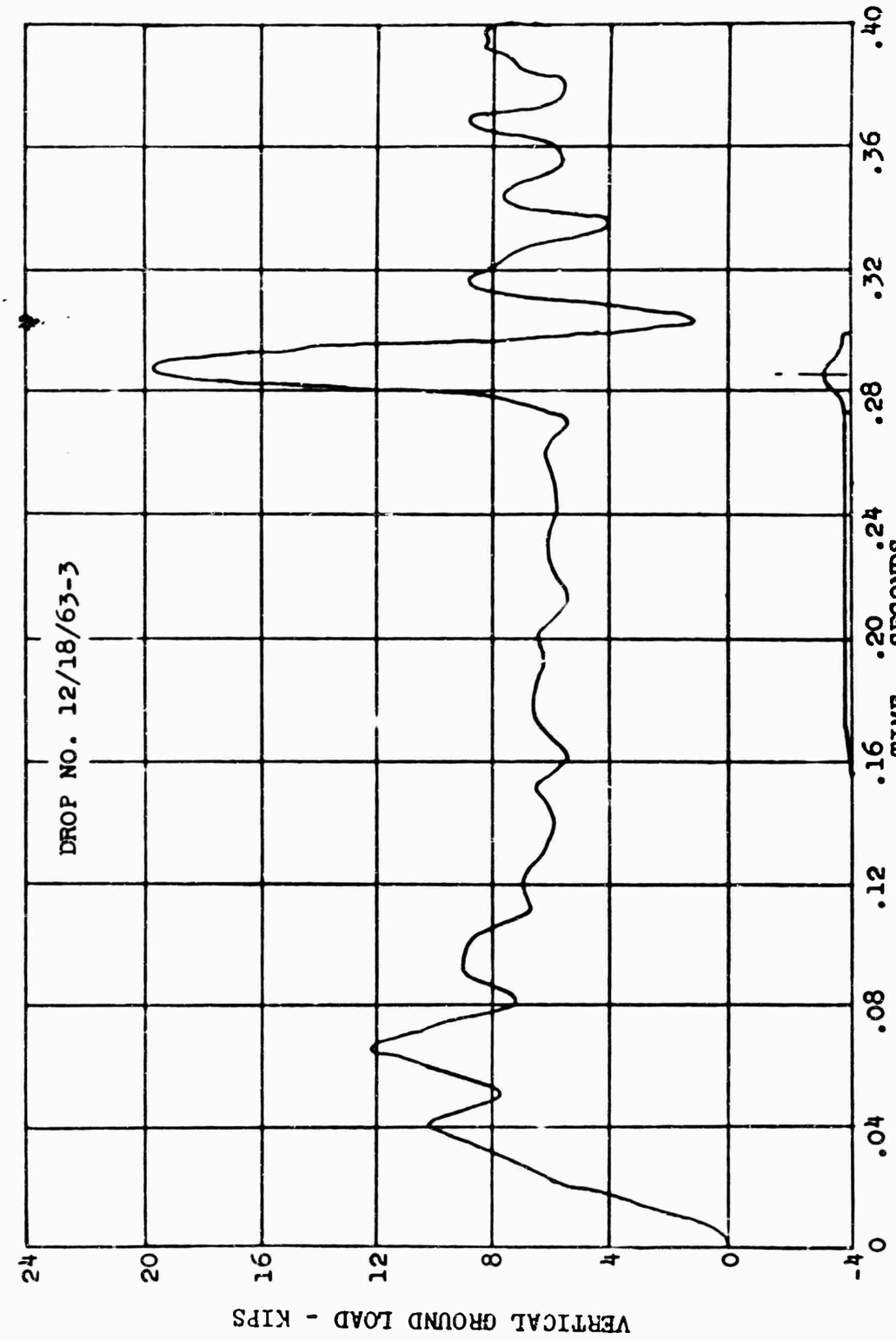

(b) Measured Vertical Loads at Ground.

Figure 36. Continued.

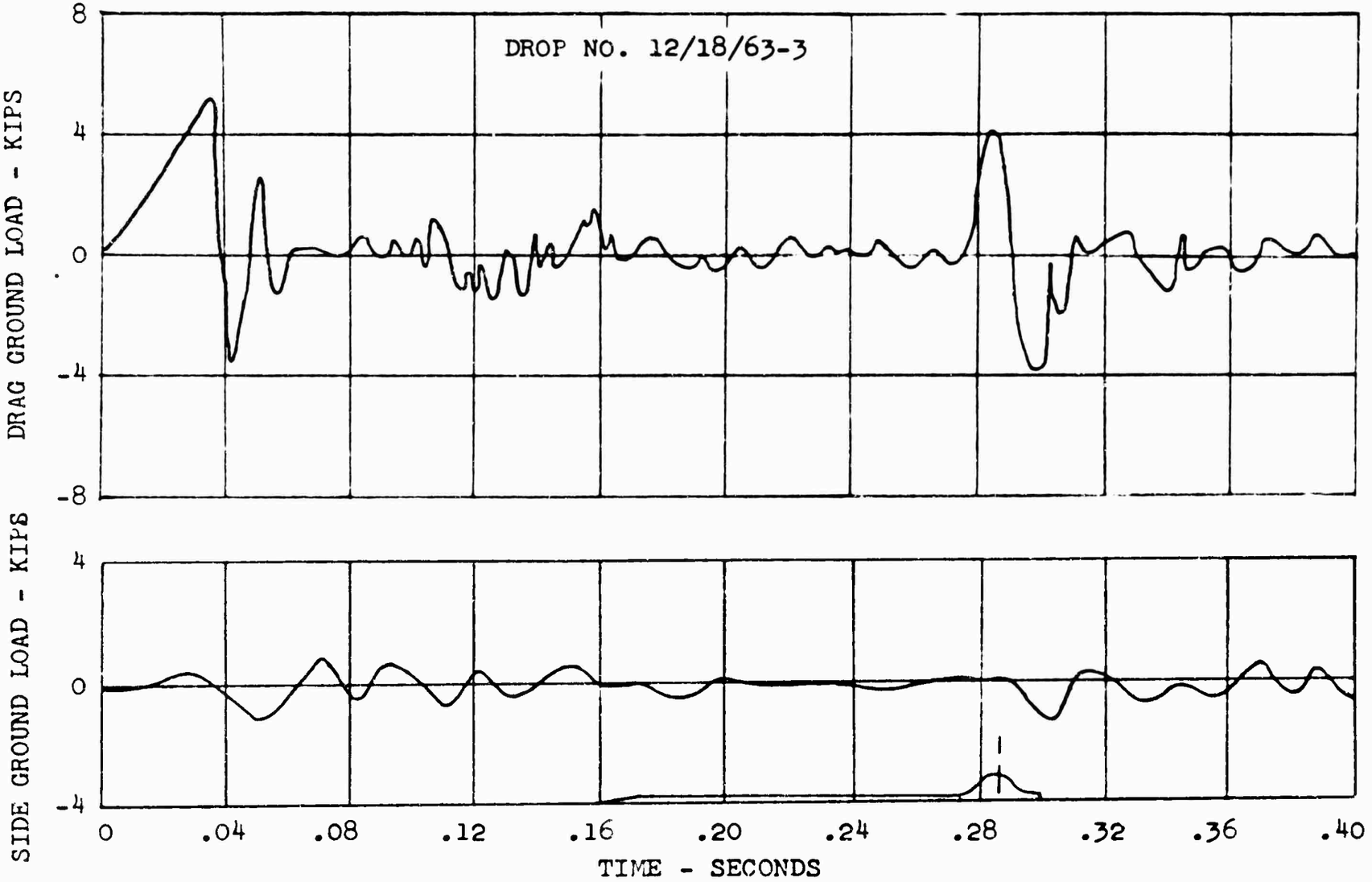

(c) Measured Horizontal and Side Load at Ground.

Figure 36. Continued.

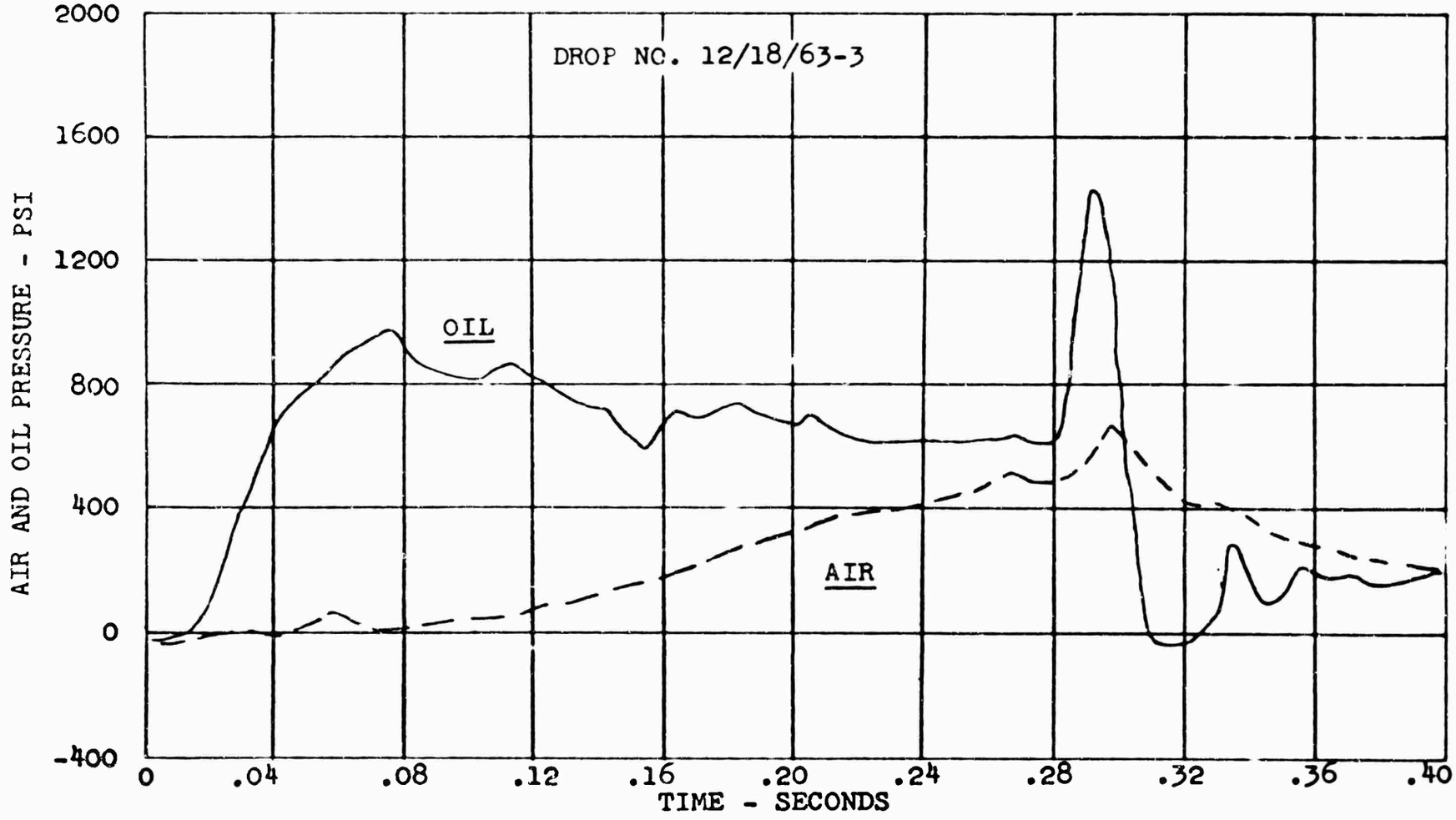

(d) Measured Strut Air and Oil Pressures.

Figure 36. Continued.

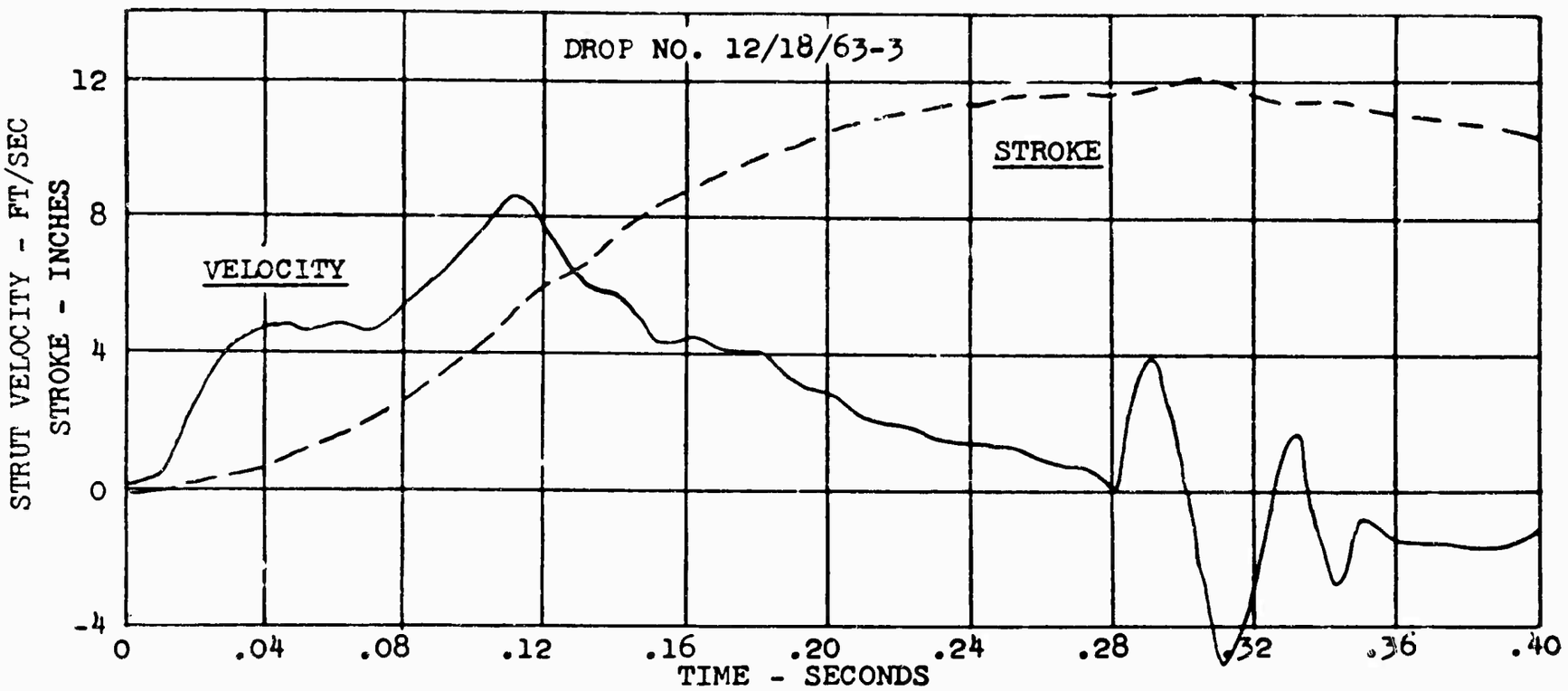

(e) Measured Strut Stroke and Compressing Velocity.

Figure 36. Concluded.

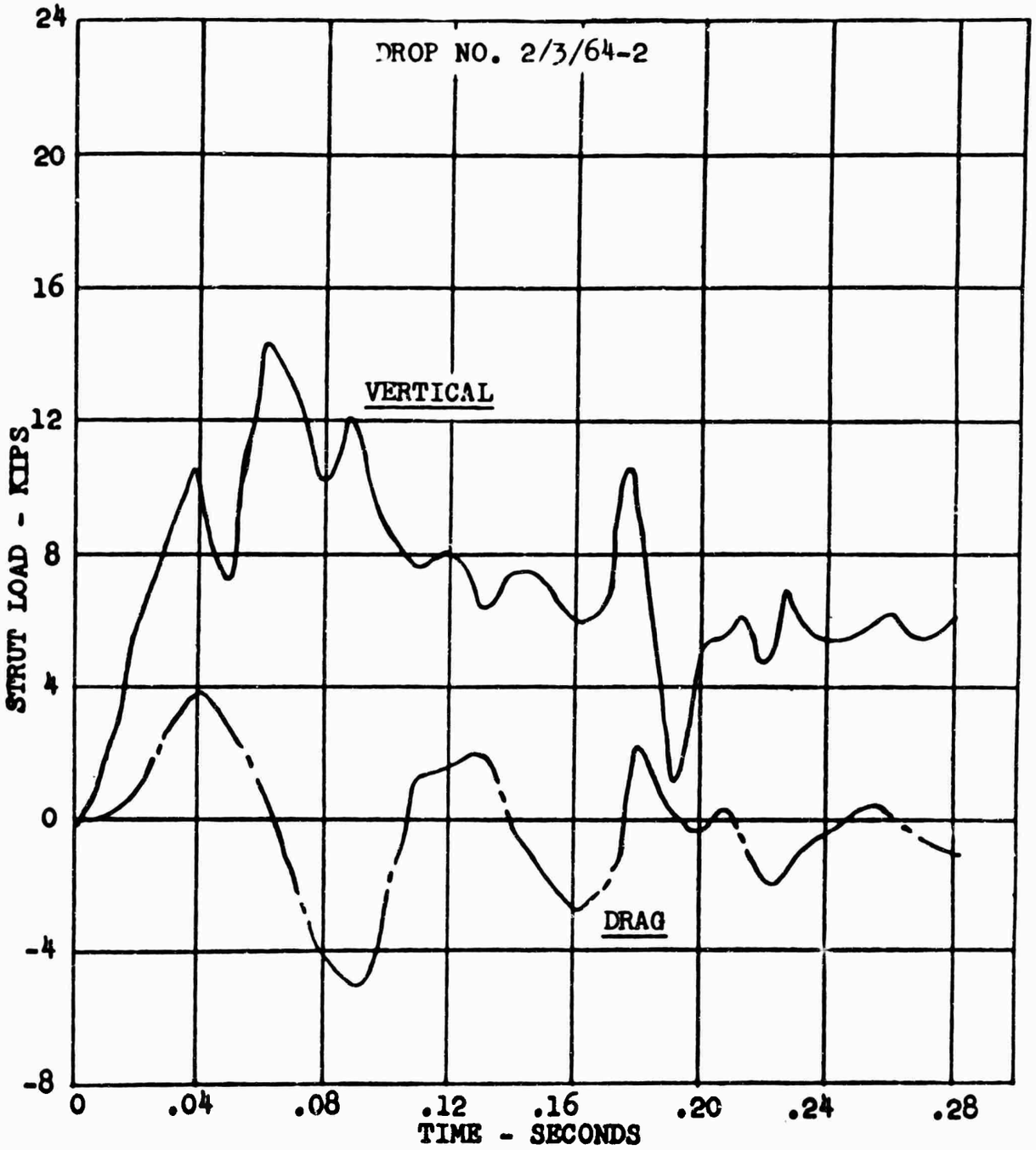

(a) Measured Loads at Axle.

Figure 37. Measured Loads, Pressures, and Axle Motion for a 7.7-FPS Drop on a 3-Inch Half Cylinder.

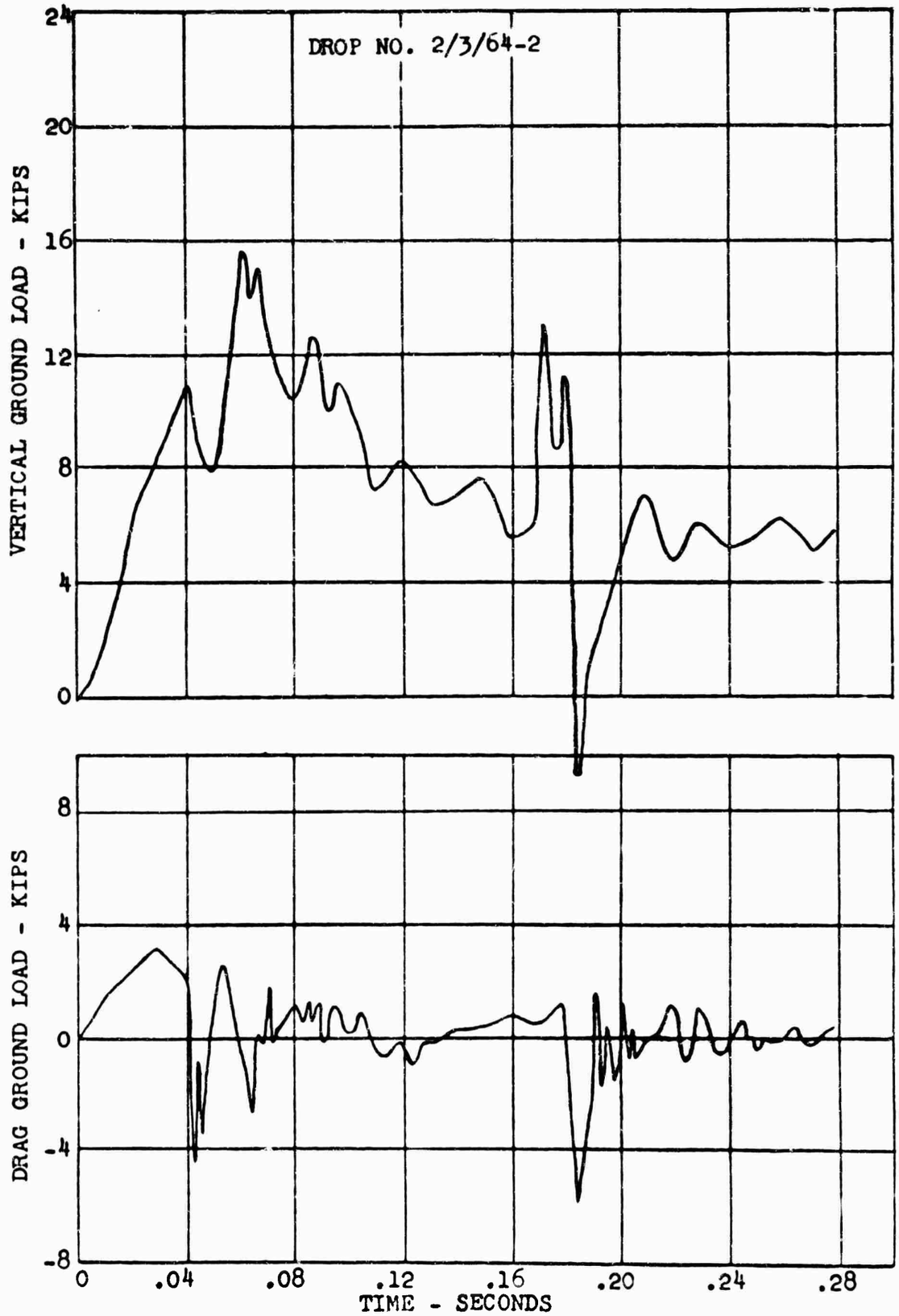

(b) Measured Loads at Ground.

Figure 37. Continued.

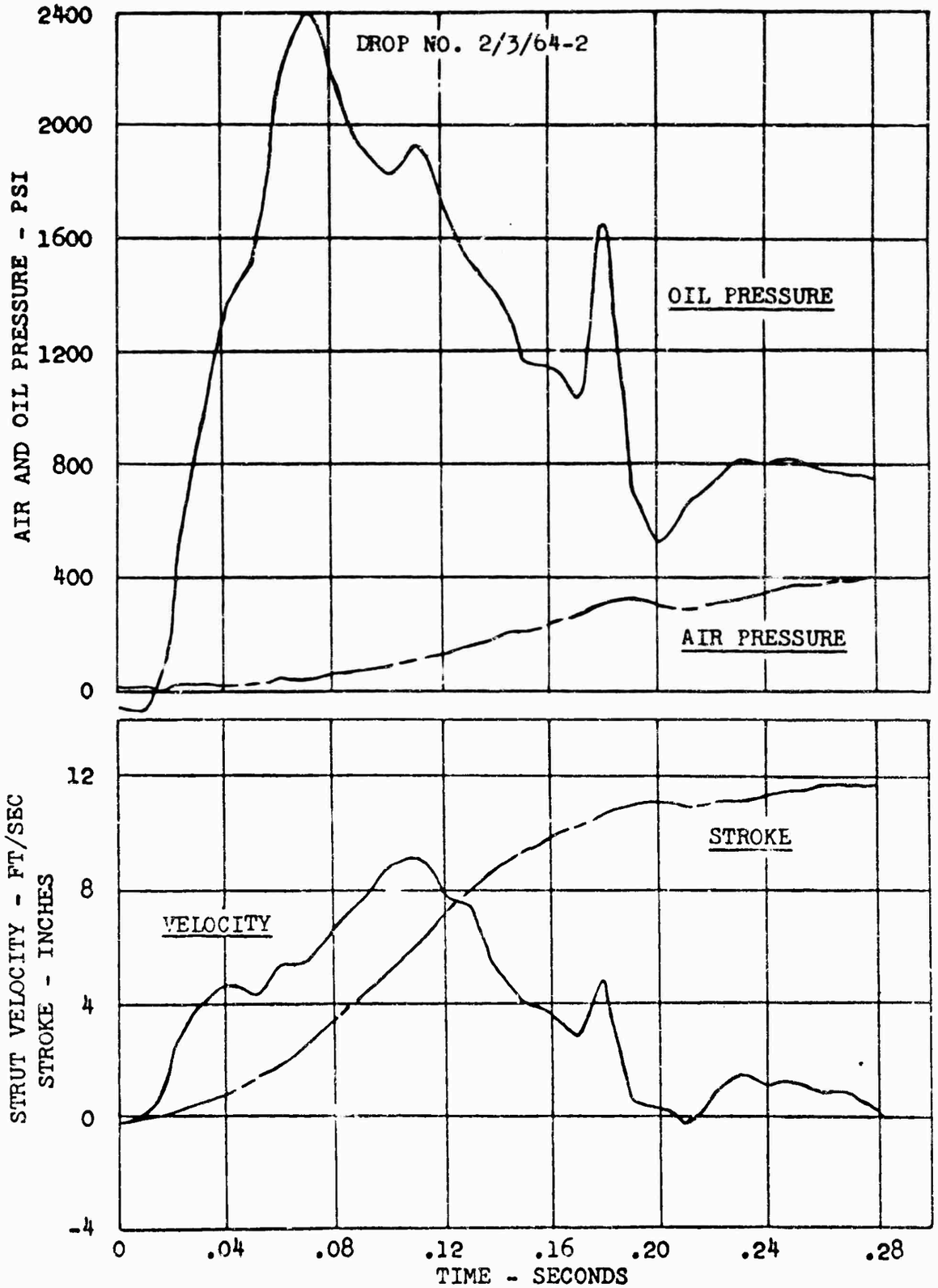

(c) Measured Strut Pressures and Measured Strut Stroke and Velocity.

Figure 37. Concluded.

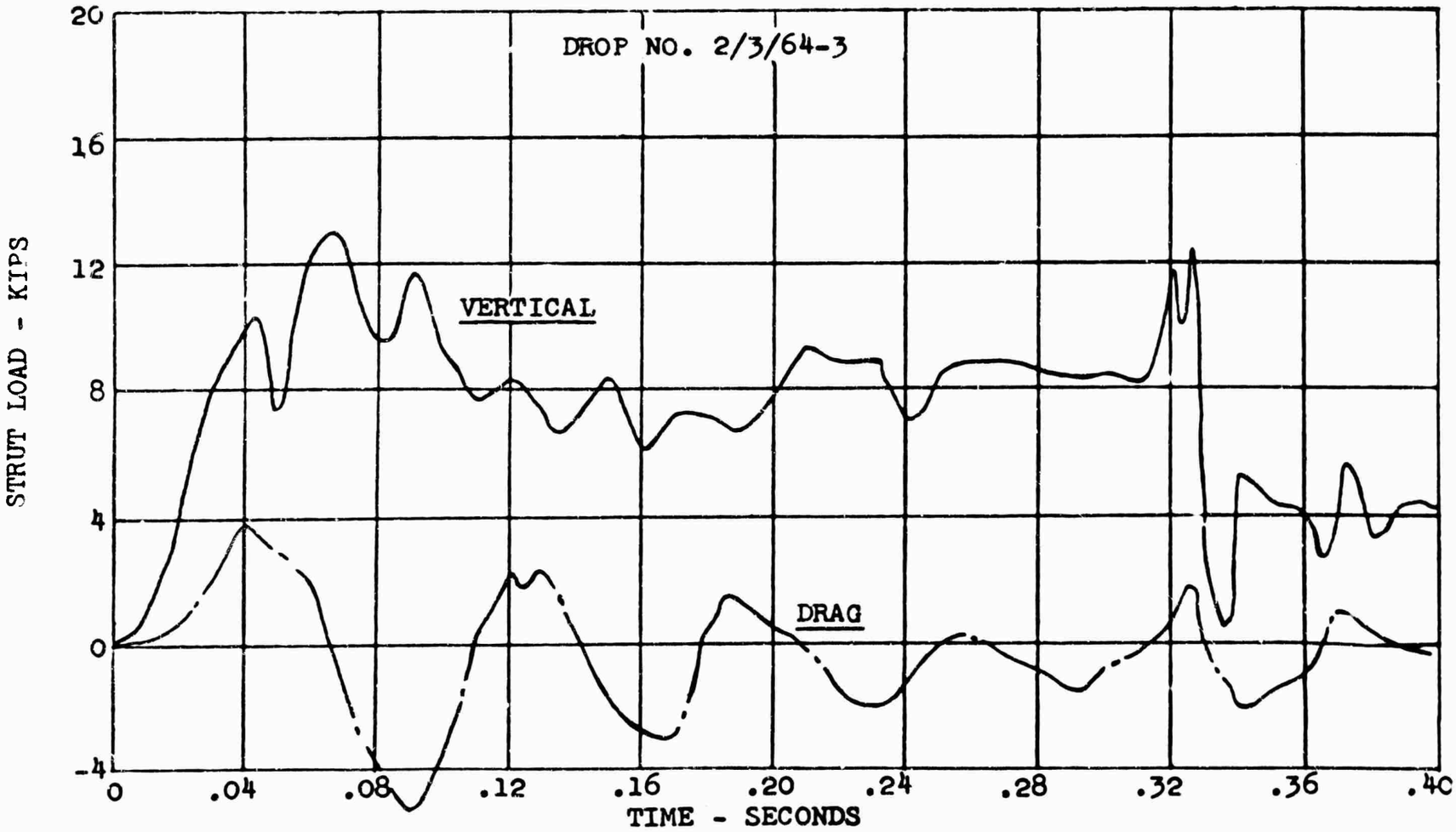

(a) Measured Loads at Axle.

Figure 38. Measured Loads, Pressures and Axle Motion for a 7.5-FPS Drop on a 3-Inch Half Cylinder.

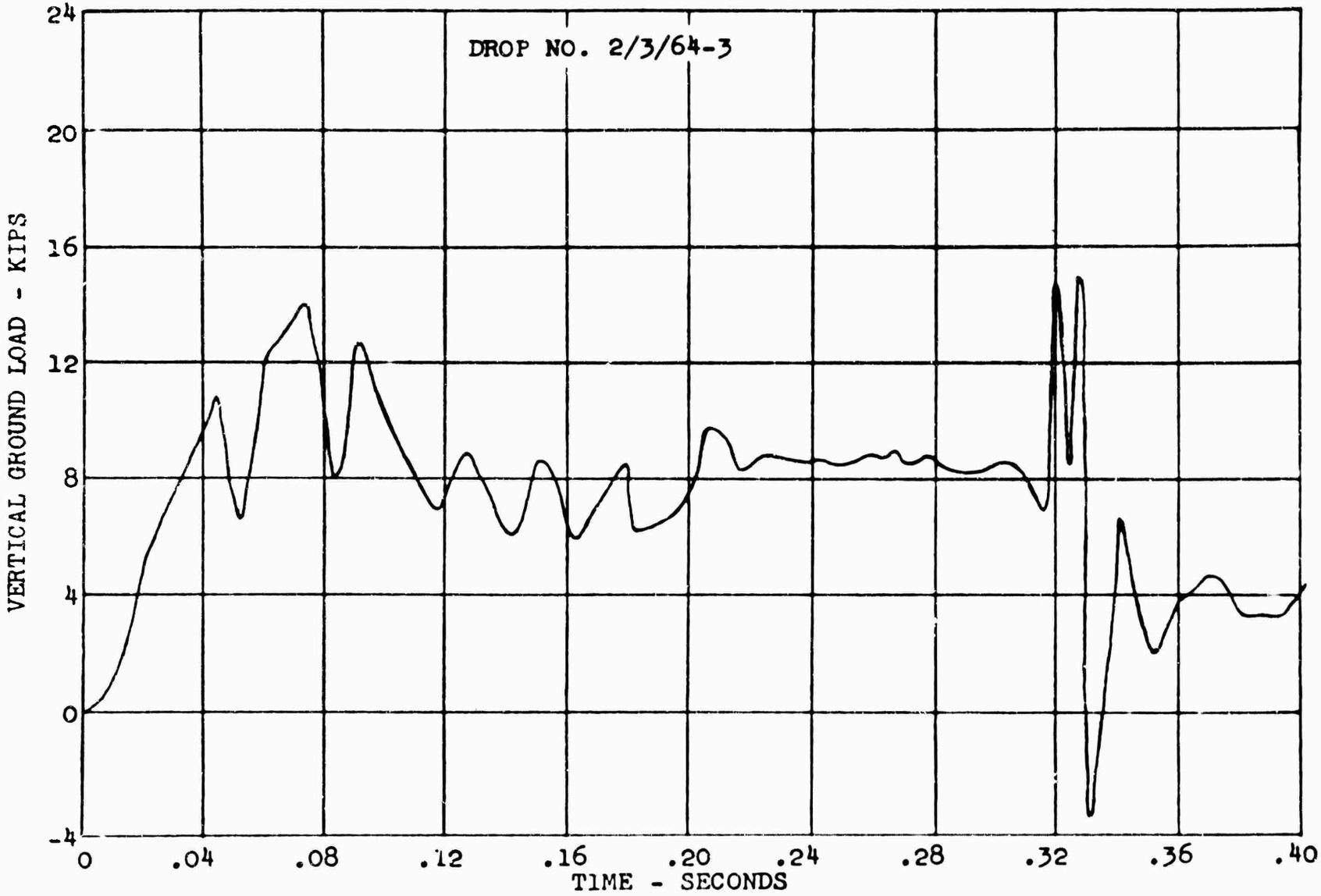

(b) Measured Vertical Load at Ground.

Figure 38. Continued.

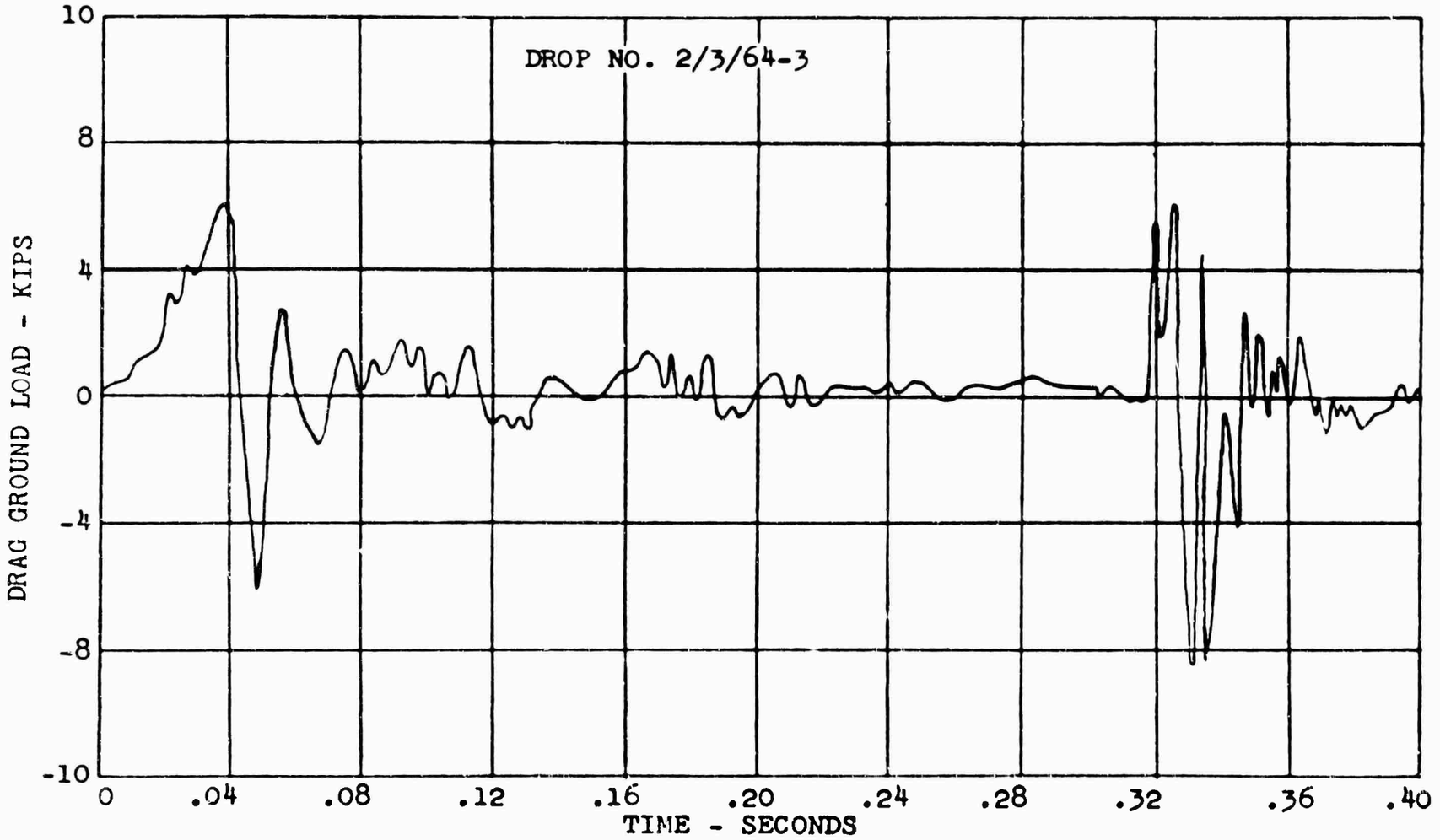

(c) Measured Horizontal Load at Ground.

Figure 38. Continued.

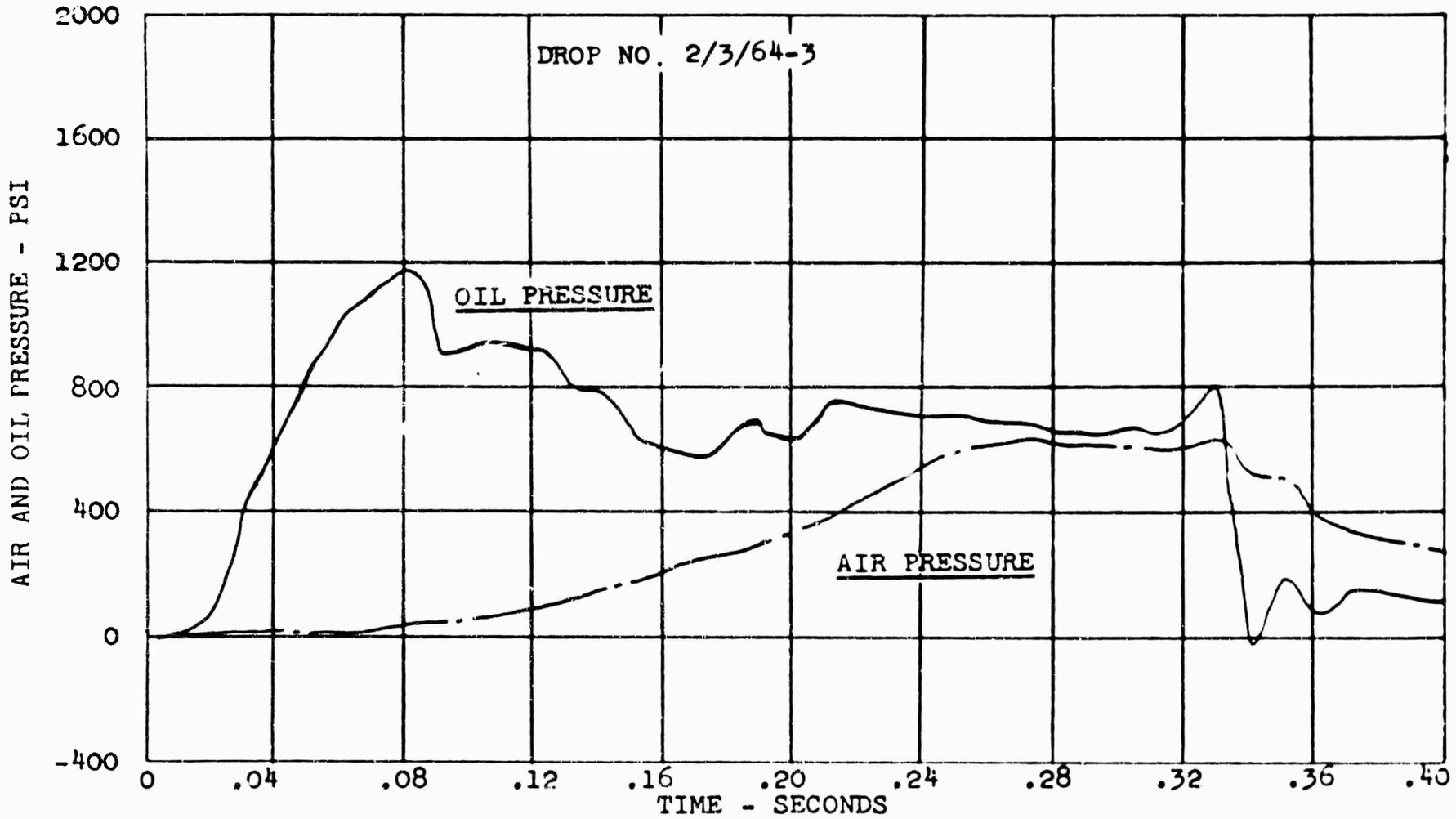

(d) Measured Strut Air and Oil Pressures.

Figure 38. Continued.

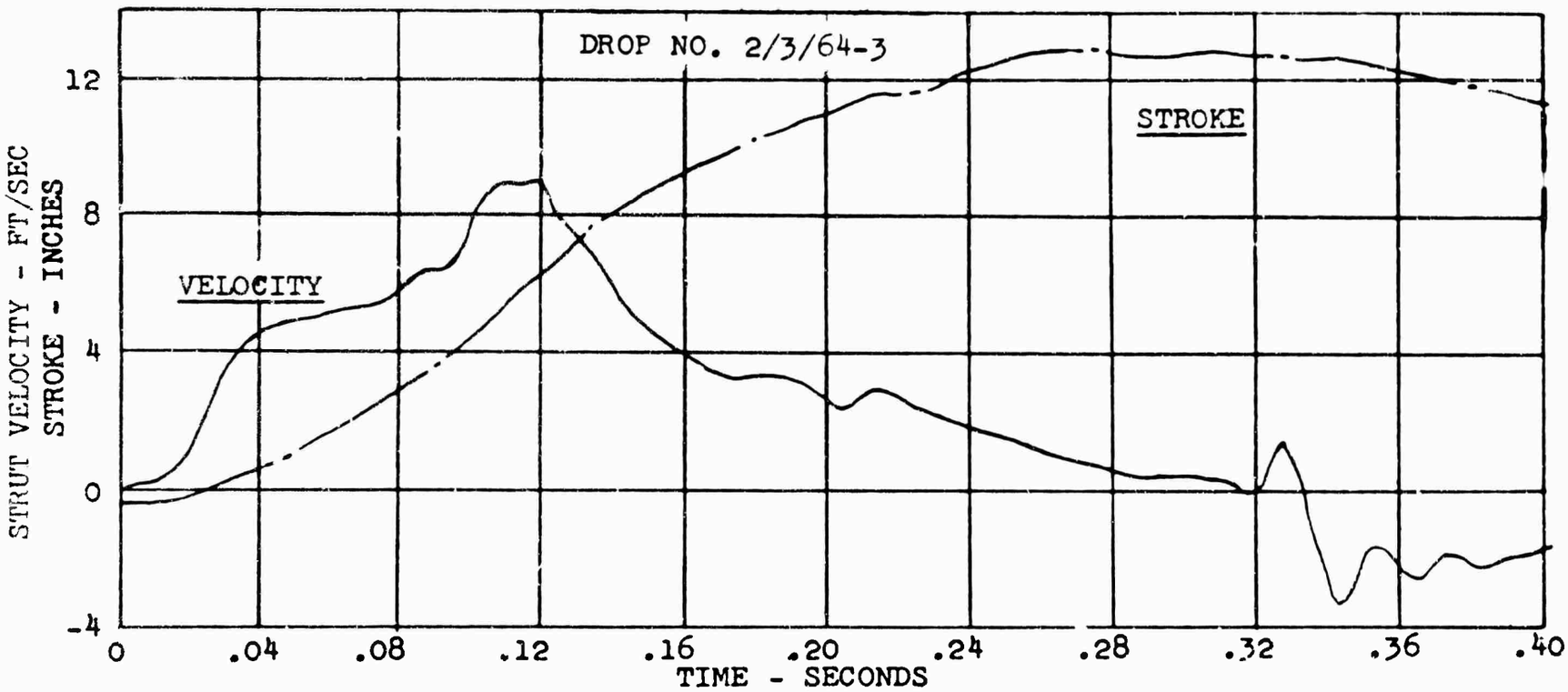

(e) Measured Strut Stroke and Compressing Velocity.

Figure 38. Concluded.

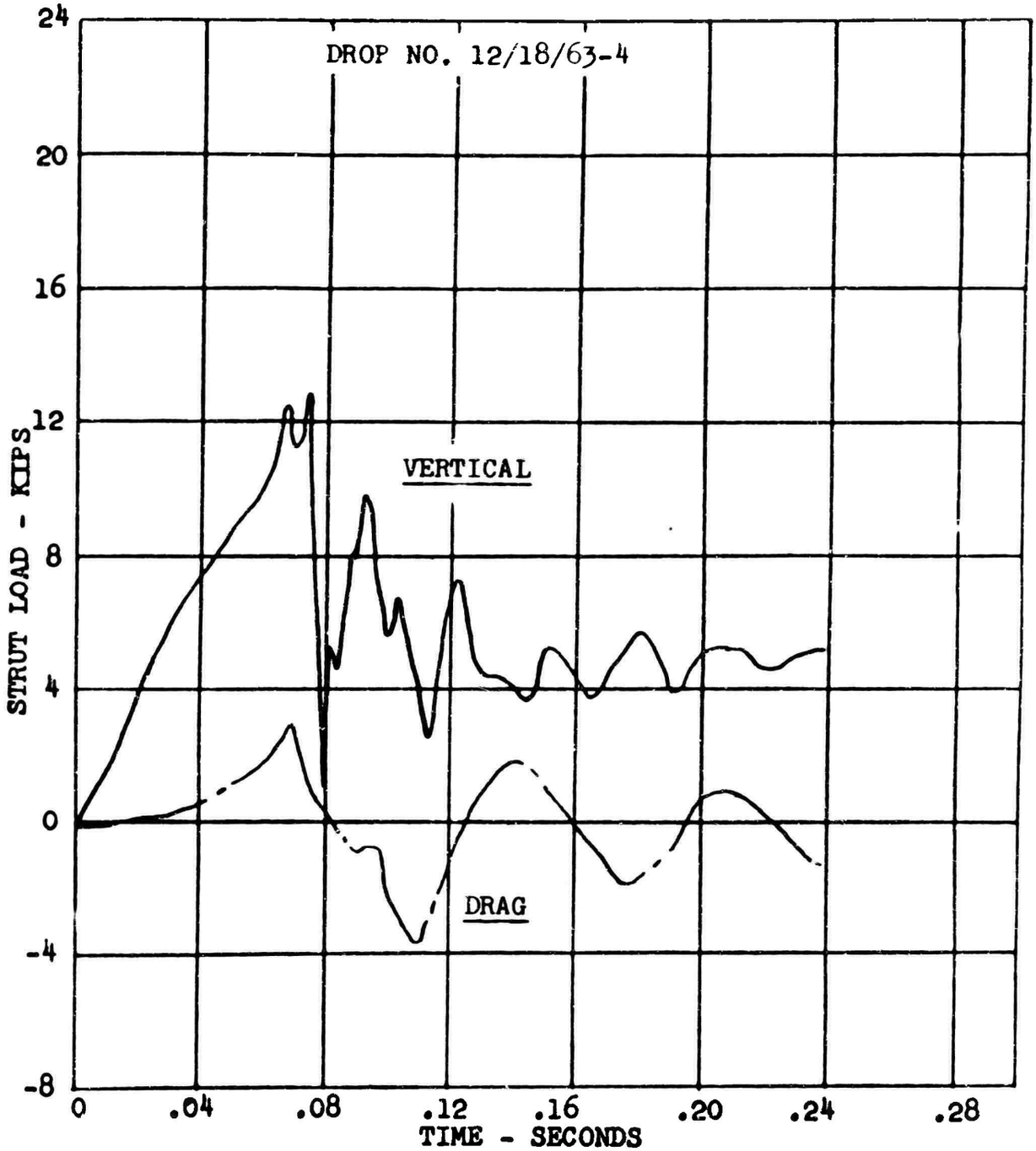

(a) Measured Loads at Axle.

Figure 39. Measured Loads, Pressures and Axle Motion for a 7.9-FPS Drop on a 3-Inch Hemisphere.

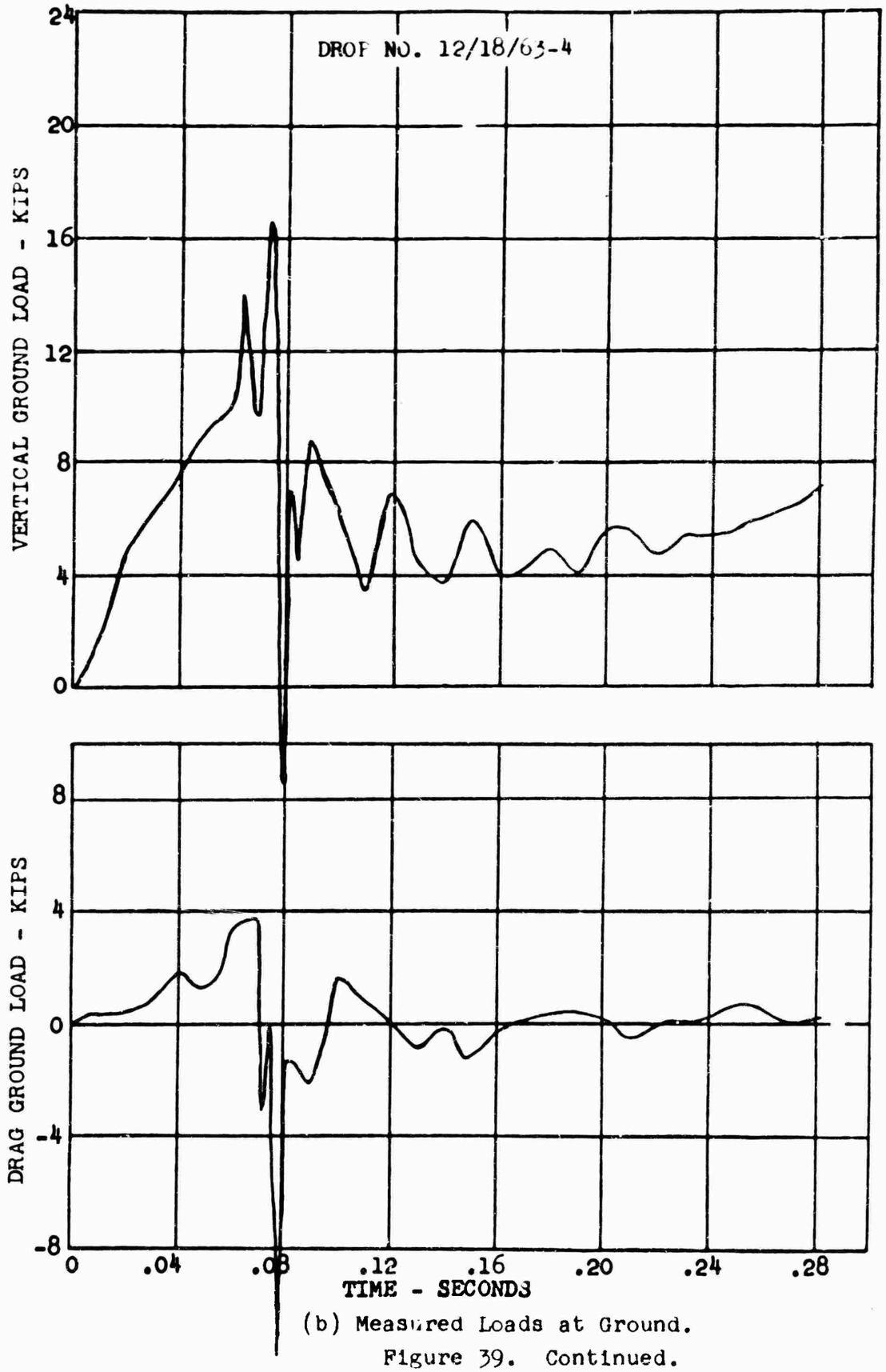

(b) Measured Loads at Ground.

Figure 39. Continued.

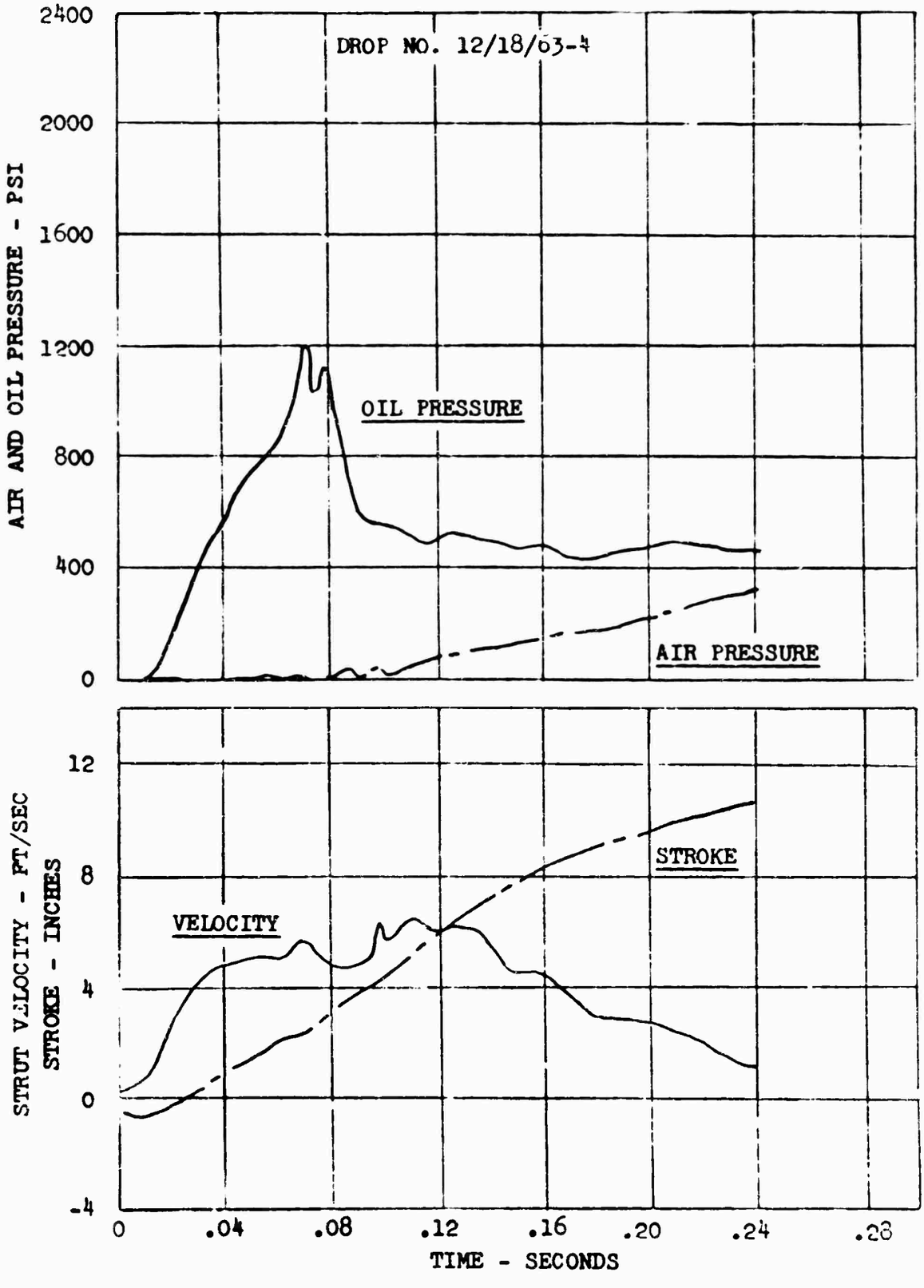

(c) Measured Strut Pressures and Measured Strut Stroke and Velocity.

Figure 39. Concluded.

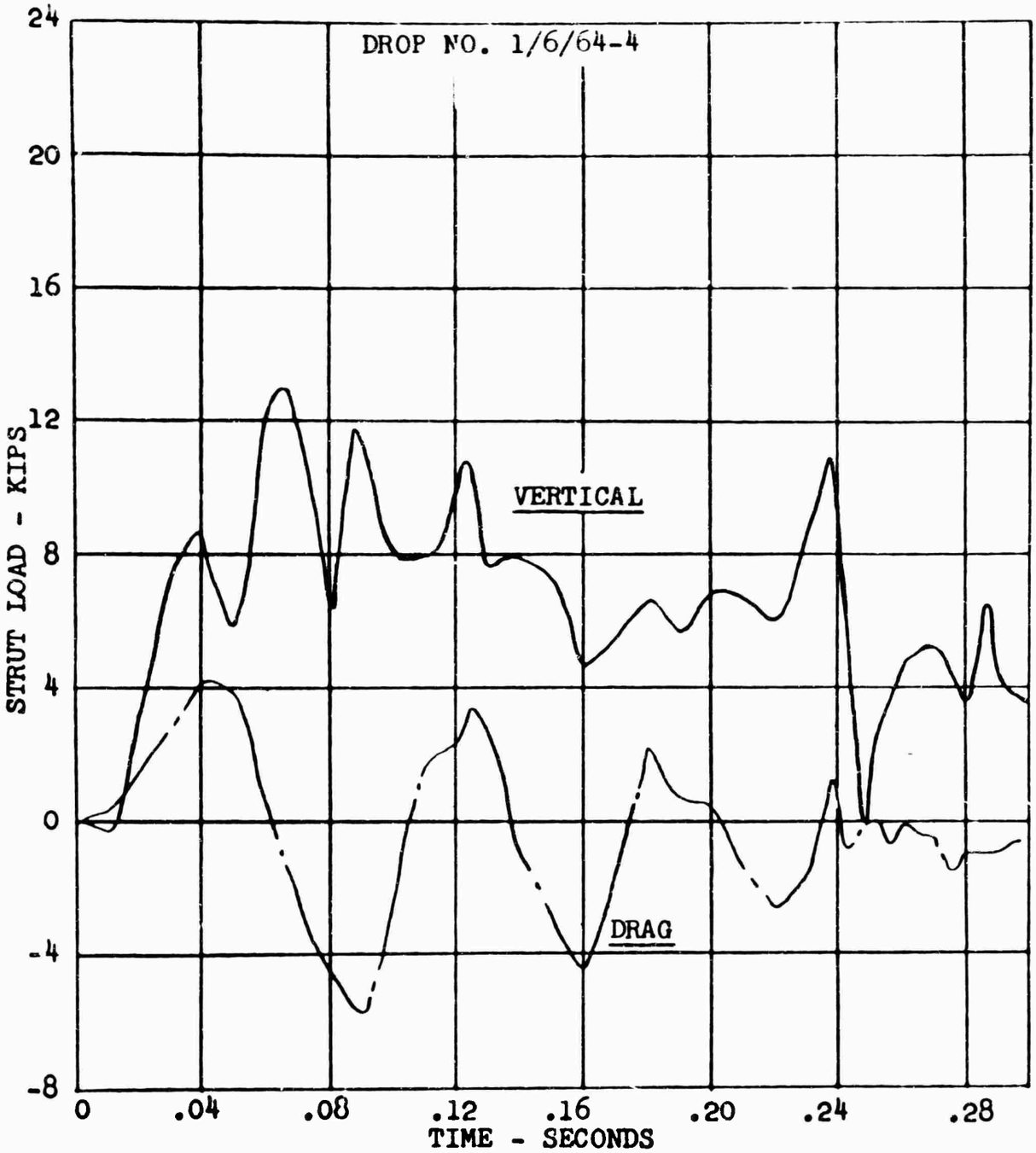

(a) Measured Loads at Axle.

Figure 40. Measured Loads, Pressures and Axle Motion for a 9.5-FPS Drop on a 3-Inch Hemisphere.

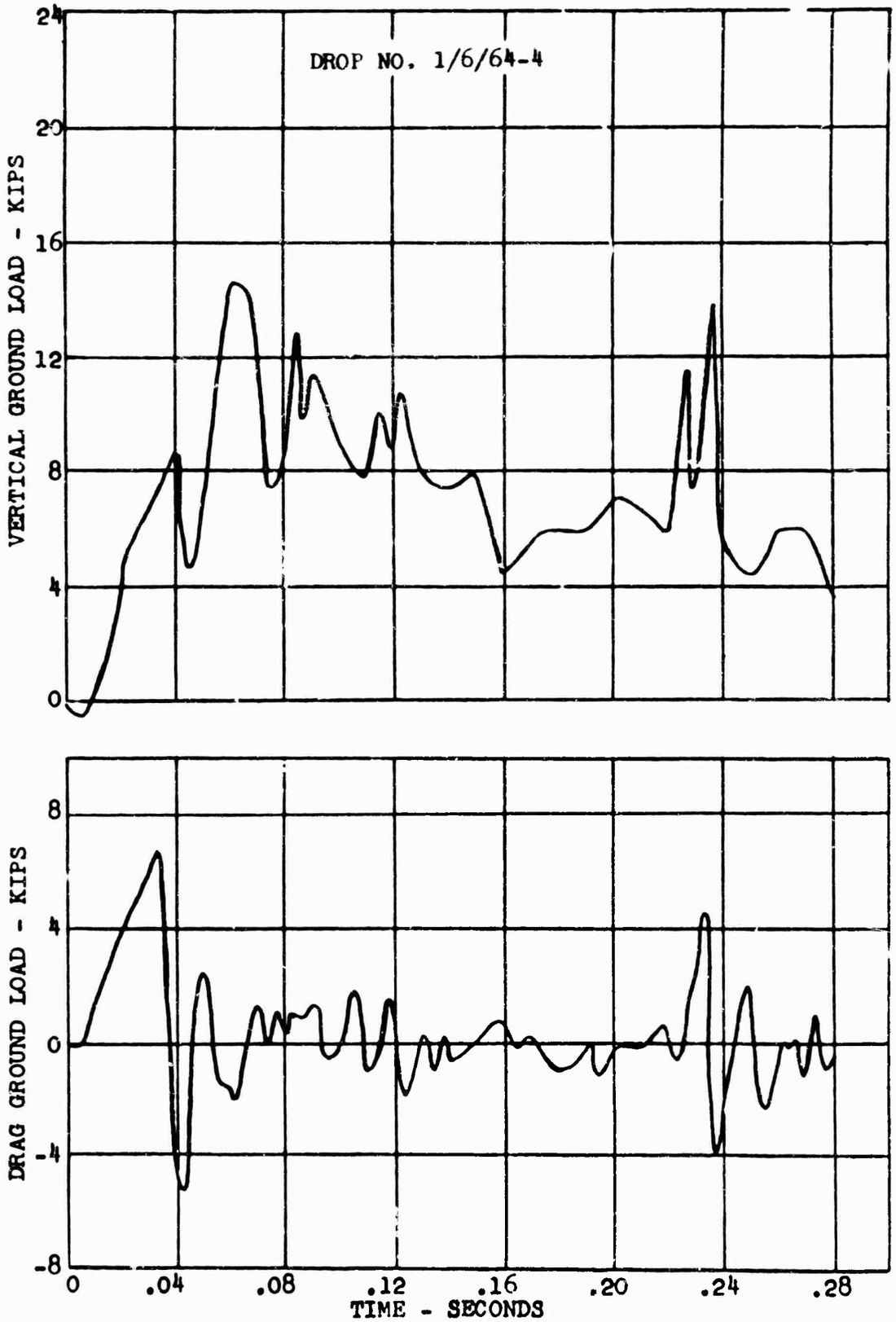

(b) Measured Loads at Ground.

Figure 40. Continued.

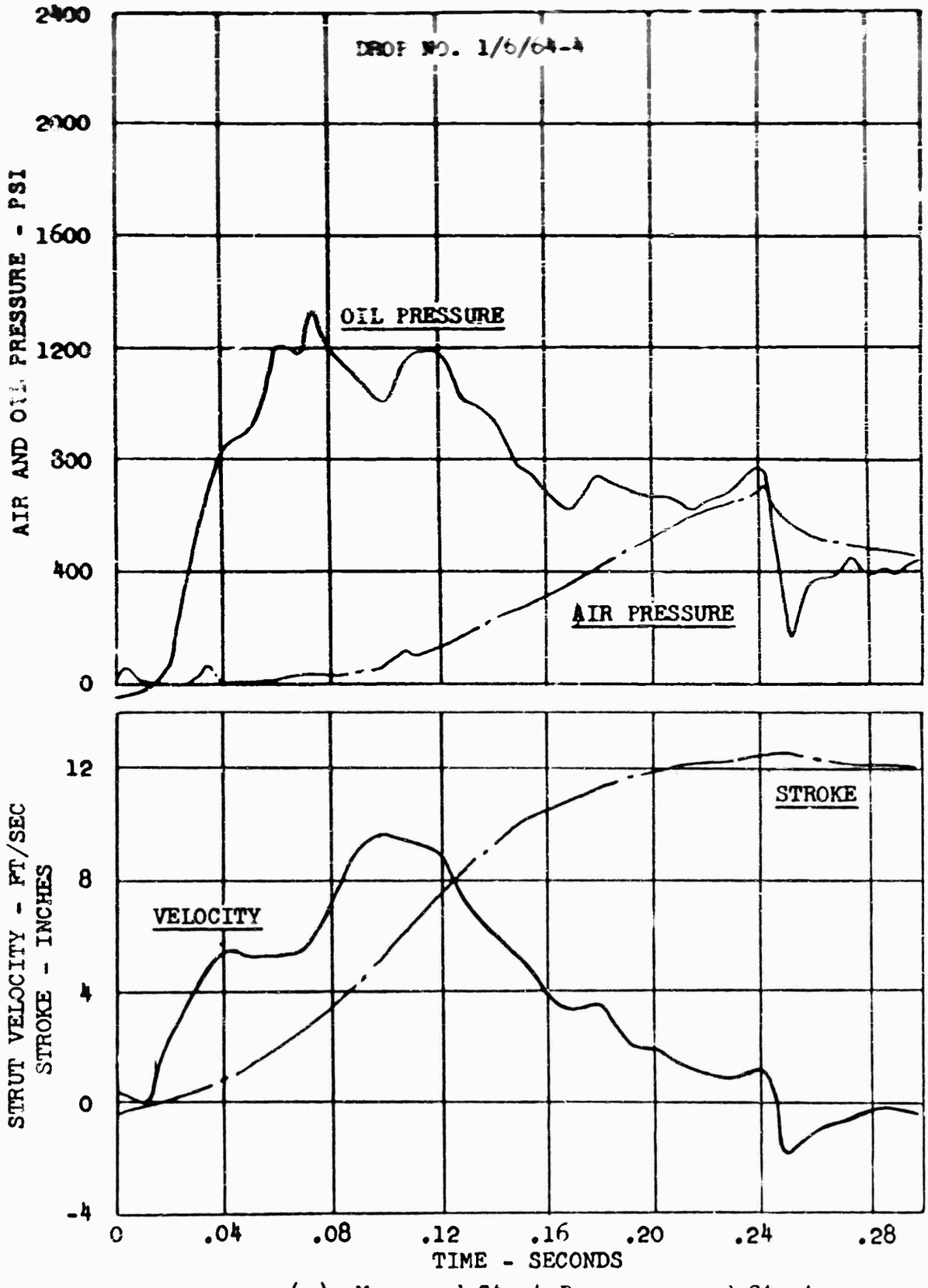

(c) Measured Strut Pressures and Strut Stroke and Velocity.

Figure 40. Concluded.

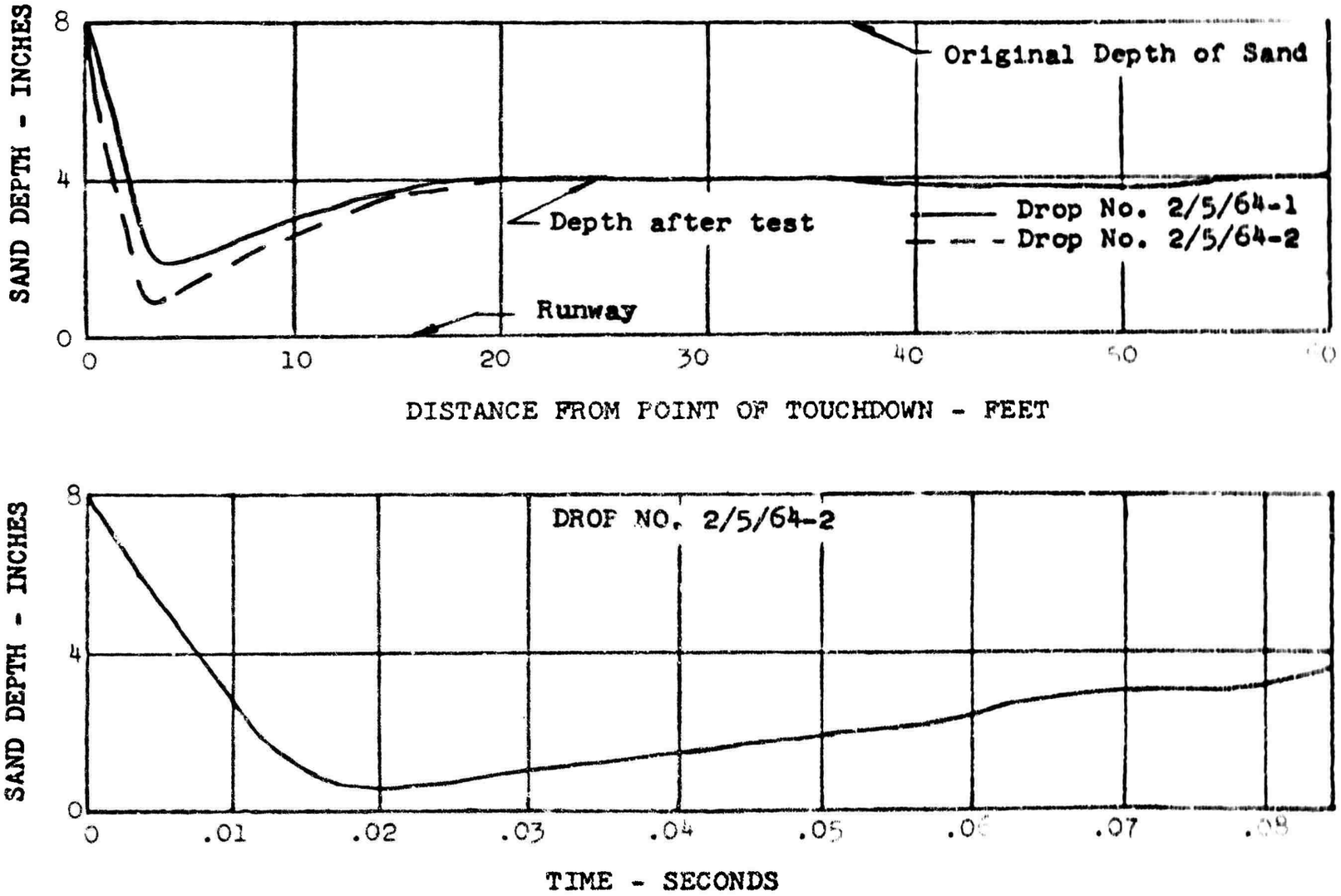

Figure 41. Depth of Sand in Rut After Test Versus Distance and Time

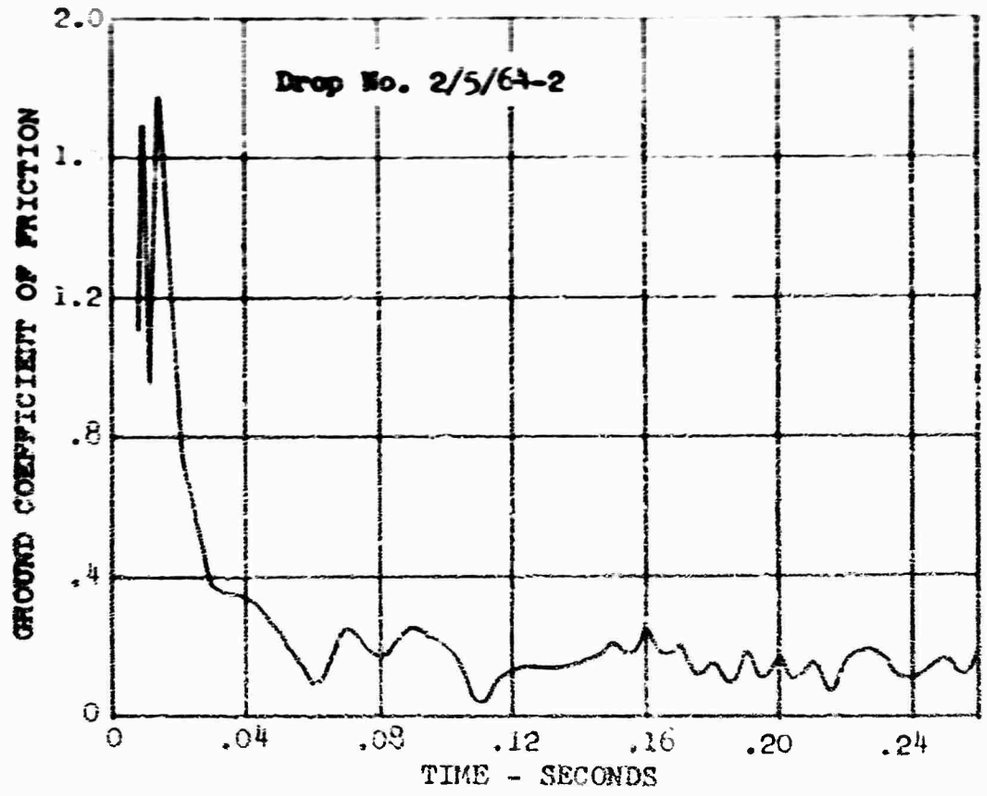

(a) Sinking Speed = 9.0 FPS, Horiz Speed = 148 FPS

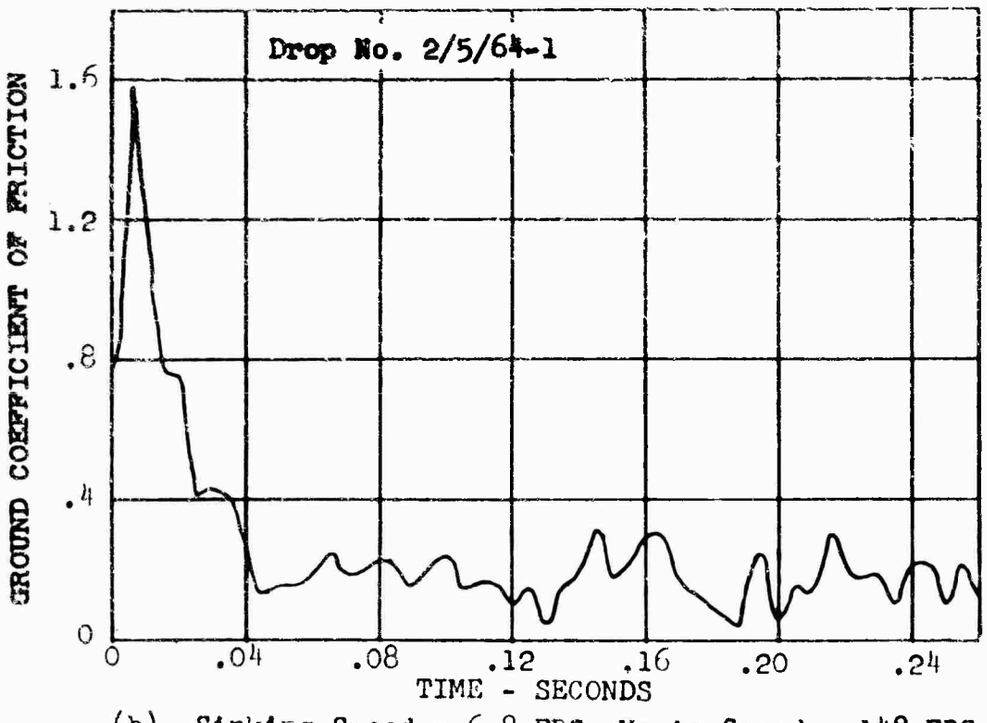

(b) Sinking Speed = 6.8 FPS, Horiz Speed = 148 FPS

Figure 42. Ground Coefficients of Friction for Drops on Sand.

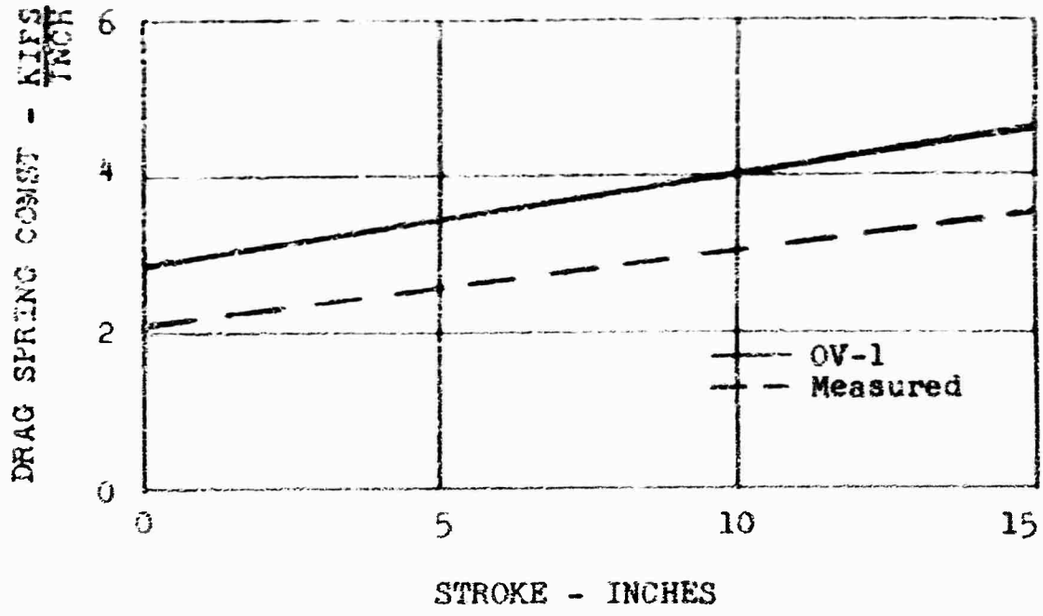

Figure 43. Comparison of OV-1 Stiffness Versus Stroke, and Stiffness Derived From Measured Data.

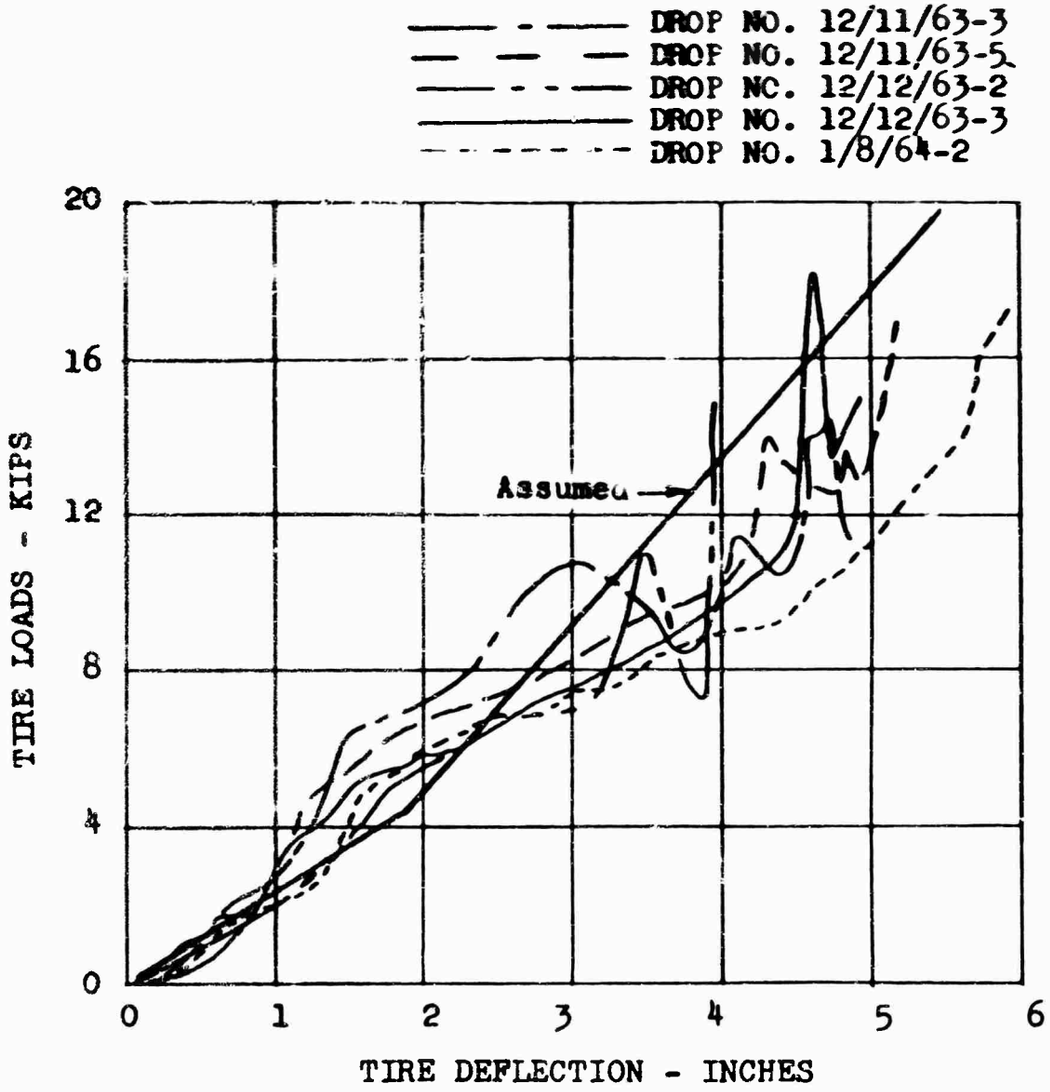

Figure 44. Comparison of Measured and Assumed Tire Load-Deflection Curves. Tire Impressed on Flat Hard Surface.

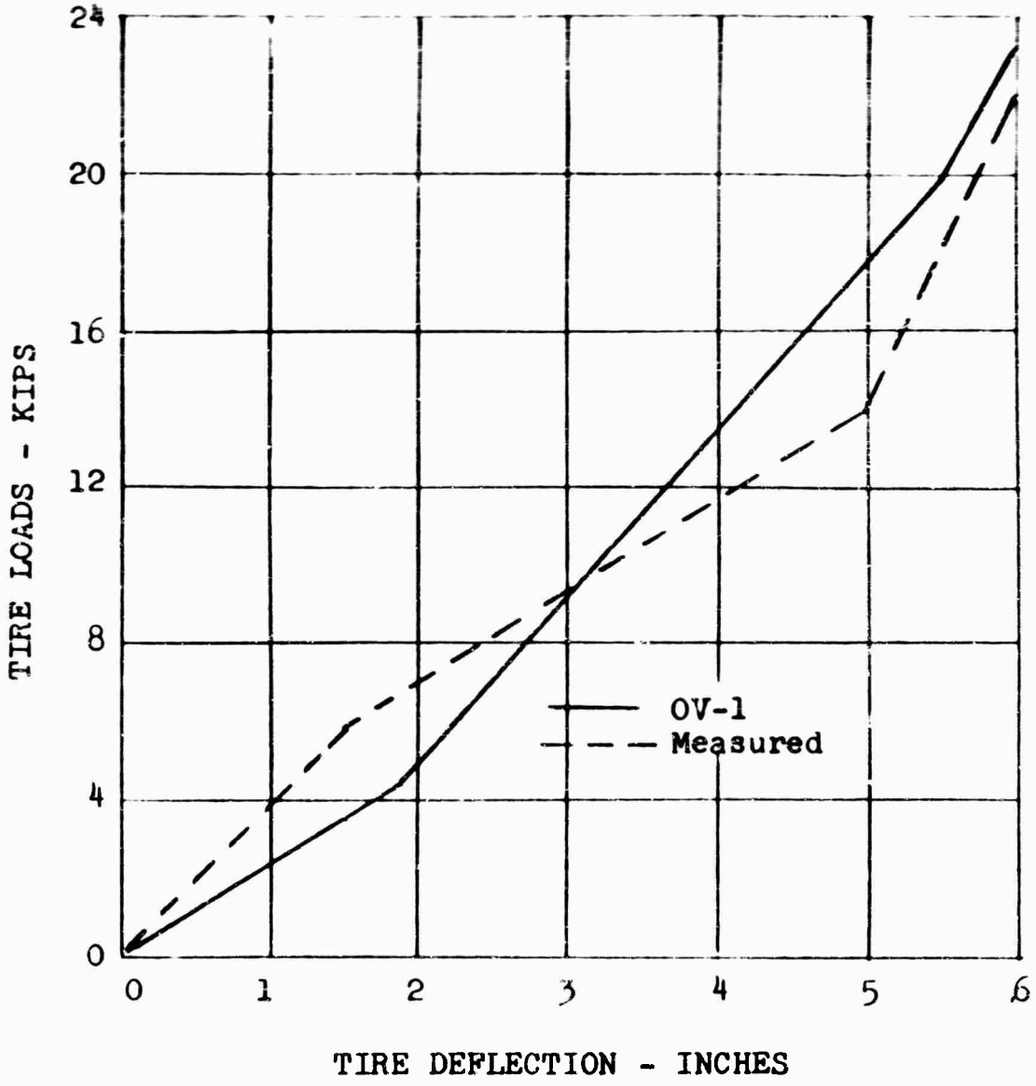

Figure 45. Comparison of OV-1 Main Gear Tire Load-Deflection Curve and Curve Derived From Measured Data.

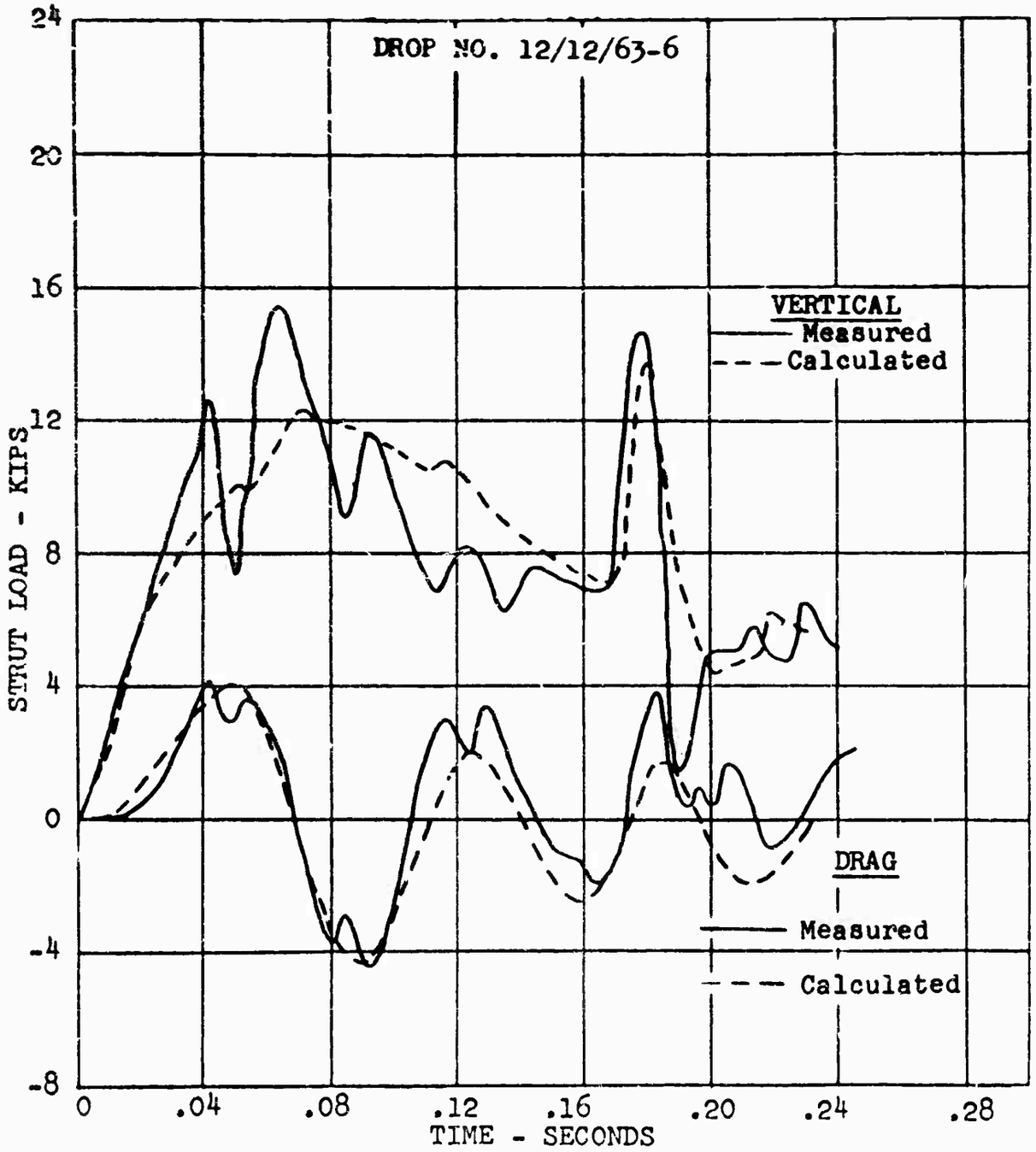

Figure 46. Comparison of Measured and Calculated Loads for an 8.8-FPS Drop on a 3-Inch 1-Cosine Bump. Calculations Revised to Improve Drag Load Correlation.

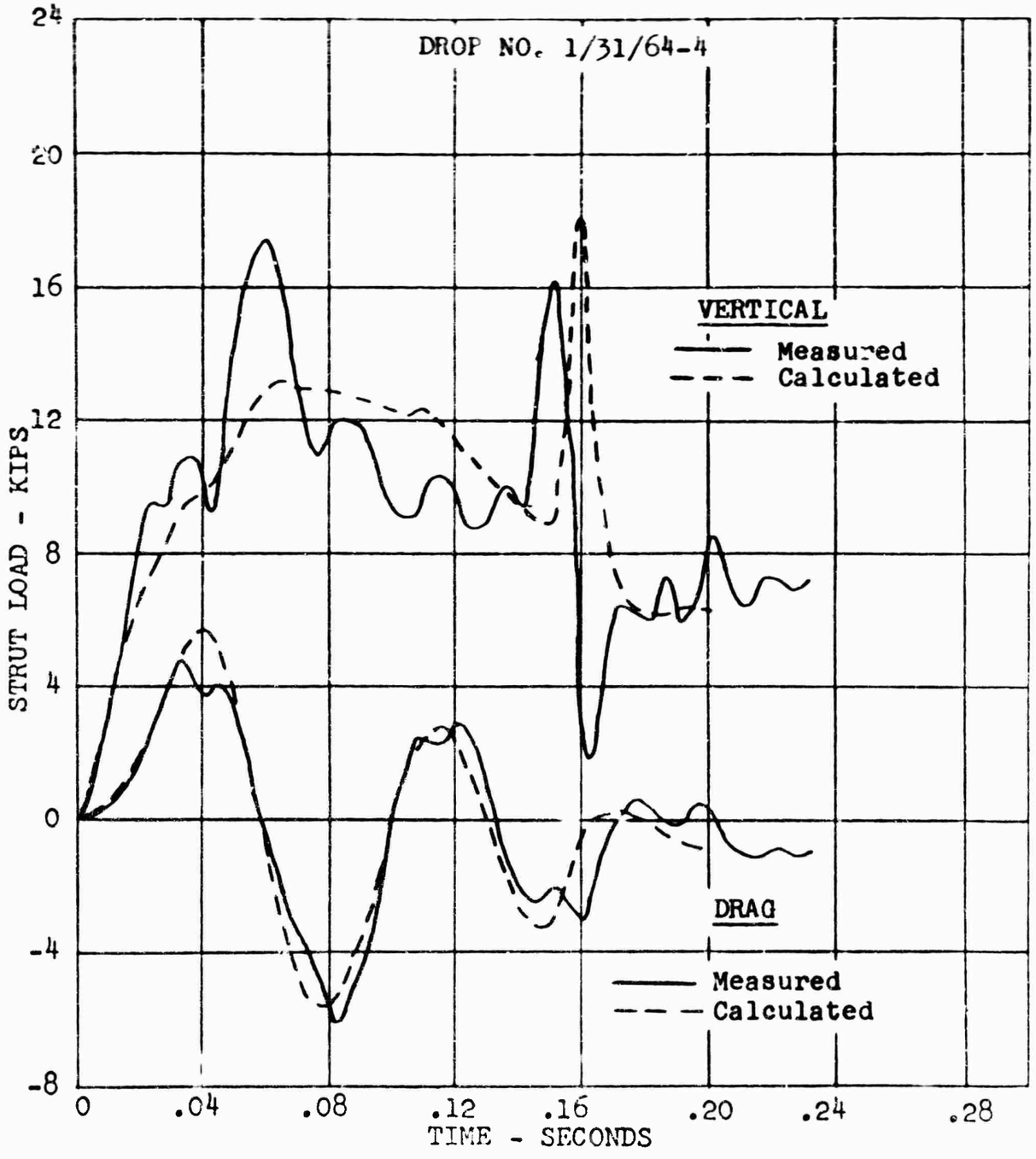

Figure 47. Comparison of Measured and Calculated Axle Loads for a 9.8-FPS Drop on a 3-Inch 1-Cosine Bump. Calculations Revised to Improve Drag Load Correlation.

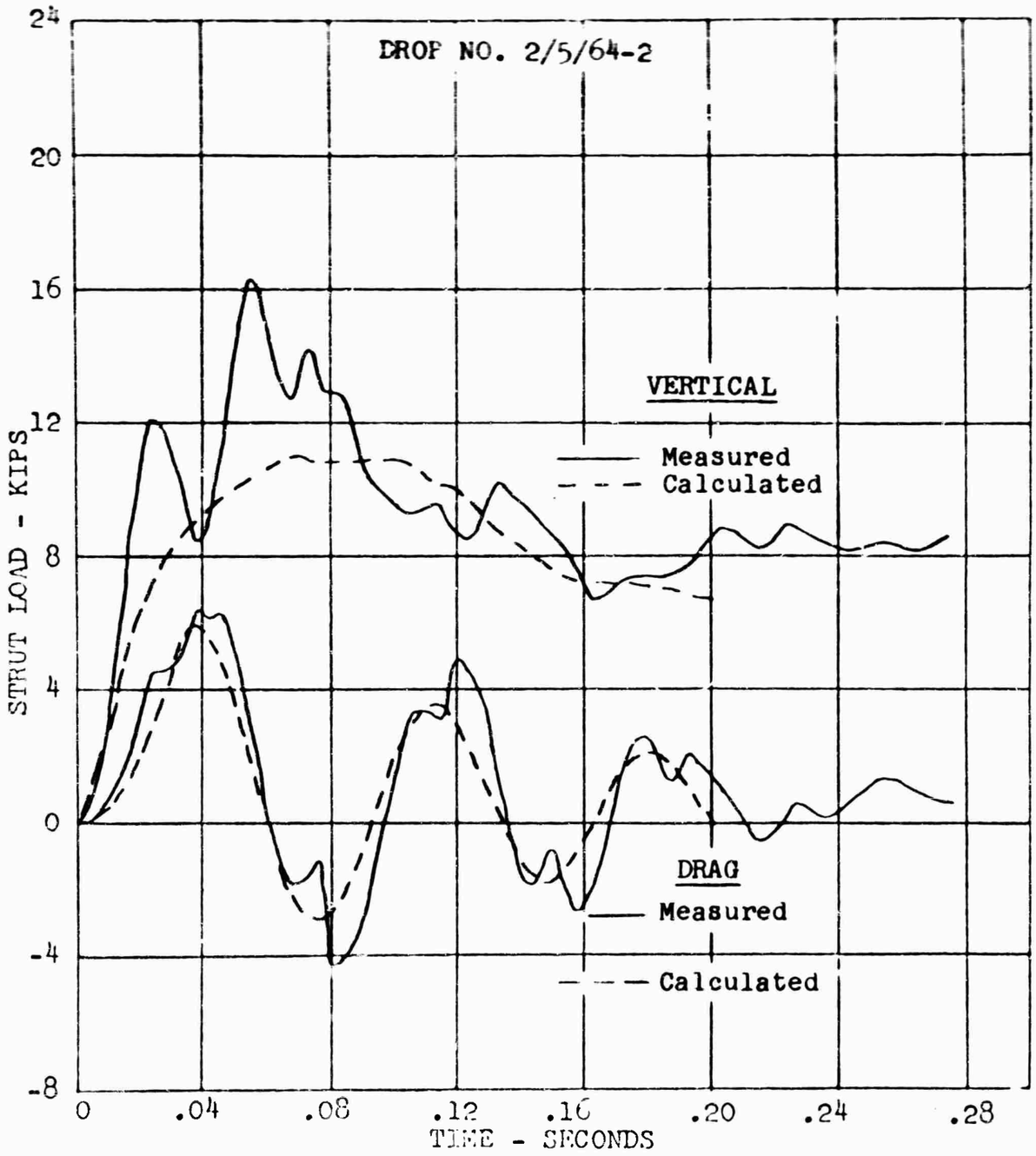

Figure 48. Comparison of Measured and Calculated Axle Loads for a 9.0-FPS Drop on Sand. Calculations Revised to Improve Drag Load Correlation.

UNCLASSIFIED
Security Classification

DOCUMENT CONTROL DATA - R&D

(Security classification of title, body of abstract and indexing annotation must be entered when the overall report is classified)

1 ORIGINATING ACTIVITY (Corporate author)
US Army Aviation Materiel Laboratories
Fort Eustis, Virginia 23604

2a REPORT SECURITY CLASSIFICATION
UNCLASSIFIED

2b GROUP

3 REPORT TITLE
A Study of Rough-Terrain-Induced Structural Landing Loads
Phase III - Simulated Landings of an OV-1 Aircraft Over Rough Terrain and Comparison of Experimental Loads with Theoretical Predictions

4 DESCRIPTIVE NOTES (Type of report and inclusive dates)

5 AUTHOR(S) (Last name, first name, initial)

6 REPORT DATE	7a TOTAL NO OF PAGES	7b NO OF REFS
May 1965	120	4

8a CONTRACT OR GRANT NO	9a ORIGINATOR'S REPORT NUMBER(S)
DA 44-177-TC-735	USAAML Technical Report 65-5
b PROJECT NO	
c Task 1P125901A14602	9b OTHER REPORT NO(S) (Any other numbers that may be assigned this report)
d	

10 AVAILABILITY/LIMITATION NOTICES
Qualified requesters may obtain copies of this report from DDC.
This report has been furnished to the Department of Commerce for sale to the public.

11 SUPPLEMENTARY NOTES	12 SPONSORING MILITARY ACTIVITY
	US Army Aviation Materiel Laboratories

13 ABSTRACT

This report describes the third phase of a project directed toward the establishment of aircraft design criteria for rough terrain landing operations.

The report presents the results of moving drop tests in which an OV-1 main landing gear was made to traverse simulated terrain irregularities of various sizes and shapes during landing impact. Test results for several cases are compared with the results of dynamic loads calculations performed on a digital computer. Recommendations for improvement of the analysis are made based on this comparison

DD FORM 1 JAN 64 1473

UNCLASSIFIED
Security Classification